

**Theory and Phenomenology Beyond the Standard Model
and Dark Matter Physics**

BY

KUO-HSING TSAO

B.S. National Chung Cheng University, Chiayi, Taiwan, 2007

M.S. National Taiwan Normal University, Taipei, Taiwan, 2009

THESIS

Submitted as partial fulfillment of the requirements
for the degree of Doctor of Philosophy in Physics
in the Graduate School of the
Univeristy of Illinois at Chicago, 2017

Chicago, Illinois

Defense Committee:

Wai-Yee Keung, Chair and Advisor

Richard Cavanaugh

Tom Imbo

James Unwin

Ian Low, Northwestern University, Evanston, Illinois, USA

To My Parents
Ming-Yueh Lin and Chin Tsao
Their Love is Beyond the Standard Model

Acknowledgements

I would like to extend my deepest appreciation to my advisor Wai-Yee Keung for his exceptional guidance during my graduate student career at UIC. His endless curiosity, keen observation and touch-ground calculation has shown me phenomenal invaluable lessons in being a great physicist. I also want to thank Ahmed Ismail for his collaborations and illuminating discussions. I further extend my appreciation to James Unwin for his brilliant inspirations on multiple projects, collaborations and assistance on my thesis manuscript.

In addition, I extend my thanks to Tom Imbo for his two-year legendary Quantum Field Theory lectures and inspiring hall-way conversations. I am grateful to Richard Cavanaugh who taught me particle physics in my first year at UIC and continuously educates me about particle physics since then. Also I extend my appreciation to Ian Low for his guidance on my thesis.

Enduring graduate school would be difficult without friends' support. I would like to thank my class fellows Bo-Yan Huang, Ben Rickman, Francisco Restrepo, John Van Dyke and Martin Winslow. I also want to thanks Bo Hsu, Yi-Yu Huang, Anvi Chen, Chun-Shan (Sandie) Yi, Ya-Ju Wang, Yi-Hsuan Chen, Nai-Ning Hsueh, Meng-Yin Wu, Yun-An Chou, Yi-Ping Lin, I-Ming Lin and friends I met at Taiwanese Student Association at UIC. I am thankful to Ya-Ching Chan and Yen-Fu Lin who always inspire me with music and their life experience. I also extend my appreciation to Victor Yu and Tai-Chi Kuo who helped me a lot in Chicago.

I have truly enjoyed my time with my violin teacher Sam Sharp, who is always patient and encouraging for my immature musical skills and my music school fellows Jisoo Jeong, Sara Kobaissi, Eva Gonzalez-Heredia, Raquel Gonzalez-Heredia and Carlos Javier Cruz Camello for their loving friendship.

Many thanks to my first physics teacher Zheng-Sheng Chen, who guided me into the physics world. I also would like to extend my appreciation to Chia-Hung Chang and Tzu-Chiang Yuan for their inspiring advice and helps of applying for UIC PhD program when I was in Taiwan.

Finally, I am grateful to my parents and Sunny Seto. This work would not be done without their unlimited support and love.

Contribution of Authors

Chapter 1 is an introduction to the background considered in this thesis. Chapter 2 is based on unpublished work by Ahmed Ismail, Wai-Yee Keung, Kuo-Hsing Tsao and James Unwin. All the authors produced the figures, performed the calculations and contributed to the writing of the manuscript. Chapter 3 and Chapter 4 are based on one published manuscript by Ahmed Ismail, Wai-Yee Keung, Kuo-Hsing Tsao and James Unwin. *Nuclear Physics B* ([dx.doi.org/10.1016/j.nuclphysb.2017.03.001](https://doi.org/10.1016/j.nuclphysb.2017.03.001)). All the authors performed the calculations, produced the figures and tables and contributed to the writing of the manuscript. Chapter 5 is a summary of this thesis.

TABLE OF CONTENTS

1	INTRODUCTION AND BACKGROUND	1
1.1	The Standard Model and Beyond the Standard Model	1
1.2	Gauge Extension of the Standard Model	4
1.2.1	The Gauge Structure of the Standard Model and Higgs Mechanism	5
1.2.2	$U(1)'$ Extension	9
1.2.3	Anomaly Cancellation	12
1.3	Dark Matter Physics	13
1.3.1	Dark Matter Relic Density	15
1.3.2	Search of Dark Matter in Simplified Models and Effective Field Theory	17
2	TOP-PHILIC VECTOR PORTAL DARK MATTER	23
2.1	Introduction	23
2.2	LHC Constraints of Z' coupled to only t_R	25
2.2.1	Effective Field Theory Approach	27
2.2.2	Simplified Models Approach	31
2.3	Relic Density and In-direct Detection	34
2.4	Direct Detection	38
2.5	Mono-jet v.s. Mono-photon in t_R -philic Z' Models	41
2.5.1	Mono- j /Mono- γ Complementarity	41
2.5.2	The Inverse Problem	43
2.6	UV Complete Theory and Mass Gereneration	45
2.6.1	Top Mass Generation and Mixing	46
2.6.1.1	EFT	46
2.6.1.2	UV Complete Model	47
2.6.2	Electroweak Precision and LHC Constraints on Top Quark Partner Fermion	49
2.6.3	Kinetic and Mass Mixing of Z - Z'	50
2.6.4	Majorana Dark Matter and Scalar Portal Model	52
2.7	Future Outlook and Discussion	54
3	ANOMALY CANCELLATION WITH AXIAL VECTOR Z'	56
3.1	Introduction	56
3.2	Gauge Anomalies and Axial Vectors	58
3.2.1	$U(1)'$ Anomaly Conditions	59
3.2.2	Coloured Exotics and Anomaly Free $U(1)'$ Extensions	60

3.3	Construction of Anomaly-Free Axial Vector Models	61
3.3.1	Mirror Constructions	62
3.3.2	An Algebraic Construction	64
3.3.3	General Algebraic Constructions	66
3.3.4	A Selection of Axial Vector Models	67
3.4	A Selection of Anomaly Free Vector Models	68
3.5	An Alternative Set of Anomaly Free Axial Vector Models	70
3.6	Algebraic Construction of Axial Vector Examples	71
4	AXIAL VECTOR Z' MODELS	73
4.1	Mass Generation	73
4.1.1	Mass Generation for Standard Model Fermions	73
4.1.2	Mass Generation for Pairs of Exotic Fermions	74
4.1.3	The Scalar Sector of Model #1	76
4.1.4	Mass Generation for Exotic Mirror Fermions	78
4.2	Breakdown of Low Energy Theories	79
4.2.1	The Non-Perturbative Limit	79
4.2.2	The Non-Renormalisable Limit	81
4.3	Dark Matter Freeze-out via an Axial Vector	83
4.4	Discussion	86
5	CONCLUSION	88
A	AXIAL VECTOR VERSUS VECTOR IN SM AND BSM	90
A.1	Axial-Vector Versus Vector in $gg \rightarrow Z(\text{or } Z') + j$	90
A.1.1	In Standard Model $M_Z = 91$ GeV	91
A.1.2	Heavy Z' with fixed couplings $g_A=g_V=0.1$	96
B	Copyright Permissions	98
	CITED LITERATURE	100
	Vita	114

List of Figures

1.1	Bullet Cluster of Dark Matter.	3
1.2	NGC2403 rotation velocity curve.	3
1.3	Kinetic mixing of Z-Z' at fermion loop.	10
1.4	The axial vector anomaly triangle loop diagram.	13
1.5	DM detection and search.	14
1.6	Schematic diagram illustrates freeze-out mechanism.	17
1.7	Spin-independent DM-nucleon scattering cross section limit from LUX. . .	20
1.8	Spin-dependent DM-nucleon scattering cross section limit from LUX and LZ projected with several relevant direct detection experiments bounds. .	21
1.9	The Fermi-LAT upper bounds for $\chi\bar{\chi} \rightarrow b\bar{b}$ or $\chi\bar{\chi} \rightarrow \tau\bar{\tau}$ annihilation cross sections.	22
2.1	Mono-jet lower bound limit in EFT.	29
2.2	$t\bar{t}$ +MET	29
2.3	$t\bar{t}$ +MET lower bound limit in EFT	30
2.4	Mono-jet limits in Simplified Model for $m_{Z'}$ and m_χ with $g_t = g_\chi = 1$. .	32
2.5	$t\bar{t}$ +MET limits in Simplified Model for $m_{Z'}$ and m_χ with $g_t = g_\chi = 1$. .	32
2.6	Mono-jet limits in Simplified Model for $m_{Z'}$ and m_χ with $g_t = g_\chi = 0.5$.	33
2.7	$t\bar{t}$ +MET limits in Simplified Model for $m_{Z'}$ and m_χ with $g_t = g_\chi = 0.5$.	33
2.8	$\chi\bar{\chi} \rightarrow Z'Z'$	35
2.9	$\chi\bar{\chi} \rightarrow Z' \rightarrow t\bar{t}$ via Z' when $m_{Z'} > 2m_t$	35
2.10	$\chi\bar{\chi} \rightarrow Z' \rightarrow tWb$ though one off-shell top and $\chi\bar{\chi} \rightarrow Z' \rightarrow Zh$ via top-loop when $(m_Z + m_h)/2 < m_{Z'} < 2m_t$	35
2.11	$\chi\bar{\chi} \rightarrow Z' \rightarrow b\bar{b}$ via top-loop when $m_{Z'} < (m_Z + m_h)/2$	36
2.12	Top-philic DM relic density contour plot	37
2.13	The direct detection of DM in top-philic simplified model	38
2.14	Top-philic DM relic density and direct detection contour plot	40
2.15	The Feynman diagrams for mono-jet V.S. mono-photon in top-philic model	42
2.16	The cross section difference between mono-jet and mono-photon and $F(p_t)$ function trend in t_R -philic model.	42
2.17	The additional tree Feynman diagrams when Z' couples to Q_L in the Q_L -philic model	44
2.18	The cross section difference between tree and loop contribution when Z' couples to Q_L	44
2.19	The cross section difference between mono-jet and mono-photon and $F(p_t)$ function trend when Z' couples to Q_L	44
2.20	The rapidity and the kinetic factor $F(p_t)$ of mono-jet with respect to t_R only and Q_L only.	45

2.21	Froggatt-Nielsen mechanism illustration.	46
2.22	Vector-like top partner mass and mixing angle limits and EW precision parameter ΔT limits	50
2.23	The EWPT parameter S and T for Z - Z' for top-philic model.	51
2.24	The summary of parameter space for top-philic model.	52
2.25	The di-photon or di-jet resonance of scalar S which is also the mediator of DM.	53
3.1	Anomaly Cancellation in SM.	58
4.1	The non-perturbative, unitarity and non-renormalisable limits for the axial-vector models.	82
4.2	The direct detection and collider limit of mono-jet search of DM for axial-vector DM models.	84
A.1	The Feynman diagrams for $gg \rightarrow Z(or Z') + j$	91
A.2	$g g \rightarrow Z + j$ with all favor quarks in the fermion loop.	91
A.3	LEFT: $g g \rightarrow Z + j$ with only up quark. RIGHT: $g g \rightarrow Z + j$ with only charm quark	94
A.4	LEFT: $g g \rightarrow Z + j$ with up and charm. RIGHT: $g g \rightarrow Z + j$ with up, down and charm. These two plots show the cross section combination from Eq. (A.3) and Eq. (A.6).	94
A.5	LEFT: $g g \rightarrow Z + j$ with $u+d+c+s+b'$. RIGHT: $g g \rightarrow Z + j$ with top only. The combination of these two plots will lead to Figure A.2 and cancellation effect from Eq. (A.5) only happens for axial vector coupling since the vector contribution from Eq. (A.8) is negligible.	94
A.6	The center mass energy \sqrt{s} needed for the cross section of $gg \rightarrow Z(91\text{GeV})j$ with only light loop fermion.	95
A.7	The center mass energy \sqrt{s} needed for the cross section of $gg \rightarrow Z(91\text{GeV})j$ with top.	95
A.8	LEFT: $g g \rightarrow Z + j$ with up only when $g_A=g_V=0.1$. $M_Z = 91$ GeV. RIGHT: $g g \rightarrow Z + j$ with top only when $g_A=g_V=0.1$. $M_Z = 91$ GeV	96
A.9	LEFT: $g g \rightarrow Z' + j$ with up only when $g_A=g_V=0.1$. $M_{Z'} = 1$ TeV. RIGHT: $g g \rightarrow Z + j$ with top only when $g_A=g_V=0.1$. $M_{Z'} = 1$ TeV	96
A.10	LEFT: $g g \rightarrow Z_{1\text{TeV}}(\text{Axial}) + j$ with up quark only. RIGHT: $g g \rightarrow Z_{91\text{GeV}}(\text{Vector}) + j$ with up quark only	97
A.11	LEFT: $g g \rightarrow Z_{1\text{TeV}}(\text{Axial}) + j$ with top quark only. RIGHT: $g g \rightarrow Z_{91\text{GeV}}(\text{Vector}) + j$ with top quark only	97

List of Tables

1.1	The gauge structure of the SM contents.	5
2.1	Mono-jet Inclusive Signal Region.	28
2.2	The gauge charges assignments of UV complete top-philic model.	47
3.1	The gauge representation of the anomaly cancelling exotics.	62
3.2	The anomaly free spectrum for different motivated axial-vector models. . .	64
3.3	Summary of the models we study. n_G is the number of SM generations charged under $U(1)'$	69
3.4	The anomaly free spectrum for different motivated pure vector models. . .	69
3.5	The anomaly free spectrum for different motivated axial-vector models by introducing extra right-handed neutrinos.	70
4.1	The $U(1)'$ charge bilinears for the axial-vector models.	75

Abbreviations

BSM	B eyond the S tandard M odel
DM	D ark M atter
EFT	E ffective F ield T heory
EW	E lectro- W eak
EWPT	E lectro- W eak P recision T ests
GUT	G rand U nified T heory
LHC	L arge H adron C ollider
MET	M issing T ransverse E nergy
QFT	Q uantum F ield T heory
RG	R enormalization G roup
SM	S tandard M odel
SUSY	S Uper S Ymmetry
UV	U ltra V iolet
VEV	V acuum E xpectation V alue
WIMP	W eakly I nteracting M assive P article

Summary

This thesis is dedicated to the study of theories of physics Beyond the Standard Model (BSM), specifically minimal extensions in which the Standard Model (SM) gauge group is extended by a new $U(1)'$ factor. We study the implications and applications of such $U(1)'$ extensions in the context of BSM and, in particular, in connection to Dark Matter (DM).

We consider the possibility that DM interactions with the SM states are mediated through a new Z' gauge boson which couples only to top quarks and DM. We call this scenario the *Top-philic Vector Portal*. We present a comprehensive study of top-philic DM models which can reproduce the correct DM relic density via the conventional freeze-out mechanism and which satisfy the current constraints from: the Large Hadron Collider (LHC), direct detection, indirect detection and electroweak precision tests. Additionally, we develop a method for identifying whether a vector is truly top-philic, or couples to both t and b , by considering the ratio of cross sections in the mono-jet and mono-photon searches for DM at the LHC.

Subsequently, we discuss the case that the Z' gauge boson only has axial couplings to the SM fermions. Such axial vector mediators are particularly interesting as portals between the SM and DM, as the direct detection constraints on such models are weak. However, additional $U(1)'$ gauge groups, under which the SM states are charged, generically lead to gauge anomalies unless new exotic anomaly cancelling fermions are introduced. We provide explicit examples and general methods for constructing anomaly free spectra and argue that in certain classes of models the axial vector Z' mass is expected to be comparable to the fermion exotics, in which case these models may be tested at current and forthcoming experiments.

Chapter 1

INTRODUCTION AND BACKGROUND

1.1 The Standard Model and Beyond the Standard Model

The Standard Model (SM) of particle physics describes our visible world of fundamental particles and interactions nearly perfectly so far. Written in the language of quantum field theory (QFT) and gauge theory, the SM explains the electromagnetic and weak force between leptons and an additional strong nuclear force among quarks by the gauge mediators photon, W and Z bosons, and gluons respectively. Moreover, the Higgs mechanism [1] successfully addresses the difficulties of generating the SM massive particles in the gauge theory framework including fundamental particles and gauge bosons except photon and gluon. By introducing a fundamental scalar boson, Higgs boson, which plays the role to give masses to the above mentioned massive gauge bosons via spontaneous symmetry breaking (SSB) of electro-weak(EW) gauge symmetry and Yukawa couplings to massive fermions respectively. On July 4 2012, a SM-like Higgs boson with mass 125 GeV [2, 3] and the SM predicted interactions with fermions and decay channels was discovered at the Large Hadron Collider (LHC) which affirms the foundation of the SM.

The understanding of our visible world is not complete since the SM still has several theoretical and phenomenological loopholes and issues even though it has the above mentioned successes. First of all, the *Hierarchy Problem* challenges the SM with the large discrepancy between electro-weak interaction and gravity force. More explicitly, it is an

open question why Higgs is so light compared to the Planck scale $M_{Planck} \sim 10^{18}$ GeV and how the Higgs boson mass survives the quantum correct divergence. According to QFT, the Higgs boson mass receives divergent quantum corrections which requires one cutoff regulation and it further implies there must be new physics present at about the cutoff energy scale. If there is no new physics, then the Higgs mass correction is expected to be order of M_{Planck} and is phenomenologically impossible to be the 125 GeV boson found at the LHC without large fine tuning. Therefore, physics beyond the Standard Model (BSM) is believed to be the answer to the hierarchy problem. Supersymmetry (SUSY) is one of the most acceptable theories beyond Standard Model to solve the hierarchy problem. It also can lead to unification of the gauge couplings at high scale. SUSY is a symmetry that relates bosons and fermions which form *superpartners* pairs, i.e. fermions and bosons are mass degenerate at M_{SUSY} unless SUSY is broken. This can address the Higgs mass issue due to cancellations between quantum corrections contribution from fermions and bosons.

In addition to the hierarchy problem, the SM is short of explaining the existence of dark matter (DM) which was initially inferred from deviations in long range gravitational measurements by Fritz Zwicky in 1933 [4]. Zwicky observed the motion of the galaxies in Coma galaxy cluster and found that there was a two-order of deviation on the total mass by the luminosity of the Coma cluster and the number of galaxies. He further proposed the deviation was caused by non-visible particle, dark matter which dominates the gravitational force contribution since the visible matter is not sufficient enough to stabilize the galaxy cluster. Moreover, there is more evidence in support of the existence of from both the collisions between galaxy clusters, the *Bullet Cluster* [5] shown in Figure 1.1 and rotation velocity curves of galaxy [6] shown in Figure 1.2.

This thesis is dedicated to the study of theories beyond the SM involving minimal extensions of the SM, $U(1)'$ *Extension of the SM*, the application of BSM to DM and collider searching of DM at the LHC. In the following sections of this chapter, $U(1)'$ Extension of the SM will be discussed first. Followed by DM physics discussion including DM relic density production, DM phenomenology and searching for DM at the LHC.

In *Chapter 2*, we present the possibility that DM interactions with the SM are mediated though a new vector Z' which couples to top quarks solely. We call this scenario the *top-philic vector portal*. Moreover, we construct a comprehensive study of top-philic DM

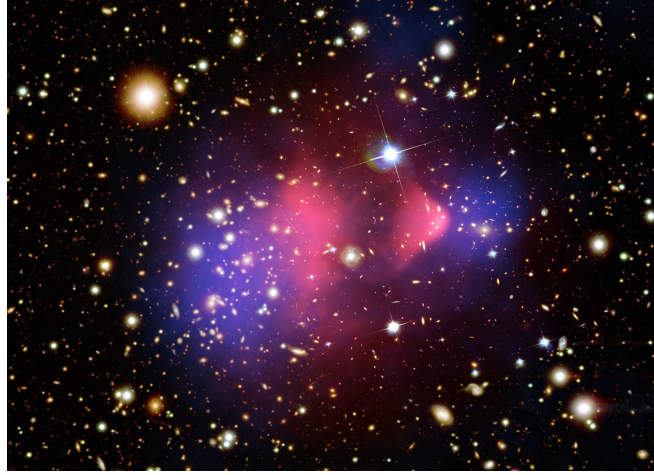


FIGURE 1.1: The *Bullet Cluster* provides the evidence for dark matter where the central red region in this figure refers the hot gas distribution of the two colliding cluster components observed in X-ray emission by the Chandra telescope. On the two separated ends of this figure, the blue region infers the gravitational lensing of dark matter which does not get affected by the cluster collision. In other words, if dark matter doesn't exist then there should be just hot gas red regions after the collision.

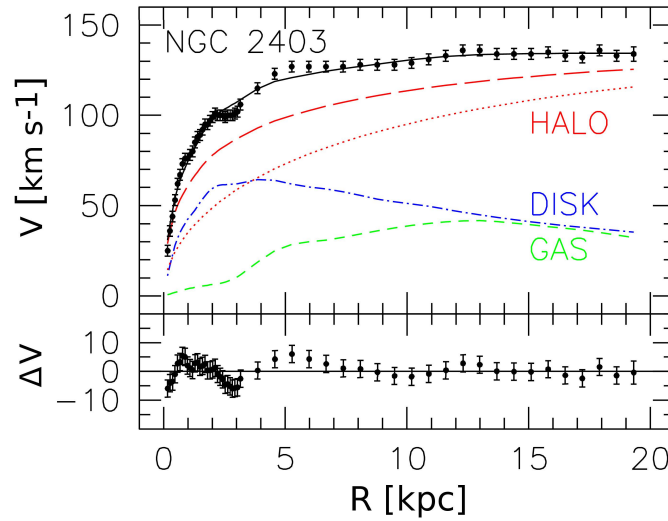


FIGURE 1.2: The observation on the interstellar rotation velocity respect to the distance from the center of galaxy NGC 2403 indicates the visible matter lacks the explanation to the deviation of rotation velocity at the far edge of galaxy. According to Newton gravity, the rotation velocity drops as the distance increases for a constant mass distribution object, however, this figure shows the majority of the galaxy is dominated by a hypothesis dark matter halo which contributes the rotation velocity distribution.

models with the correct DM relic density via conventional freeze-out mechanism and current LHC collider, direct and indirect detection limits.

In *Chapter 3* and *4*, we will discuss Z' gauge boson with only axial coupling to the SM fermions by constructing several motivated models. With the introduction of the new abelian $U(1)'$, anomaly cancellation requires new exotics fermions. We argue that in certain classes of models the axial vector Z' mass is comparable to the exotics. Furthermore, axial vector mediators can be portals between the SM and DM and the study of the parameter space of DM density due to freeze-out via the axial vector is presented. A summary of this thesis is presented in *Chapter 5*.

1.2 Gauge Extension of the Standard Model

This section follows treatments of [7, 8]

There are many proposed extensions of gauge symmetries in the SM or even in the Minimal Supersymmetric Standard Model (MSSM) involving the extension of EW symmetry $SU(2)_L \times U(1)_Y$. For example, $SU(2)_L \times U(1)_Y \times U(1)'$ with addition abelian $U(1)$ symmetry, which is considered as the minimal extension of the SM from the bottom-up point of view. If we consider a top-down example with a larger symmetry group, say $SU(N)$ which is broken spontaneously by a real adjoint scalar ϕ with its vacuum expectation value $\langle\phi\rangle$ (VEV or vev) and $\langle\phi\rangle$ can be presented by an $SU(N)$ transformation with unbroken $U(1)^N$ subgroup. There are extra gauge bosons correlate with the introduction of extended gauge symmetries. In this thesis, we focus on the neutral gauge bosons Z' 's which is widely studied in the context of BSM, especially for being mediators between the SM and DM.

In this section, the SM gauge structure and Higgs mechanism will be reviewed first. Then we will focus on $U(1)'$ extension of the SM and the searches for the new neutral boson Z' . Finally we will discuss anomaly cancellation in the SM and in the case when a new gauge is introduced.

1.2.1 The Gauge Structure of the Standard Model and Higgs Mechanism

The SM is formed by the gauge symmetries $SU(3)_C \times SU(2)_L \times U(1)_Y$ and we summarize the fermion contents and gauge bosons with their $SU(3)_C \times SU(2)_L \times U(1)_Y$ gauge representations and charges in Table 1.1:

Fermion ($N_f=3$)	$SU(3)$	$SU(2)_L$	$U(1)_Y$
Q_L	3	2	1/3
u_R	3	1	4/3
d_R	3	1	-2/3
L_L	1	2	-1
e_R	1	1	-2
Scalar Boson	$SU(3)$	$SU(2)_L$	$U(1)_Y$
$\Phi = \begin{pmatrix} \phi^+ \\ \phi^0 \end{pmatrix}$	1	2	1
Vector Bosons	g	W^i	B

TABLE 1.1: The gauge structure of the SM contents.

where $Q_L = \begin{pmatrix} u_L \\ d_L \end{pmatrix}$ and $L_L = \begin{pmatrix} e_L \\ \nu_L \end{pmatrix}$ are the $SU(2)_L$ doublets for left-handed quarks and leptons.

The generic gauge invariant Lagrangian of the SM:

$$\mathcal{L}_{SM} = -\frac{1}{4}F^{\mu\nu}F_{\mu\nu} + i\bar{f}_i \not{D} f_i + Y_{ij}\bar{f}_L^i \Phi f_R^j + |D_\mu \Phi|^2 - V(\Phi) + h.c. \quad (1.1)$$

where $F^{\mu\nu}F_{\mu\nu}$ is the field strength tensor operator of gauge field interactions, f_i are the three flavor fermion content of the SM including quarks and leptons and \not{D} is the corresponding gauge invariant and Lorentz invariant covariant derivative.

$$\not{D} \equiv D_\mu \gamma^\mu; \quad (1.2)$$

$$D_\mu = \partial_\mu + ig\vec{W} \cdot \vec{T} + \frac{1}{2}ig'B_\mu Q_Y, \quad \text{for } SU(2)_L \times U(1)_Y \quad (1.3)$$

$$D_\mu = \partial_\mu + ig_s\vec{G} \cdot \vec{T}, \quad \text{for } SU(3)_C \quad (1.4)$$

\vec{W} and \vec{G} are $SU(2)_L$ and $SU(3)_C$ gauge fields with isospin operator $\vec{T} = \vec{\sigma}/2$ where $\vec{\sigma}$ are 2×2 Pauli matrices. We can further express $\vec{W} \cdot \vec{T} = W^+T^+ + W^-T^- + W_3T_3$ in

terms of raising and lower operators of isospin $T^\pm = (T_1 \pm iT_2)/\sqrt{2}$. g' , g , g_s are the $U(1)_Y$, $SU(2)_L$ and $SU(3)_C$ gauge couplings respectively.

Y_{ij} is the Yukawa matrix of the SM fermion, $D_\mu\phi$ is Higgs field kinetic term and $V(\Phi)$ is Higgs potential.

$$V(\Phi) = -\mu^2|\Phi|^2 + \lambda|\Phi|^4, \quad (\mu^2 > 0, \lambda > 0) \quad (1.5)$$

When Φ acquires a non-zero vev $v = \pm\sqrt{\frac{\mu^2}{\lambda}}$ from Higgs potential, it breaks EW symmetry $SU(2)_L \times U(1)_Y \rightarrow U(1)_{EM}$ spontaneously¹ and gives mass to the $SU(2)_L$ gauge bosons W^\pm and Z .

$$\Phi = \begin{pmatrix} 0 \\ \frac{v+H}{\sqrt{2}} \end{pmatrix} \quad (1.6)$$

where H is the Higgs Boson and its Lagrangian becomes

$$\mathcal{L}_{Higgs} = \frac{1}{2}(\partial H)^2 + \frac{1}{4}g^2W^+W^-(v+H)^2 + \frac{1}{8}g_Z^2ZZ(v+H)^2 - V\left(\frac{1}{2}(v+H)^2\right) \quad (1.7)$$

which gives the mass of gauge bosons and Higgs boson:

$$m_W = \frac{1}{2}gv; \quad m_Z = \frac{m_W}{\cos\theta_W}; \quad m_H = \sqrt{\frac{\lambda}{2}}v \quad (1.8)$$

and photon is still massless after rotating the mass matrix of gauge bosons with Weinberg angle θ_W :

$$\begin{pmatrix} Z \\ A \end{pmatrix} \equiv \begin{pmatrix} \cos\theta_W & -\sin\theta_W \\ \sin\theta_W & \cos\theta_W \end{pmatrix} \begin{pmatrix} W_3 \\ B \end{pmatrix}. \quad (1.9)$$

On the other hand, the SM fermions f^i also receive mass from the Yukawa interaction in Eq. (1.1) when Φ gets vev and mass Lagrangian is²:

$$\mathcal{L}_{mass} = -\mathcal{M}_{ij}^e \bar{e}_L^i e_R^j - \mathcal{M}_{ij}^u \bar{u}_L^i u_R^j - \mathcal{M}_{ij}^d \bar{d}_L^i d_R^j + h.c. \quad (1.10)$$

¹ $SU(2)_L \times U(1)$ symmetry is still invariant in Eq. (1.1) but not for the ground state at non-zero vev.

²Neutrinos are massless in the SM since there is no right-handed neutrino in the SM. However, neutrino oscillations observation provides the experimental evidence for non-zero neutrino masses and this will lead to a mixing matrix as known as Pontecorvo-Maki-Nakagawa-Sakata (PMNS) matrix in the leptonic sector. [9, 10]

where M_{ij}^u and M_{ij}^d are in the EW gauge eigenstate basis. These can be diagonalized into flavor basis by applying unitary matrices:

$$\mathcal{U}_R^{-1} \mathcal{M}^u \mathcal{U}_L = \begin{pmatrix} m_u & 0 & 0 \\ 0 & m_c & 0 \\ 0 & 0 & m_t \end{pmatrix} \quad (1.11)$$

and

$$\mathcal{D}_R^{-1} \mathcal{M}^d \mathcal{D}_L = \begin{pmatrix} m_d & 0 & 0 \\ 0 & m_s & 0 \\ 0 & 0 & m_b \end{pmatrix} \quad (1.12)$$

where the unitary matrices are:

$$\begin{pmatrix} u_1 \\ u_2 \\ u_3 \end{pmatrix}_{L,R} = \mathcal{U}_{L,R} \begin{pmatrix} u \\ c \\ t \end{pmatrix}_{L,R} \quad (1.13)$$

$$\begin{pmatrix} d_1 \\ d_2 \\ d_3 \end{pmatrix}_{L,R} = \mathcal{D}_{L,R} \begin{pmatrix} d \\ s \\ b \end{pmatrix}_{L,R} \quad (1.14)$$

The EW charge current term from Eq. (1.1) indeed indicates there are flavor mixing features for the SM quarks sector:

$$-\mathcal{L}_{CC} = i \frac{g}{\sqrt{2}} W_\mu^+ \begin{pmatrix} \bar{u}_{1L} & \bar{u}_{2L} & \bar{u}_{3L} \end{pmatrix} \gamma^\mu \begin{pmatrix} d_{1L} \\ d_{2L} \\ d_{3L} \end{pmatrix} + h.c. \quad (1.15)$$

$$= i \frac{g}{\sqrt{2}} W_\mu^\pm \begin{pmatrix} \bar{u}_L & \bar{c}_L & \bar{t}_L \end{pmatrix} \mathcal{U}_L^\dagger \mathcal{D}_L \gamma^\mu \begin{pmatrix} d_L \\ s_L \\ b_L \end{pmatrix} + h.c. \quad (1.16)$$

and we define the mixing matrix

$$\mathcal{V} \equiv \mathcal{U}_L^\dagger \mathcal{D}_L \quad (1.17)$$

which leads to standard Cabibbo-Kobayashi-Maskawa (CKM) matrix [11, 12] with three rotation matrices and one CP violation phase [13].

$$\begin{aligned}\mathcal{V} &\equiv \mathcal{R}_2(\theta_{23})\mathcal{R}_3(\theta_{13}, \delta)R_1(\theta_{12}) \\ &= \begin{pmatrix} c_{12}c_{13} & s_{12}c_{13} & s_{13}e^{-i\delta} \\ -c_{23}s_{12} - c_{12}s_{23}s_{13}e^{-i\delta} & -c_{12}c_{23} - s_{12}s_{23}s_{13}e^{-i\delta} & c_{13}s_{23} \\ s_{12}s_{23} - c_{12}c_{23}s_{13}e^{-i\delta} & -c_{12}s_{23} - c_{23}s_{12}s_{13}e^{-i\delta} & c_{12}c_{23} \end{pmatrix} \quad (1.18)\end{aligned}$$

where c_{ij} and s_{ij} are $\cos\theta_{ij}$ and $\sin\theta_{ij}$ the mixing angles of generation i with j the rotation matrices are :

$$\mathcal{R}_1(\theta_{ij}) = \begin{pmatrix} c_{ij} & s_{ij} & 0 \\ -s_{ij} & c_{ij} & 0 \\ 0 & 0 & 1 \end{pmatrix}, \quad (1.19)$$

$$\mathcal{R}_2(\theta_{ij}) = \begin{pmatrix} 1 & 0 & 0 \\ 0 & c_{ij} & s_{ij} \\ 0 & -s_{ij} & c_{ij} \end{pmatrix}, \quad (1.20)$$

$$\mathcal{R}_3(\theta_{ij}, \delta) = \begin{pmatrix} c_{ij} & 0 & s_{ij}e^{-i\delta} \\ 0 & 1 & 0 \\ -s_{ij}e^{-i\delta} & 0 & c_{ij} \end{pmatrix} \quad (1.21)$$

The diagonal values of CKM matrix in (1.18) are $\mathcal{O}(1)$ and off-diagonal values are small and the current experiment measurement is reviewed in *Review of Particle Physics* from *Particle Data Group* [14].

The neutral current of Z boson in Eq. (1.1) doesn't have mixing behaviors since

$$-\mathcal{L}_{NC} \equiv g_Z J_Z^\mu Z_\mu \quad (1.22)$$

$$= ig_L Z_\mu \begin{pmatrix} \bar{u}_{1L} & \bar{u}_{2L} & \bar{u}_{3L} \end{pmatrix} \gamma^\mu \begin{pmatrix} d_{1L} \\ d_{2L} \\ d_{3L} \end{pmatrix} + L \leftrightarrow R \quad (1.23)$$

$$= ig_L Z_\mu \begin{pmatrix} \bar{u}_L & \bar{c}_L & \bar{t}_L \end{pmatrix} \gamma^\mu \mathcal{U}_L^\dagger \mathcal{U}_L \begin{pmatrix} u_L \\ c_L \\ t_L \end{pmatrix} + L \leftrightarrow R \quad (1.24)$$

$$= ig_L Z_\mu \begin{pmatrix} \bar{u}_L & \bar{c}_L & \bar{t}_L \end{pmatrix} \gamma^\mu \begin{pmatrix} u_L \\ c_L \\ t_L \end{pmatrix} + L \leftrightarrow R \quad (1.25)$$

where $g_{L,R} \equiv g_Z P_{L,R}$ and the projector operator $P_L \equiv \frac{1-\gamma^5}{2}$ and $P_R \equiv \frac{1+\gamma^5}{2}$.

Due to the chirality of the SM fermion sector, the neutral current can be further expressed into the vector and axial-vector:

$$-\mathcal{L}_{NC} = \sum_f Z_\mu \bar{f} (g_f^V \gamma^\mu + g_f^A \gamma^\mu \gamma^5) f \quad (1.26)$$

with $g_f^V \equiv \frac{1}{2}(g_{fL} + g_{fR})$ and $g_f^A \equiv \frac{1}{2}(g_{fR} - g_{fL})$. A more detail discussion of vector and axial-vector coupling will be discussed in the context of a new gauge $U(1)'$ symmetry below.

1.2.2 $U(1)'$ Extension

The generic neutral current Lagrangian of $U(1)'$ with the SM fermions (without the kinetic mixing) can be expressed in terms of the SM neutral current with additional $U(1)'$ current:

$$\begin{aligned} -\mathcal{L}_{NC} &= g' J_Y^\mu B_\mu + g J_3^\mu W_\mu^3 + g_X J_X^\mu X_\mu \\ &= e J_Q^\mu A_\mu + g_Z J_Z^\mu Z_\mu + g_{Z'} J_{Z'}^\mu Z'_\mu \end{aligned} \quad (1.27)$$

where X and Z' are the new gauge boson in gauge and mass eigenstate. g'_Z is the new $U(1)'$ gauge coupling and Z_μ and A_μ are the SM neutral currents. Then we can express the neutral current into vector and axial-vector combination as in Eq. (1.26) for the SM:

$$\begin{aligned} J_i^\mu &= g_i \bar{f} \gamma^\mu (Q_L P_L + Q_R P_R) f \\ &= \bar{f} \gamma^\mu (g_i^V + g_i^A \gamma^5) f \end{aligned} \quad (1.28)$$

where $i = Z, Z'$ and Q_L and Q_R are the gauge charges of left-handed and right-handed fermions respectively. Using the chirality projector operators $P_L = \frac{1-\gamma^5}{2}$ and $P_R = \frac{1+\gamma^5}{2}$. This leads to the vector coupling $g_i^V = \frac{g_i}{2}(Q_L + Q_R)$ and axial vector coupling $g_i^A = \frac{g_i}{2}(Q_L - Q_R)$. There are rich phenomenology studies arising due to the vector and axial vector couplings. Here we present one example to illustrate the consequence for the case of DM mono-jet searches at the LHC with the final state Z (or Z') with an energetic jet in Appendix A. Furthermore, note that the vector coupling vanishes if it couples to Majorana fermions Ψ_M due to Majorana fermion's charge conjugation definition:

$$\mathcal{C}^{-1} \Psi_M \mathcal{C} = \Psi_M, \quad \mathcal{C}^{-1} \bar{\Psi}_M \mathcal{C} = \bar{\Psi}_M \quad (1.29)$$

and

$$\mathcal{C}^{-1}(\gamma^\mu) \mathcal{C} = -\gamma^\mu \quad (1.30)$$

leads to $\bar{\Psi}_M \gamma^\mu \Psi_M = 0$ for Majorana fermions. In SUSY, the fermionic superpartner of neutral gauge bosons, *neutralinos*, are good theoretical candidates for Majorana fermions.

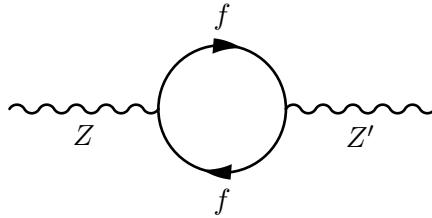


FIGURE 1.3: Kinetic mixing appears at loop when fermions have both $U(1)$ and $U(1)'$ charges.

Kinetic mixing effect arises though loop correction when fermions carry both $U(1)$ and $U(1)'$ charges. [15] Figure 1.3 and mass mixing between the SM neutral bosons and new

gauge boson can also arise. Consider a Lagrangian [16]:

$$\begin{aligned}\mathcal{L}_{\text{mixing}} = & -\frac{1}{4}\hat{B}^{\mu\nu}\hat{B}_{\mu\nu} - \frac{1}{4}\hat{X}^{\mu\nu}\hat{X}_{\mu\nu} + \frac{1}{2}m_{\hat{Z}}^2\hat{Z}^\mu\hat{Z}_\mu + \frac{1}{2}m_{\hat{X}}^2\hat{X}^\mu\hat{X}_\mu \\ & -\frac{1}{2}\text{sin}\epsilon\hat{B}^{\mu\nu}\hat{X}_{\mu\nu} + \delta m^2\hat{Z}^\mu\hat{X}_\mu\end{aligned}\quad (1.31)$$

where the hatted field contents are the canonical gauge interaction fields with mixing effects. The mass mixing term can be realized if the SM Higgs has non-zero $U(1)'$ charge $\delta m^2 = \frac{1}{2}\frac{eg'}{\hat{s}_W\hat{c}_W}Q'_H v^2$ or loop-induced if Higgs is neutral under $U(1)'$. The SM neutral gauge boson $\hat{Z} \equiv \hat{c}_W\hat{W}^3 - \hat{s}_W\hat{B}$ with sine (\hat{s}_W) and cosine (\hat{c}_W) of Weinberg angle.

The mass eigenstates of neutral bosons in Eq. (1.31) can be expressed by applying a rotation matrix to the hatted gauge fields to the canonical (non-hatted) gauge interaction bases first and then diagonalized:

$$\begin{pmatrix} B_\mu \\ W_\mu^3 \\ X_\mu \end{pmatrix} = \begin{pmatrix} 1 & 0 & t_\epsilon \\ 0 & 1 & 0 \\ 0 & 0 & c_\epsilon \end{pmatrix} \begin{pmatrix} \hat{B}_\mu \\ \hat{W}_\mu^3 \\ \hat{X}_\mu \end{pmatrix} \quad (1.32)$$

$$\begin{pmatrix} A_\mu \\ Z_\mu \\ Z'_\mu \end{pmatrix} = \begin{pmatrix} 1/\hat{c}_W & \hat{s}_W c_\xi & -\hat{s}_W s_\xi \\ -\hat{s}_W & 1/\hat{c}_W c_\xi & \hat{c}_W s_\xi \\ 0 & -s_\xi & 1/c_\xi \end{pmatrix} \begin{pmatrix} B_\mu \\ W_\mu^3 \\ X_\mu \end{pmatrix} \quad (1.33)$$

where

$$t_{2\xi} = \frac{-2c_\epsilon(\delta m^2 + m_{\hat{Z}}^2\hat{s}_W s_\epsilon)}{m_{\hat{X}}^2 - m_{\hat{Z}}^2 c_\epsilon^2 + m_{\hat{Z}}^2\hat{s}_W^2 s_\epsilon^2 + 2\delta m^2\hat{s}_W s_\epsilon} \quad (1.34)$$

Here we omit the mass mixing term $\hat{A}^\mu\hat{X}_\mu$, although this can have implication for DM *millicharge* studies.[17] The resulting Z' neutral current interaction becomes:

$$\mathcal{L}_{Z'} = -\frac{e}{2\hat{c}_W\hat{s}_W}c_\xi Z'_\mu \bar{f}\gamma^\mu \left(T_3^f (\hat{s}_W t_\epsilon - t_\xi) + Q^f (\hat{s}_W^2 - \hat{s}_W t_\epsilon) \right) f \quad (1.35)$$

and the SM neutral current can be expressed in the terms of electroweak precision tests parameters (EWPT) [16, 18] with constraint of new physics [19–21]:

$$\mathcal{L}_Z = -\frac{e}{2\hat{s}_W\hat{c}_W} \left(1 + \frac{\alpha T}{2} \right) Z_\mu \bar{f}\gamma^\mu \left(\left(T_3^f - 2Q^f \left(\hat{s}_W^2 + \frac{\alpha S - 4\hat{c}_W^2\hat{s}_W^2\alpha T}{4(\hat{c}_W^2 - \hat{s}_W^2)} \right) \right) - T_3^f \gamma^5 \right) f \quad (1.36)$$

where T_3^f and Q^f are the fermion weak isospin and electric charge. The electric charge

here remains *non-hatted* so $\alpha = \frac{e^2}{4\pi}$ in Eq. (1.36). The EWPT parameters S and T are defined:

$$S = \frac{4}{\alpha} \hat{c}_W^2 \hat{s}_W \xi (\epsilon - \hat{s}_W \xi) \quad (1.37)$$

$$T = \frac{\xi^2}{\alpha} \left(\frac{m_{Z'}^2}{m_Z^2} - 2 \right) + 2 \hat{s}_W \xi \epsilon \quad (1.38)$$

where m_Z and $m_{Z'}$ are physical masses of the Z and Z' . The current limits on new contribution to the EWPT parameters are referenced in [14].

The physical massive neutral bosons Z and Z' masses are obtained after we diagonalize Eq. (1.33):

$$m_Z = \sqrt{m_{\hat{Z}^2} (1 + \hat{s}_W t_\xi t_\epsilon) + \delta m^2 c_\epsilon^{-1} t_\xi} \quad (1.39)$$

$$m_{Z'} = \sqrt{\frac{m_{\hat{X}^2 + \delta m^2 (\hat{s}_W s_\epsilon - c_\epsilon t_\xi)}{c_\epsilon^2 (1 + \hat{s}_W t_\xi t_\epsilon)}} \quad (1.40)$$

and the physical Weinberg angle and physical m_Z satisfy the identity

$$s_W c_W m_Z = \hat{s}_W \hat{c}_W m_{\hat{Z}}. \quad (1.41)$$

If we fix \hat{s}_W and $m_{\hat{Z}}$, then Fermi constant is correct:

$$s_W^2 c_W^2 = \frac{\pi \alpha(m_Z)}{\sqrt{2} G_F m_Z^2} \quad (1.42)$$

Searching for new neutral bosons at the LHC is model-dependent which includes conventional Drell-Yan production [22], $pp \rightarrow Z' \rightarrow l\bar{l}$ or di-jet and in general there are a total 21 possible couplings to the SM fermions u_i , d_{iL} , e_{iL} , ($L \leftrightarrow R$) and ν_{iL} . In addition to the final states of the SM fermions, Z' could also be a mediator to exotics fermions or scalars and even DM which implies Z' decays to missing transverse energy (MET) and other final state contents.

1.2.3 Anomaly Cancellation

When we introduce a new $U(1)$ gauge symmetry with the SM gauge symmetries, there is a fundamental constraint arising: the requirement is that there are no gauge anomalies

since the SM is gauge anomaly free unless there are extra exotic fermions involved. Gauge anomalies appear when conserved currents of a gauge theory is no longer conserved in the presence of quantum corrections. For example, the vector current for a fermion with $U(1)$ gauge charge α is conserved when $\psi \rightarrow e^{i\alpha}\psi$:

$$J^\mu \equiv \bar{\psi}\gamma^\mu\psi, \quad \text{and} \quad \partial_\mu J^\mu = 0 \quad (1.43)$$

However, the chirality of ψ leads to the non-conserved axial current for a massive fermion:

$$J^{\mu 5} \equiv \bar{\psi}\gamma^\mu\gamma^5\psi, \quad \text{and} \quad \partial_\mu J^{\mu 5} = 2im_\psi\bar{\psi}\gamma^5\psi \neq 0 \quad (1.44)$$

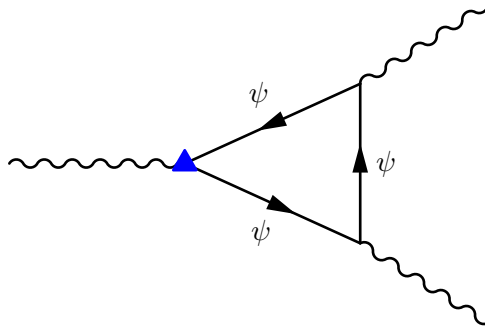


FIGURE 1.4: The BLUE TRIANGULAR vertex refers $J^{5\mu}$ which has the chiral anomaly contribution $\partial_\mu J^{\mu 5} = 2im_\psi\bar{\psi}\gamma^5\psi \neq 0$ in Eq. (1.44).

Anomaly cancellation generally requires additional exotics or non-chiral structure, e.g. vector-like exotics in new physics. However, model-building of anomaly-free spectrum is not trivial as many works have shown either by the bottom-up construction [5, 23] or top-down approaches [24, 25]. In *Chapter 3* and *4*, we consider the case of anomaly cancellation when Z' is a pure axial vector which has rich phenomenology especially in DM searches. We further highlight the additional constraints from gauge coupling running effect and the unitarity condition of Z' s-channel scattering process.

1.3 Dark Matter Physics

The majority of this thesis is related to the study of DM which has both theoretical and phenomenological motivation from BSM. For a experimental point of view, DM can be detected in three main methods:

- Direct detection: When DM scatters with the SM particles at the detectors, the scattering signal can produce the recoil energy for atomic nuclei in the direct detection experiments, e.g. LUX and PandaX, which have the most recent direct detection limits from the null result of DM searches [26–28]. The direct detection is illustrated in Figure 1.5(a).
- In-direct detection: The annihilation process of DM not only settles the relic abundance but also provides a source of the cosmic rays from galaxies, e.g. Fermi-LAT, AMS-02 and PAMELA [29–31]. The illustration of in-direct detection is shown in Figure 1.5(b)
- Collider search at the LHC: If DM is produced at the LHC, it will become an apparent imbalance of the total transverse momentum with SM final states, for example, mono-jet or mono-photon with MET[32, 33] shown in Figure 1.5(c). There are other search channels at the LHC which are model-dependent. In *Chapter 2*, we focus on a simplified model in which the new vector boson Z' only couples to right-handed top quark and DM. We will discuss the mono-jet and $t\bar{t} + MET$ [34] search of DM.

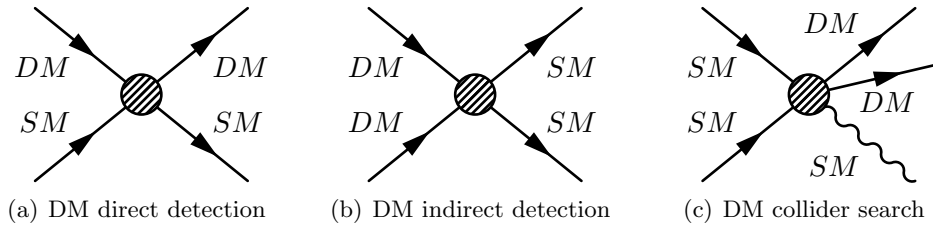


FIGURE 1.5: The three different DM detection and search channels: (a) the scattering between DM and the SM particles at the detector gives us the direct detection of DM; (b) the annihilation of DM from the galaxies provides the search of cosmic rays excess experiments; (c) searching DM at the LHC requires the associate the SM state along with DM production which becomes MET.

In this section, DM relic density will be discussed since it provides a good foundation for the discussion of parameters space in phenomenological studies. Following we discuss the search for DM in both effective field theory (EFT) and simplified model scenarios.

1.3.1 Dark Matter Relic Density

In the early Universe, most of the elements of the Universe were in the thermal equilibrium and then it expanded and cooled with the Hubble rate H . The number density abundance of massive particles (mass = M) becomes exponentially small and frozen when the temperature is not able to produce those massive particles from the hot bath ($T_{bath} < M$) in the expanding universe. The number density is called *Relic Density* which is controlled by two factors: the expansion rate of the Universe H and the thermal annihilation cross section $\langle\sigma_{ann}\rangle$ of the species. The Boltzman equation of the number density of a massive particle X with respect to time:

$$\frac{d}{dt}n_X + 3Hn_X = -\langle\sigma_{ann}v\rangle(n_X^2 - n_X^{(eq)2}) \quad (1.45)$$

where $\langle\sigma_{ann}v\rangle$ is the particle-antiparticle $X\bar{X}$ annihilation cross section times the relative velocity of two particles annihilating, $n_X^{(eq)}$ is the equilibrium density without the chemical potential:

$$n_X^{(eq)} \sim \frac{g_X}{2\pi^3} \int \frac{1}{e^{E/kT} \pm 1} d^3p \quad (1.46)$$

g_X is the degrees of freedom(d.o.g.) ($g_X = 1$ for a real scalar, $g_X=2$ for a massive vector boson or a fermion). In the non-relativistic limit ($kT \ll m$),

$$n_X^{(eq)} = g_X \left(\frac{mkT}{2\pi}\right)^{3/2} e^{m/kT} \quad (1.47)$$

where $3Hn_X$ tells us the expanding effect of the Universe and the number density of particle in a co-volume $n_X a^3$ or in terms of temperature $n_X T^{-3}$ shall be a constant without the annihilation process. Here we further define two parameters to rewrite Eq. (1.45):

$$Y_X \equiv \frac{n_X}{s}, \quad s = \frac{2\pi^2}{45} g_*^s T^3, \quad g_*^s(T_i) = \sum_{boson} g_i \left(\frac{T_i}{T}\right)^3 + \frac{7}{8} \sum_{fermion} g_i \left(\frac{T_i}{T}\right)^3 \quad (1.48)$$

and a new defined parameter

$$x \equiv \frac{m_X}{T}. \quad (1.49)$$

Thus Boltzman equation Eq. (1.45) becomes:

$$\begin{aligned}\frac{d}{dx}Y_X &\equiv -\lambda x^{-n-2}(Y_X^2 - Y_X^{(eq)2}) \\ &= -\frac{1}{x^{n+2}} \frac{s}{H(m_X)} \langle \sigma_{ann} v \rangle (Y_X^2 - Y_X^{(eq)2})\end{aligned}\quad (1.50)$$

where

$$\lambda = 0.264 M_{pl} \left(\frac{g_*^s}{\sqrt{g_*}} \right) m_X \langle \sigma_{ann} v \rangle \quad (1.51)$$

$$Y_{eq} = 0.145 \left(\frac{g}{g_*^s} \right) x^{3/2} e^{-x} \quad (1.52)$$

The Boltzman equation in Eq. (1.50) can be solved in the mechanism of *freeze-out* which means at early time ($x \ll x_f$) the co-moving number density Y follows the thermal equilibrium co-volume number density Y_{eq} very closely $Y \approx Y_{eq}$. At the later time ($x \gg x_f$), Y loses tracking Y_{eq} and becomes Y_∞ at freeze-out temperature x_f :

$$Y_\infty = \frac{n+1}{\lambda} x_f^{n+1} \quad (1.53)$$

$$x_f = \text{Log} \left((2+c) \lambda a c - \left(n + \frac{1}{2} \right) \text{Log} (\text{Log} (2+c)) + \dots \right) \quad (1.54)$$

with the numerical input constant $c \sim \mathcal{O}(1)$, $a = 0.145 \left(\frac{g}{g_*^s} \right)$, and the order n of Taylor expansion of annihilation cross section refers to *s-wave* channel ($n=0$), *p-wave* ($n=1$) channel, etc.

We illustrate the evolution of Y from solving Eq. (1.50) with respect to x in Figure 1.6 for freeze-out mechanism. In general, the freeze-out co-moving number density of particle X is controlled by the mass of particle and the thermal annihilation cross section $\langle \sigma_{ann} v \rangle$:

$$Y_\infty^{FO} \sim \frac{1}{m_X \langle \sigma_{ann} v \rangle M_{pl}} \quad (1.55)$$

where $M_{pl} \approx 10^{18}$ GeV.

The measured relic density of DM is related to Y by:

$$\Omega_\chi = \frac{s_o m_\chi}{\rho_c} Y_\chi \quad (1.56)$$

where the entropy density today $s_o = 2.8 \times 10^{-3} \text{cm}^{-3}$ and the critical density $\rho_c = 10^{-5} h^2 \text{GeVcm}^{-3}$.

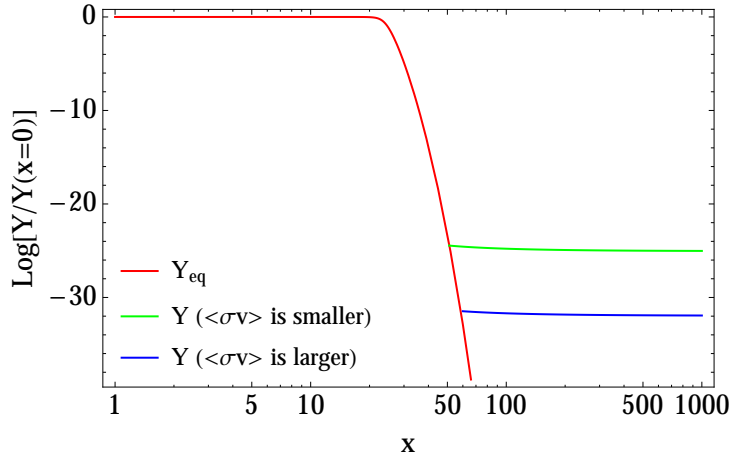


FIGURE 1.6: The co-volume number density Y keeps tracking along with Y_{eq} at the early universe and then freezes-out at temperature x_f . Note that the co-volume density after freeze-out depends on the thermal average annihilation cross section $\langle\sigma_{ann}v\rangle$.

DM relic density is observed $\Omega_\chi h^2 \simeq 0.12$ and it applies $\langle\sigma_{ann}v\rangle \approx \mathcal{O}(10^{-26}) \text{ cm}^3\text{s}^{-1}$ from freeze-out DM [35].

1.3.2 Search of Dark Matter in Simplified Models and Effective Field Theory

Following the discussion of the DM relic density, if there is such a weakly interacting massive particle (WIMP) with the correct relic density $\Omega_\chi h^2 \simeq 0.12$ (WIMP miracle), then the search for DM can be understood using the three methods highlighted above. However, the knowledge of hidden sectors is the missing part of the SM and the current detection results nearly rule out the possibility of Higgs or Z as the mediators of DM [36]. Therefore new physics is needed to construct viable DM models. In this thesis, we consider a minimal extension of the SM by considering *DM simplified models* [37, 38]. The models can be *s-channel portal* which are further categorized into two groups by the spin-state of DM mediator³:

$$\mathcal{L}_V \supset \sum_f \bar{f} V_\mu (g_f^V \gamma^\mu + g_f^A \gamma^\mu \gamma^5) f + \bar{\chi} (g_\chi^V \gamma^\mu + g_\chi^A \gamma^\mu \gamma^5) \chi \quad (1.57)$$

$$\mathcal{L}_\phi \supset \sum_f \bar{f} \phi (y_f^S + y_f^P \gamma^5) f + \phi \bar{\chi} (y_\chi^S + y_\chi^P \gamma^5) \chi \quad (1.58)$$

³Here DM is assumed to be Dirac fermion. Majorana DM only has axial-vector or pseudo-scalar interaction and there is a factor of 1/2 for the couplings compared to Dirac DM cases.

where Eq. (1.57) and Eq. (1.58) are the *vector portal* and *scalar portal* DM simplified models respectively. This thesis is mainly focus on the vector portal models. The couplings of the mediators refer to the $g(y)_f^i$ for the SM couplings and $g(y)_\chi^i$ for DM couplings where i can be V for vector, A for axial-vector, S for scalar and P for pseudo-scalar mediators respectively. For s-channel simplified models, DM search is controlled by five parameters (m_χ , m_{med} , $g(y)_f^i$, $g(y)_\chi^i$, Γ_{med}): DM mass, mediator mass, the SM coupling, DM coupling and the decay width of the mediator. Here the decay width is considered in the *minimal width assumption*:

$$\Gamma \equiv \Gamma_{V(\phi) \rightarrow \chi\bar{\chi}} + \Gamma_{V(\phi) \rightarrow f\bar{f}} + \Gamma_{\phi \rightarrow gg} \quad (1.59)$$

where the last term is forbidden for vector mediators due to Landau-Yang theorem. [39, 40]

In the collider search for DM with simplified models, the mediator can be produced either *on-shell* ($m_{med} > 2m_{\chi(q)}$) or *off-shell* ($m_{med} < 2m_{\chi(q)}$). Furthermore, if the mediator mass is heavier than the collider kinetic allowed region, i.e. $m_{med} \gg \sqrt{s}$, (where \sqrt{s} is the center mass energy of the collider) then simplified models reach the effective field theory (EFT) region which means we can integrate the mediator mass and then study DM search with the effective operator \mathcal{O}_{eff} .

$$\mathcal{L}_{eff} = \frac{1}{\Lambda^n} \mathcal{O}_{eff}^{4+n} \quad (1.60)$$

where Λ is EFT scale, for example, the dimension-6 operator $\Lambda \equiv \frac{m_{med}}{\sqrt{g_f g_\chi}}$. In the collider search for DM, we can express the matrix element for the production cross section of DM with EFT scale:

$$\mathcal{M} \propto \frac{g_f g_\chi}{m_{med}^2 - s} \approx \frac{1}{\Lambda^2} \quad (1.61)$$

and the null DM search result from the LHC provides the lower limits for the different search channels. Thus far, the current LHC model-dependent bound $\Lambda \sim \mathcal{O}(10^2)$ GeV to $\mathcal{O}(10^3)$ GeV for $\mathcal{O}(10^2)$ GeV DM. In *Chapter 2*, we study both EFT and simplified model scenarios within a vector portal DM simplified model in which the new gauge neutral boson Z' only couples to top quark. We name this model the *top-philic vector portal*.

Additionally, there is another simplified model which focuses on the mediator coupling one SM fermion and one DM particle:

$$\mathcal{L} \supset g_\phi \sum_f \phi_i^* \bar{\chi} f_R + \phi \bar{f}_L \chi \quad (1.62)$$

where DM χ is a SM singlet and the scalar mediator carries appropriate SM charges to keep Eq. (1.62) gauge invariant. The scalar here is similar to the sfermion in Minimal Supersymmetric Standard Model (MSSM).

In direct detection search for DM, generally speaking, the recoil energy of the detectors is below the mass of mediator, therefore we will apply low energy nuclear EFT with DM-SM EFT approach and also non-relativistic limits ($v_{DM} \sim 10^{-3}c$) for direct detections. [41, 42] Note that there are two EFTs involved in direct detection:

$$\mathcal{L}_{\chi N} = \frac{1}{m_{med}^2} \chi \mathcal{O}_{eff}^\chi \chi N \mathcal{O}_{eff}^N N \quad (1.63)$$

where \mathcal{O}_{eff}^χ is from Eq. (1.60) and \mathcal{O}_{eff}^N is EFT from nucleon energy scale by integrating out EW scale which includes the sum of quarks couplings in the nucleons of the detectors:

$$\mathcal{O}_{eff}^N \supset (\mathcal{G}_v^N \bar{N} \gamma^\mu N + \mathcal{G}_a^N \bar{N} \gamma^\mu \gamma^5 N) \quad (1.64)$$

where N is for nucleons including protons (p) and neutrons (n) and the couplings \mathcal{G}^N are the sum of quarks couplings within the nucleon:

$$\begin{aligned} \mathcal{G}_v^p &= 2\mathcal{G}_v^u + \mathcal{G}_v^d \\ \mathcal{G}_v^n &= \mathcal{G}_v^u + 2\mathcal{G}_v^d \\ \mathcal{G}_a^N &= \sum_{q=u,d,s} \mathcal{G}_a^q \Delta_q^N \end{aligned} \quad (1.65)$$

the axial vector charges Δ_q^N are the light quark contribution to the spin of the nucleon N . The details of \mathcal{G} are calculated and reviewed in [42]. After matching two EFTs and we

can evaluate DM-nucleon interaction matrix elements to non-relativistic limit:

$$\begin{aligned}
 \mathcal{M}_{\chi N} &\equiv \langle \chi N | \mathcal{L}_{\chi N}^{\mu_N} | \chi N \rangle \\
 &= \frac{1}{m_{med}^2} \mathcal{O}_{eff}^{\chi} \mathcal{O}_{eff}^N \\
 &\simeq \sum_i \mathcal{C}_{\chi,i}^N \mathcal{O}_i^{NR}
 \end{aligned} \tag{1.66}$$

where $\mathcal{C}_{\chi,i}^N$ are the non-relativistic effective operator coefficient of the model-dependent \mathcal{O}_i^{NR} operators which implies spin-independent and spin-dependent DM-nucleon scattering cross sections corresponding to different combinations of $\mathcal{O}_{eff}^{\chi} \mathcal{O}_{eff}^N$ in Eq. (1.66):

$$\begin{aligned}
 \sigma_{SI}^{\chi N} &= \sum_i \frac{\mu_{\chi N}}{\pi} \frac{(g(y)_{\chi} \mathcal{G}_i^N)^2}{m_{med}^4} \\
 \sigma_{SD}^{\chi N} &= \sum_i \frac{3\mu_{\chi N}}{\pi} \frac{(g(y)_{\chi} \mathcal{G}_i^N)^2}{m_{med}^4}
 \end{aligned} \tag{1.67}$$

with the reduce mass of DM-nucleon system $\mu_{\chi N} = \frac{m_{\chi} M_N}{m_{\chi} + M_N}$. The current direct detection limits from LUX [26, 27] for spin-independent and spin-dependent scattering cross section (including LZ projected limits) in Figure 1.7 and Figure 1.8.

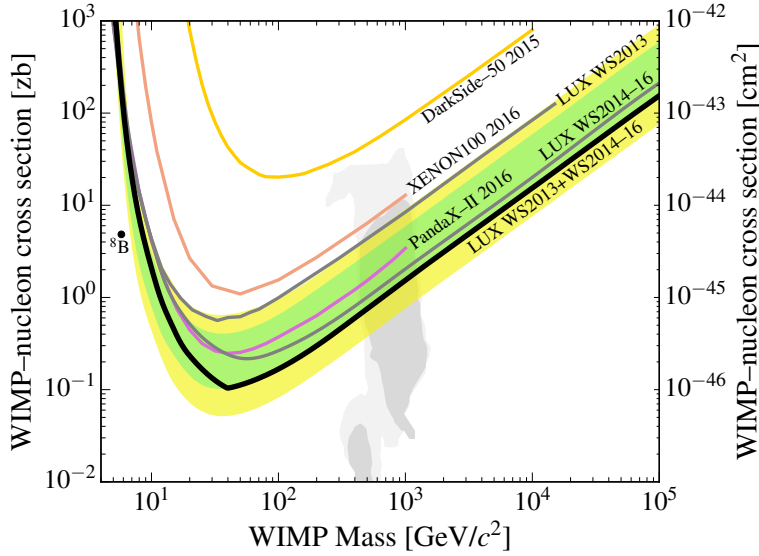


FIGURE 1.7: The current spin-independent scattering cross section between DM and nucleon from LUX [27].

If DM annihilation occurs in the high DM density region in our universe, they can produce the fluxes of cosmic rays of the SM particles, for example, the gamma rays detection from

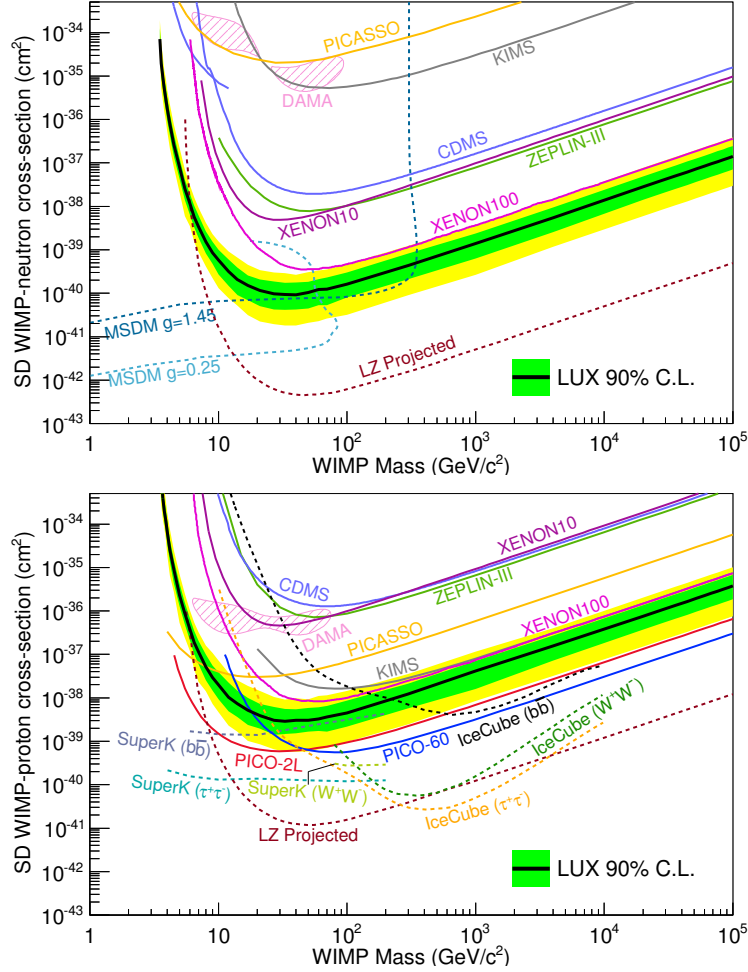


FIGURE 1.8: The current spin-independent (including neutron and proton) scattering cross section between DM and nucleon from LUX and LZ projected limits with other direct detection experiments bounds. [26]

Fermi Large Area Telescope (Fermi-LAT) [29] which presents 6 years gamma ray observation data from the dwarf spheroidal satellite galaxies (dSphs) of the Milky Way. In Fermi-LAT experiment, the gamma ray signal flux ϕ (ph cm⁻²s⁻¹, photon per cm² per second) integrated over a solid angle $\Delta\Omega$ at Fermi-LAT detector is defined:

$$\phi(\Delta\Omega) = \underbrace{\frac{1}{4\pi} \frac{\langle\sigma v\rangle}{2m_\chi^2} \int_{E_{min}}^{E_{max}} \frac{dN_\gamma}{dE_\gamma} dE_\gamma}_{\text{particle physics}} \times \underbrace{\int_{\Delta\Omega} \int_{l.o.s.} \rho_{DM}^2(r) dl d\Omega'}_{\text{J-factor}} \quad (1.68)$$

where the coordinate r in the J-factor is the Galactic Center coordinate $r = \sqrt{r_\odot^2 + l^2 - 2r_\odot l \cos\theta}$ with $r_\odot = 8.33\text{kpc}$ (kiloparsec), l is the line of sight (l.o.s.) and θ is the angle between the direction of l.o.s and the axis of connecting the Earth to the Galactic Center. Milky Way dSphs can give the gamma ray excess raise from J-factor of $\mathcal{O}(10^{19})$ GeV²cm⁻⁵ [29, 43, 44]

with $\rho_{DM} = 0.3 \text{ GeVcm}^{-3}$. However, there is no excess beyond the background gamma ray excesses being observed which leads the upper bound for DM annihilation cross sections dependent on DM primary decay channels, for example, $\chi\bar{\chi} \rightarrow b\bar{b}$ or $\chi\bar{\chi} \rightarrow \tau^+\tau^-$ which and then decay to photons in Figure 1.9. As we can see from Fermi-LAT results, the in-direct detection limits are shown on the annihilation cross sections for light DM ($m_\chi < 100 \text{ GeV}$) and we will discuss the impacts on the parameter space in our studies.

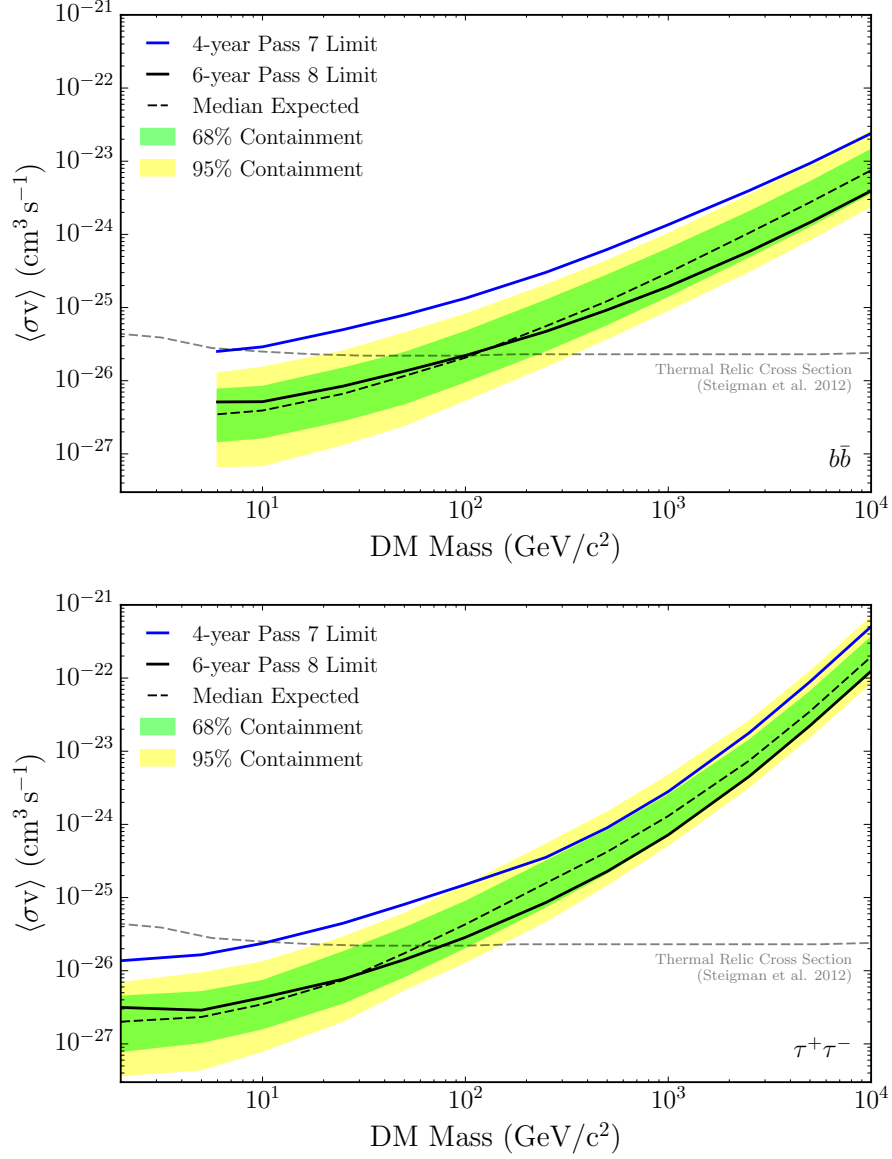


FIGURE 1.9: With the null extra gamma excess observed from Fermi-LAT, the annihilation cross section upper limits for $\chi\bar{\chi} \rightarrow b\bar{b}$ or $\chi\bar{\chi} \rightarrow \tau^+\tau^-$ from Eq. (1.68).

Chapter 2

TOP-PHILIC VECTOR PORTAL DARK MATTER

2.1 Introduction

From an effective field theory stance, *portal operators* involve a gauge and Lorentz invariant combination of both the SM fields and operators of hidden sector fields $\mathcal{O}_{\text{hidden}}$ should be present. For example, the *Higgs portal*, $|H|^2 \mathcal{O}_{\text{hidden}}$ [45, 46] is well motivated. In this case, diagrams through the SM fermions couple to hidden sector states involve a Higgs VEV insertion $\langle H \rangle$, and thus characterized by Yukawa couplings $y_q = m_q / \langle H \rangle$. For instance, the dimension six operator coupling fermion DM χ and Standard Model quarks q after electroweak symmetry breaking is typically of the form:

$$\frac{m_q}{\Lambda^2} \bar{\chi} \chi \bar{q} q , \quad (2.1)$$

where Λ is characteristically the mass of a new (heavy) scalar mediator. Indeed, deviations from Yukawa-like couplings naïvely run foul of minimal flavor violation (MFV) constraints [47].

Since interactions involving the Higgs portal are Yukawa suppressed, collider searches are typically substantially weaker than compared to universal interactions. The reason for this is that light fermions are heavily suppressed due to their small Yukawa couplings, and the heavy quark content of the nucleons is very small. Therefore the main production

process for such y_q -suppressed operators is via gluon fusion involving loops of top and bottom quarks [48].

It is intriguing to consider alternative scenarios involving different mediators states in which the dominant production of DM at colliders occurs through loops. We will primarily consider the implications of a new spin one mediator which couples to only hidden sector states and the top quark. We call this the *top-philic vector portal*. Since this new vector only couples directly to top quarks of all the Standard Model states, as with the Higgs portal DM will be essentially be only produced via loops. Moreover, the parameter space of the *universal coupling Z' or H models* suffers severe constraints on the both couplings and the masses of DM and mediator [36].

New spin one degrees of freedom are ubiquitous in BSM physics [8], and can potentially mediate interactions between the DM and SM states. At the effective field theory level, contact operators between DM χ and quarks q mediated by vector bosons are of the form $\bar{\chi}\gamma_\mu\chi\bar{q}\gamma^\mu q$, while for axial vectors the operators generated are $\bar{\chi}\gamma_\mu\gamma^5\chi\bar{q}\gamma^\mu\gamma^5q$. This implies the spin-independent and spin-dependent scattering cross sections respectively. Examples appear in the meson sector of QCD [49] exhibits a rich spectrum of spin-1 bosons, those with odd parity $J^{PC} = 1^{-\pm}$ are vectors, while even parity $J^{PC} = 1^{+\pm}$ states are axial vectors. The vector mesons and axial vector mesons are the 1^{+-} state $h_1(1170)$ and the 1^{++} state $f_1(1285)$.

The purpose of this chapter is to study the phenomenology of new vector and axial vector states which couple preferentially to top quarks. First, we start with a simplified model in which only the *right-handed* top couples to the new spin one mediator Z' . Such top-philic scenarios arise in a range of scenarios, as we discuss shortly, and aspects of the collider phenomenology [50–52] and their potential for generating interesting indirect detection signals [53, 54] have previously attracted attention. In particular, this scenario is of interest in the context of certain DM models, specifically, the Fermi 130 GeV line(s) [54, 55], and the Galactic Centre excess observed by Fermi-LAT [56]. Finally, we develop a phenomenological method for clarifying the ambiguity arising from the chirality of top quark which has not been studied in the literature.

2.2 LHC Constraints of Z' coupled to only t_R

For hidden sector states χ which interact with the SM states, in our case via their interactions with top quarks, particle collisions at the LHC can potentially produce these states. If the hidden sector states are stable on collider timescales (for instance DM which is stable on cosmological timescales). Once DM is produced, it will escape the detector and its presence can only be inferred through the observation of anomalous amounts of missing transverse energy (MET). Thus searches [57, 58] for events with missing energy, such as mono-jets ($pp \rightarrow j + \text{MET}$), mono-photons ($pp \rightarrow \gamma + \text{MET}$) or $t\bar{t} + \text{MET}$ can provide model independent limits on the interactions of χ with quarks and gluons [48, 59–70].

In this section, we explore the current bounds on hidden sector states coupled to the SM states via top-philic vectors or axial vectors. We present both a model independent effective field theory (EFT) analysis based on dimension six operators $\bar{\chi}\gamma_\mu\chi\bar{q}\gamma^\mu q$ and $\bar{\chi}\gamma_\mu\gamma^5\chi\bar{q}\gamma^\mu\gamma^5q$, and a UV complete analysis in the context of the model outlined in Section 2.6. We shall focus on the constraints which arise from the null searches for mono-jet and $t\bar{t} + \text{MET}$ events. Finally, we will discuss the prospect of using complementary channels to distinguish between vector and axial vector couplings, in the event of an observed excess in these searches for missing energy.

Searching for DM as the missing transverse energy with a high energetic jet [33, 57, 58] is a relatively clean signal at the LHC. We consider the case that $m_{Z'}$ is present from 10 GeV to 10 TeV.¹ For the current mono-jet and $t\bar{t} + \text{MET}$ studies, m_χ is taking to be in the mass range of 1 GeV to 1 TeV. We also consider that the couplings g_t and g_χ are equal (i.e. both DM and top have the same $U(1)'$ charge), the couplings of g_t and g_χ are both $\mathcal{O}(1)$ or less in order to maintain the acceptable perturbative behavior. As we shall show, if the DM relic density is set due to thermal freeze-out process via the top-philic vector, the corresponding Z' mass range consistent with LHC searches for mono-jet and $t\bar{t} + \text{MET}$ is between 100 GeV to 10 TeV and the DM mass should lie in the range 1 GeV to 1 TeV.

¹When DM coupling disappears, the lower bound of $m_{Z'}$ is constraints from the decay channels to the SM states. Here we take the conservative lower limit due to its non-zero invisible decay and small mixing angle between Z - Z' . [36]

First of all, we consider the simplest top-philic Z' DM model by coupling the top quark t_R and Dirac DM χ to a new U(1) gauge boson Z' with q_{tL} , t_R and $q_{\chi L}$, χ_R charges:

$$\begin{aligned}
\mathcal{L} &= \bar{t}\gamma^\mu (g_{Z'} q_{tL} P_L + g_{Z'} q_{tR} P_R) t Z'_\mu + \bar{\chi}\gamma^\mu (g_{Z'} q_{\chi L} P_L + g_{Z'} q_{\chi R} P_R) \chi Z'_\mu \\
&= \bar{t}\gamma^\mu \left(g_{Z'} q_{tL} \left(\frac{1-\gamma^5}{2} \right) + g_{Z'} q_{tR} \left(\frac{1+\gamma^5}{2} \right) \right) t Z'_\mu \\
&\quad + \bar{\chi}\gamma^\mu \left(g_{Z'} q_{\chi L} \left(\frac{1-\gamma^5}{2} \right) + g_{Z'} q_{\chi R} \left(\frac{1+\gamma^5}{2} \right) \right) \chi Z'_\mu \\
&= \bar{t} \left(\frac{g_{Z'}}{2} q_{tL} (1-\gamma^5) \gamma^\mu + \frac{g_{Z'}}{2} q_{tR} (1+\gamma^5) \gamma^\mu \right) t Z'_\mu \\
&\quad + \bar{\chi} \left(\frac{g_{Z'}}{2} (q_{\chi L} + q_{\chi R}) \gamma^\mu + \frac{g_{Z'}}{2} (q_{\chi L} - q_{\chi R}) \gamma^\mu \gamma^5 \right) \chi Z'_\mu \\
&\equiv \bar{t} (g_{tL} (\gamma^\mu - \gamma^\mu \gamma^5) + g_{tR} (\gamma^\mu + \gamma^\mu \gamma^5)) t Z'_\mu + \bar{\chi} (g_{\chi V} \gamma^\mu + g_{\chi A} \gamma^\mu \gamma^5) \chi Z'_\mu \quad (2.2)
\end{aligned}$$

where in the last equation we have introduced:

$$g_{tL} \equiv \frac{g_{Z'}}{2} \times q_{tL}; \quad g_{tR} \equiv \frac{g_{Z'}}{2} \times q_{tR} \quad (2.3)$$

$$g_{\chi V} \equiv \frac{g_{Z'}}{2} \times (q_{\chi L} + q_{\chi R}); \quad g_{\chi A} \equiv \frac{g_{Z'}}{2} \times (q_{\chi L} - q_{\chi R}) \quad (2.4)$$

Furthermore, we observe that in that case of $q_{tL} = 0$, Eq. (2.2) reduces to

$$\mathcal{L} = \bar{t}(g_{tR}(\gamma^\mu + \gamma^\mu \gamma^5))t Z'_\mu + \bar{\chi}(g_{\chi V}\gamma^\mu + g_{\chi A}\gamma^\mu \gamma^5)\chi Z'_\mu \quad (2.5)$$

We find that vector contributions is negligible in Eq. (2.2) due to either the center mass energy \sqrt{s} suppression i.e. the loop structure of vector coupling contributions are the box-diagrams which is relatively harder for a pair of initial gluons to generate Z' plus either mono-jet or top quark. The difference between vector and axial-vector contribution is about two orders of magnitude. More details are discussed in Appendix A.

It is not immediate to obtain information regarding the chirality of a given vector operator. We note that the fact that the SM fermion content is chiral under $SU(2)$ gives an opportunity to quickly break this ambiguity, since the left-handed top and bottom form a $SU(2)$ doublet. Thus if Z' coupled to the left handed top it must couple to the left handed bottom leading to a top-bottom-philic Z' vector boson rather than purely top-philic model. This ambiguity has been neglected in the literature and we develop a phenomenological method to address this in Section 2.5.

2.2.1 Effective Field Theory Approach

One can consider an EFT approach in which the heavy mediator Z' state is integrated out leading to effective operator description. For instance, a Z' which couples to fermion DM and quarks, when integrated out, leads to the following dimension six operator:

$$\mathcal{L} \supset \frac{1}{\Lambda^2} \mathcal{O}_6, \quad \mathcal{O}_6 = g_t g_\chi (\bar{\chi} \gamma_\mu \gamma_5 \chi) (\bar{t} \gamma^\mu \gamma^5 t) \quad (2.6)$$

where $\Lambda \equiv m_{Z'}/\sqrt{g_t g_\chi}$ is the scale of the effective operator.

The effective operator \mathcal{O}_6 can further induce the gluon fusion effective operator by applying the partial axial vector current conservation [71]

$$\begin{aligned} \mathcal{O}_6 &= g_t g_\chi (\bar{\chi} \gamma_\mu \gamma_5 \chi) (g^{\mu\nu}) (\bar{t} \gamma_\nu \gamma^5 t) \\ &= g_t g_\chi (\bar{\chi} \gamma_\mu \gamma_5 \chi) \left(\underbrace{g^{\mu\nu} - \frac{k^\mu k^\nu}{k^2}}_{=0} + \frac{k^\mu k^\nu}{k^2} \right) (\bar{t} \gamma_\nu \gamma^5 t) \\ &= \frac{g_t g_\chi}{k^2} \partial^\mu (\bar{\chi} \gamma_\mu \gamma_5 \chi) \partial^\nu (\bar{t} \gamma_\nu \gamma^5 t) \\ &= \frac{g_t g_\chi}{k^2} (2i m_\chi \bar{\chi} \gamma_5 \chi) \times \left(\underbrace{2i m_t \bar{t} \gamma^5 t}_{-\frac{\alpha_s}{4\pi} I(k^2, m_t^2) G_{\mu\nu}^{(a)} \tilde{G}^{(a)\mu\nu}} + \frac{\alpha_s}{4\pi} G_{\mu\nu}^{(a)} \tilde{G}^{(a)\mu\nu} \right) \\ \mathcal{M} &\rightarrow \left(\frac{2m_\chi}{\Lambda_*^4} \right) (\bar{\chi} i \gamma_5 \chi) \left\{ \frac{\alpha_s}{4\pi} [1 - I(k^2, m_t^2)] G_{\mu\nu}^{(a)} \tilde{G}^{(a)\mu\nu} \right\} \end{aligned} \quad (2.7)$$

where $\Lambda_* = \frac{m_{Z'}}{(g_t g_\chi)^{1/4}}$ and the loop function is given as:

$$I(k^2, m_t^2) = 2! \int_0^1 \int_0^{1-y} \frac{dx dy}{1 - k^2 xy / m_t^2 - i\epsilon} \quad (2.8)$$

This function is explicitly known, $I(k^2, m_t^2) = f(\tau)/\tau$, with $\tau = k^2/(4m_t^2)$, and

$$f(\tau) = \Theta(1 - \tau) \arcsin^2 \sqrt{\tau} - \Theta(\tau - 1) \frac{1}{4} \left(\ln \frac{1 + \sqrt{1 - 1/\tau}}{1 - \sqrt{1 - 1/\tau}} - i\pi \right)^2 \quad (2.9)$$

We study the 13 TeV LHC mono-jet limits at luminosity $\mathcal{L} = 3.2 \text{ fb}^{-1}$. Specifically, we use FeynRules [72], FeynArts[73] to generate model files, MadGraph5 [74] for the events generation, Pythia 6 [75] for parton showering and Delphes 3 for the LHC detector response simulation[76] based on the event selection rules from the ATLAS mono-jet+MET [33].

The simulation events are identified as signal events if the following critiques are *all* satisfied:

- MET > 250 GeV
- The leading jet $p_t > 250$ GeV and $|\eta| < 2.4$
- At most four jets with $p_t > 30$ GeV and $|\eta| < 2.8$
- $\Delta\phi(\text{jet}, \vec{p}_T^{\text{miss}}) > 0.4$
- No muons with $p_t > 10$ GeV or electrons with $p_t > 20$ GeV

and the *inclusive signal region* of MET:

Inclusive signal region	IM1	IM2	IM3	IM4	IM5	IM6	IM7
MET (GeV)	> 250	> 300	> 350	> 400	> 500	> 600	> 700

TABLE 2.1: The inclusive signal region.

The EFT scale Λ_* in Eq. (2.7) determines the production cross section σ_{Monojet} which sets the number of event yields $\# = \sigma_{\text{Monojet}} \times \mathcal{L} \times \text{efficiency}$ from the selection rules (the best limit in the selection inclusive regions with 95% CLs). By rescaling the Λ , we obtain from MadGraph + Pythia + Delphes (for short, we refer to these packages as MPD):

$$\frac{\#_{\text{MPD}}}{\#_{\text{ATLAS}}} = \frac{\sigma_{\text{MPD}} \times \mathcal{L} \times \text{eff.}}{\#_{\text{ATLAS}}} \propto \left(\frac{\Lambda_{\text{ATLAS}}}{\Lambda_{\text{MPD}}} \right)^8 \quad (2.10)$$

where Λ_{MPD} is given by the input parameters $\Lambda_{\text{MPD}} = \frac{m_{Z'}}{(g_{At}g_{AX})^{1/4}}$ and Λ_{ATLAS} is the effective scale Λ_* in Eq. (2.7) for the mono-jet DM search.

Eq. (2.10) can be expressed as following:

$$\Lambda_{\text{ATLAS}} = \Lambda_{\text{MPD}} \times \left(\frac{\#_{\text{MPD}}}{\#_{\text{ATLAS}}} \right)^{1/8} \quad (2.11)$$

and we extract the limits on Λ with respect to different DM masses in Figure 2.1

For the $t\bar{t}$ +MET search [34] at the 13 TeV LHC collider with luminosity $\mathcal{L} = 2.2 \text{ fb}^{-1}$, there are two event selection categories depending on the number of leptons in the final state. Since the top quark mainly decays to bW and W can either decay to di-jets or one

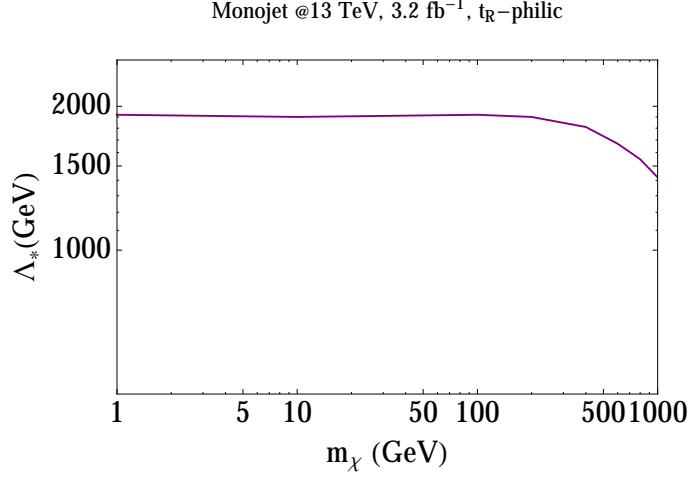


FIGURE 2.1: EFT scale Λ_* lower limit respect to DM mass 1 GeV to 1TeV from ATLAS mono-jet search. We use Eq. (2.11) to interpret Λ_* in Eq. (2.7) from MPD simulation results.

lepton and one neutrino: *semi-leptonic* final state which has exactly one lepton and *fully hadronic* final state which has no leptons shown in Figure 2.2:

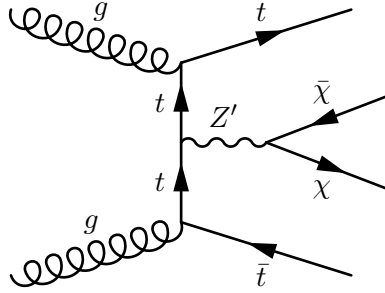


FIGURE 2.2: DM production with top quark pair via gluon t-channel at LHC which leads to EFT after integrating out Z' .

The semi-leptonic selection rules are:

- $\text{MET} > 160 \text{ GeV}$
- Jet $p_t > 30 \text{ GeV}$, 3 or more jets of which at least *one* b-tagged jet
- $|\eta| < 4$ and $\Delta\phi(\vec{p}_T^{\text{miss}}, \text{jet}_i) > 1.2$ up to the two leading jets
- Exactly *one* lepton which has $p_t > 30 \text{ GeV}$ and $|\eta| < 2.1$
- The transverse mass $m_T = \sqrt{2p_t^l E_T^{\text{miss}} (1 - \cos\Delta\phi(\vec{p}_T^{\text{miss}}, \text{lepton}))} > 160 \text{ GeV}$
- No muons with $p_t > 10 \text{ GeV}$ or electrons with $p_t > 20 \text{ GeV}$

- $M_{T2}^W > 200 \text{ GeV}$

where the M_{T2}^W [77] variable is defined as the minimal mass for the mother particle which is compatible enough for all the transverse momenta and production W boson in top quark pair system. The M_{T2}^W contains a kinematic end-point which can help us to address the ambiguity of MET arising from neutrinos or DM.

While the fully hadronic selection rules are:

- $\text{MET} > 200 \text{ GeV}$
- Jet $p_t > 30 \text{ GeV}$, at least 4 jets of which at least *two* b-tagged jet
- $|\eta| < 4$ and $\Delta\phi(\vec{p}_T^{\text{miss}}, \text{jet}_i) > 1$ up to the six leading jets
- Leptons with looser criteria which has $p_t > 10 \text{ GeV}$ and $|\eta| < 2.1$

The lower limit on Λ arises from the maximum number of event yields allowed by null searches with respect to different DM masses from (95% CL) given in Figure 2.3.

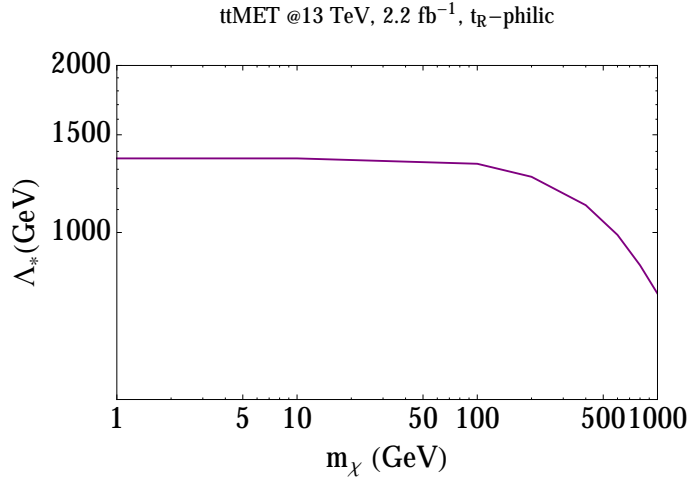


FIGURE 2.3: EFT scale Λ_* lower limit respect to DM mass 1 GeV to 1TeV from CMS $\bar{t}t$ +MET search. We use Eq. (2.11) to interpret Λ_* in Eq. (2.7) from MPD simulation results.

To summarize, we use the null result of the DM search at LHC to set up the lower limit bounds of EFT scale Λ from two different searching channels mono-jet and $\bar{t}t$ +MET. The mono-jet search has about a 20% stronger bound than $\bar{t}t$ +MET for the same DM mass and both bounds are $\Lambda_* \sim \mathcal{O}(1.5 \text{ TeV})$.

2.2.2 Simplified Models Approach

We further study the light Z' mass ($m_{Z'} < 1$ TeV) parameter space by considering the simplified model of Eq. (2.2). In addition to the above discussed collider limits, the unitarity of self-scattering amplitude of top-quark or DM provides another bound [20]:

$$m_{Z'} \gtrsim \left(\frac{g_f}{1}\right) \left(\frac{m_f}{1 \text{ GeV}}\right) \text{ GeV}, \quad (2.12)$$

where m_f, g_f are top-quark, DM or further exotics [78] mass and coupling. Moreover, the decay width of the Z' needs to be considered in the simplified model scenario. Here we use MadGraph to generate the decay width with the narrow width approximation so that the Z' is produced on-shell within certain kinetic regions. The production cross section for either mono-jet or a top pair with DM is determined by $(m_{Z'}, m_\chi, g_\chi, g_t)$. Here we fix the couplings of Z' to investigate the allowed parameter space of $(m_{Z'}, m_\chi)$ with $\mathcal{O}(1)$ couplings. Following the same process for the effective operator approach, we simulate the events with MadGraph 5, Pythia 6 and Delphes 3.

First, we consider the case in which Z' couples to DM axially and right-handed top solely:

$$\begin{aligned} \mathcal{L} &= \bar{t}(g_{tR}(\underbrace{\gamma^\mu + \gamma^\mu \gamma^5}_{\ll})t)Z'_\mu + g_{\chi A}\bar{\chi}\gamma^\mu\gamma^5\chi Z'_\mu \\ &\equiv g_t\bar{t}\gamma^\mu\gamma^5tZ'_\mu + g_\chi\bar{\chi}\gamma^\mu\gamma^5\chi Z'_\mu \end{aligned} \quad (2.13)$$

and we fix the couplings to make $g_t = g_\chi = 1$ such that the collider bounds are highly constraining, but the couplings remain in the acceptable perturbative region. Note that the vector contribution is negligible compared to the axial-vector contribution.

We show the constraints from the mono-jet and $t\bar{t}$ +MET searches in Figure 2.4 and Figure 2.5. These figures show the unitarity bounds and the LHC limits on the mono-jet and a top pair with DM production cross section based on the number of events from [33] and [34] respectively. The gray shaded area indicates the unitarity bound and this overlaps with the collider limits. Then in Figure 2.6 and Figure 2.7 we take $g_t = g_\chi = 0.5$ to show how the parameter space changes.

The parameter space allowed regions from mono-jet or $t\bar{t}$ +MET are both larger than the Z' universal coupling simplified models [79] with $g_t = 0.25$ and $g_\chi = 1$. This indicates that the LHC search limits have severe constraints on universal simplified models compared

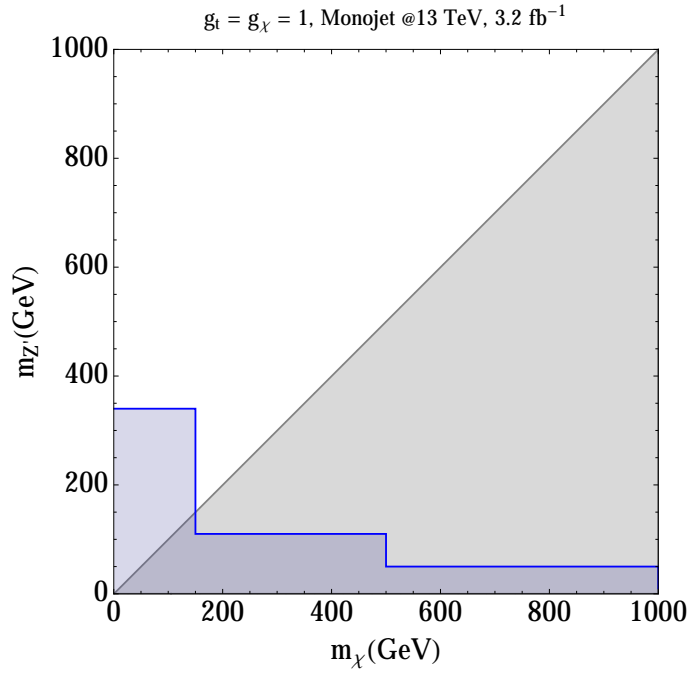


FIGURE 2.4: LHC mono-jet bounds $m_{Z'}$ and m_χ with $g_t = g_\chi = 1$. The *Gray* area is excluded by the unitary constraints $m_{Z'} \gtrsim g_\chi m_\chi$ and $m_{Z'} \gtrsim g_t m_t$ since $g_t = g_\chi = 1$ the boundary of the grey area is simply $m_{Z'} = \text{Max}(m_\chi, m_t)$. The *Blue* region presents the excluded parameter space form the null result of mono-jet search at LHC at 13 TeV.

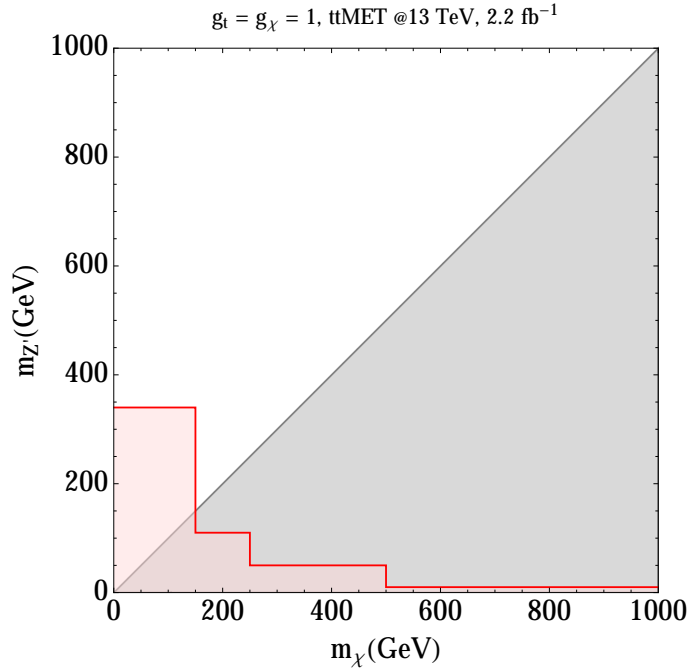


FIGURE 2.5: LHC $\bar{t}t$ +MET bounds $m_{Z'}$ and m_χ with $g_t = g_\chi = 1$. The *Gray* area is excluded by the unitary constraints $m_{Z'} \gtrsim g_\chi m_\chi$ and $m_{Z'} \gtrsim g_t m_t$ since $g_t = g_\chi = 1$ the boundary of the grey area is simply $m_{Z'} = \text{Max}(m_\chi, m_t)$. The *Red* region presents the excluded parameter space form the null result of $\bar{t}t$ +MET search at LHC at 13 TeV.

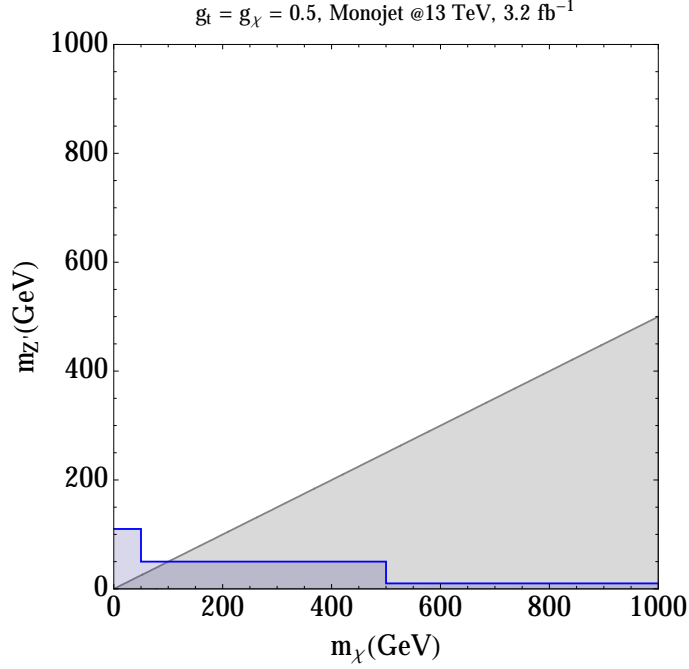


FIGURE 2.6: LHC mono-jet bounds $m_{Z'}$ and m_χ with $g_t = g_\chi = 0.5$. The *Gray* area is excluded by the unitary constraints $m_{Z'} \gtrsim g_\chi m_\chi$ and $m_{Z'} \gtrsim g_t m_t$ since now $g_t = g_\chi = 0.5$ the boundary of the grey area is simply $m_{Z'} = \frac{1}{2} \times \text{Max}(m_\chi, m_t)$. The *Blue* region presents the excluded parameter space form the null result of mono-jet search at LHC at 13 TeV.

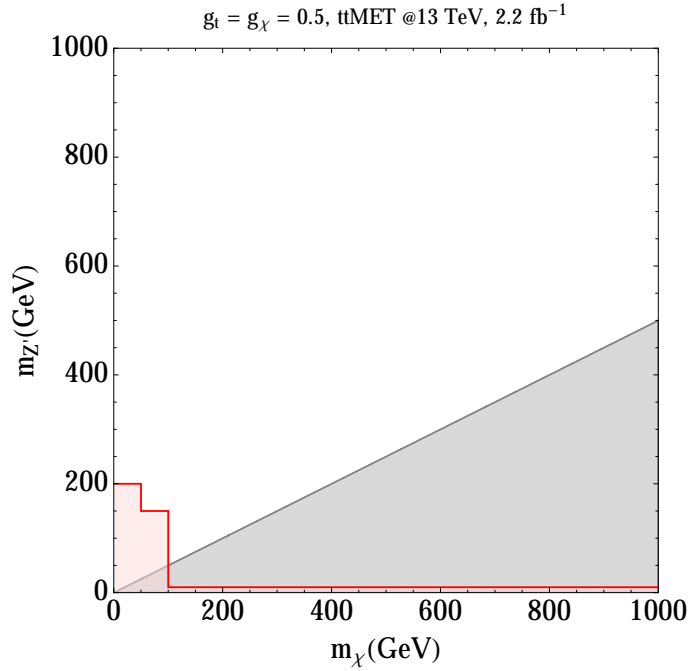


FIGURE 2.7: LHC $t\bar{t}$ +MET bounds $m_{Z'}$ and m_χ with $g_t = g_\chi = 0.5$. The *Gray* area is excluded by the unitary constraints $m_{Z'} \gtrsim g_\chi m_\chi$ and $m_{Z'} \gtrsim g_t m_t$ since now $g_t = g_\chi = 0.5$ the boundary of the grey area is simply $m_{Z'} = \frac{1}{2} \times \text{Max}(m_\chi, m_t)$. The *Red* region presents the excluded parameter space form the null result of $t\bar{t}$ +MET search at LHC at 13 TeV.

to the top-philic simplified model presented here. Moreover, both mono-jet and $t\bar{t}$ +MET constraints become smaller when couplings g_t and g_χ are made smaller, and the excluded area quickly reduces to the unitary bounds, which is also weaker for reduced couplings.

To summarize the DM collider search based on mono-jet and $t\bar{t}$ +MET of top-philic Z' models here are present for both EFT and simplified models. We find the lower limits for the EFT cut-off scale is $\Lambda \sim \mathcal{O}(1.5\text{TeV})$ and these are relatively weaker collider limits compared to unitary bounds which are stringent for simplified top-philic model when $g_t = g_\chi \lesssim \mathcal{O}(1)$. These collider limits will be weaker or even negligible for $g_t = g_\chi \ll \mathcal{O}(1)$. This will be relevant when we discuss the DM relic density in the following [Section 2.3](#) since the dominate annihilation channels, $\chi\bar{\chi} \rightarrow t\bar{t}$ and $\chi\bar{\chi} \rightarrow Z'Z'$, require relatively small couplings in order to reproduce the DM relic density $\Omega_\chi h^2 \approx 0.12$. [[35](#), [80](#)]

2.3 Relic Density and In-direct Detection

If the DM relic density is set by its annihilation cross section, as in the traditional WIMP picture, then the requirement that the scenario reproduces the observed value fixes the annihilation cross section for a given mass.² Following the previous discussion on the parameter spaces $(m_{Z'}, m_\chi, g_\chi, g_t)$. DM annihilation channels naturally can be categorized into two cases:

- For $m_\chi > m_{Z'}$, then $\chi\bar{\chi} \rightarrow Z'Z'$ via t/u-channel shown in [Figure 2.8](#)

$$\langle\sigma v\rangle(\chi\bar{\chi} \rightarrow Z'Z') \approx \frac{g_\chi^4}{16\pi m_\chi^2 (1 - \frac{m_{Z'}^2}{2m_\chi^2})^2} (1 - \frac{m_{Z'}^2}{m_\chi^2})^{3/2} \quad (2.14)$$

- $m_\chi < m_{Z'}$, the annihilation of DM is controlled by the decay branching ratios of Z' which depends on $m_{Z'}$. This behavior can be classified into three subgroups:

1. $m_{Z'} > 2m_t$, $\chi\bar{\chi} \rightarrow Z' \rightarrow t\bar{t}$ shown in [Figure 2.9](#)

$$\langle\sigma v\rangle(\chi\bar{\chi} \rightarrow t\bar{t}) \approx \frac{3g_t^2 g_\chi^2 m_t^2}{8\pi m_{Z'}^4} \sqrt{1 - \frac{m_t^2}{m_\chi^2}} \quad (2.15)$$

²We focus on the minimal freeze-out scenario, however that if the DM relic density is set due to annihilation to other hidden sectors states, or is diluted due to subsequent entropy generation, then the constraints derived below will be different. [[81](#), [82](#)]

2. $(m_Z + m_h)/2 < m_{Z'} < 2m_t$, $\bar{\chi}\chi \rightarrow Z' \rightarrow tWb$ though one off-shell top and $\bar{\chi}\chi \rightarrow Z' \rightarrow Zh$ via top-loop shown in Figure 2.10(a) and 2.10(b) and we use the form factors from [54].
3. $m_{Z'} < (m_Z + m_h)/2$, $\bar{\chi}\chi \rightarrow Z' \rightarrow \bar{b}b$ via top-W-loop shown in Figure 2.11

$$\langle\sigma v\rangle(\chi\bar{\chi} \rightarrow \bar{b}b) \approx \frac{3g_{b,\text{eff}}^2 g_\chi^2 m_b^2}{8\pi m_{Z'}^4} \sqrt{1 - \frac{m_b^2}{m_\chi^2}} \quad (2.16)$$

where $g_{b,\text{eff}} \approx g_t \times 7.5 \times 10^{-3}$ [56] and the final state bottom quarks are *left-handed*. However, the last two are suppressed by the either three-body phase space or loop effects.

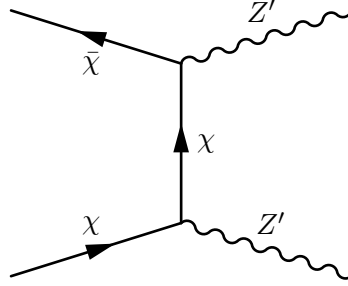


FIGURE 2.8: $\bar{\chi}\chi \rightarrow Z'Z'$ via t/u-channel when $m_\chi > m_{Z'}$.

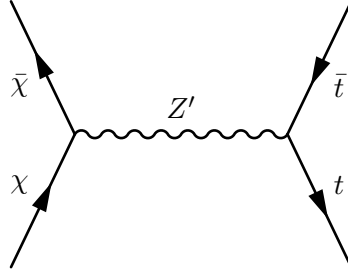


FIGURE 2.9: $\bar{\chi}\chi \rightarrow Z' \rightarrow \bar{t}t$ via Z' when $m_{Z'} > 2m_t$.

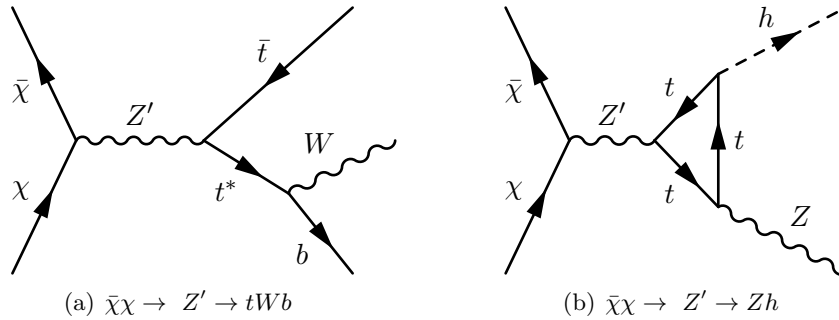
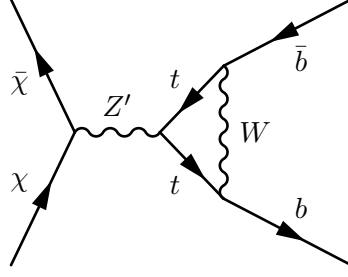


FIGURE 2.10: $\bar{\chi}\chi \rightarrow Z' \rightarrow tWb$ though one off-shell top and $\bar{\chi}\chi \rightarrow Z' \rightarrow Zh$ via top-loop when $(m_Z + m_h)/2 < m_{Z'} < 2m_t$.

FIGURE 2.11: $\bar{\chi}\chi \rightarrow Z' \rightarrow \bar{b}b$ via top-loop when $m_{Z'} < (m_Z + m_h)/2$.

All of the above annihilation channels contribute to the total annihilation cross section $\langle\sigma_{ann}v\rangle$. The thermal relic density of DM can be calculated via the Boltzmann equation of DM number density. From which one can derive the following form of the thermal freeze-out abundance assuming s-wave annihilation:

$$\Omega_\chi h^2 \simeq \frac{1.07 \times 10^9}{GeV} \frac{x_f}{M_{Pl} \times \sqrt{g_*} \times \langle\sigma_{ann}v\rangle} \simeq 0.12 \quad (2.17)$$

where g_* is the degree of freedom at the freeze-out temperature T_f and $x_f = \frac{m_\chi}{T_f} \approx 20$ for $m_\chi \approx 100$ GeV and $\mathcal{O}(0.1)$ couplings.

For fixed couplings $g_\chi = g_t$, we present the coupling required to make the relic density $\Omega_\chi h^2 \approx 0.12$ in the parameter space of m_χ and $m_{Z'}$ and only logarithm sensitive to changes in g_i and m_χ in Figure 2.12

The plot shows contours with values of g_χ which reproduces $\Omega_\chi h^2 \approx 0.12$. This can be understood in three parts:

- $\mathcal{O}(0.1)$ couplings region refers to when $t\bar{t}$ and $Z'Z'$ annihilation are accessible and dominate the most of bottom-right region in Figure 2.12.
- When Zh channel is open but $Z'Z'$ is closed, the coupling is about $\mathcal{O}(1)$ and appears in the upper-right and bottom-left region in Figure 2.12.
- Finally, when $b\bar{b}$ channel becomes the only annihilation channel leads larger couplings $\mathcal{O}(10)$ or even larger than 4π . (the gray shaded region in Figure 2.12.)

So far, we have discussed the requirements that the DM relic abundance is produced due to DM freeze-out via the top-philic portal. DM annihilation today may occur in the high DM density region in our universe and produce the fluxes of cosmic rays of

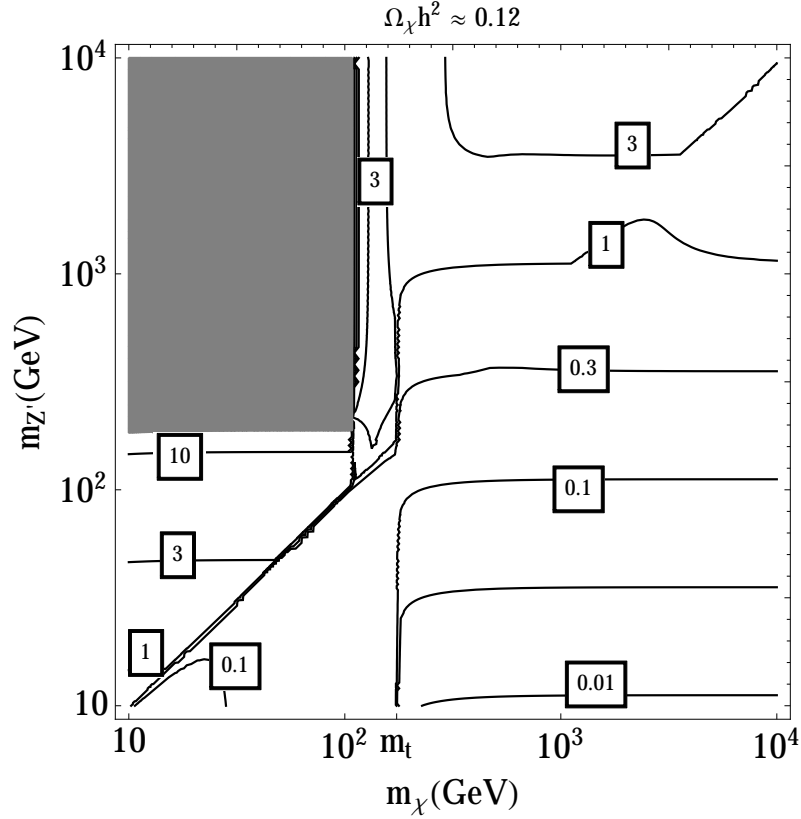


FIGURE 2.12: The contours show the value of $g_t = g_{\chi}$ to make $\Omega_{\chi} h^2 \approx 0.12$ and the framed-boxes show values of $g_t = g_{\chi}$. The right-bottom part of the plot indicates the relic abundance is dominated by $t\bar{t}$ and $Z'Z'$ channel whereas $g_t = g_{\chi} \ll \mathcal{O}(1)$ and the right-top part is for Zh channel with $g_t = g_{\chi} \approx \mathcal{O}(1)$. On the left side of the plot are $b\bar{b}$ annihilation channel with $g_t = g_{\chi} \gg \mathcal{O}(1)$. Note that we do not include the mass resonance region of $m_{Z'} = 2m_{\chi}$ in our parameter space. The GRAY region indicates regions of parameter space where the coupling is non-perturbative $g_t = g_{\chi} \gtrsim \mathcal{O}(10)$.

the SM particles dependent on the primary annihilation channels. Here the majority of DM annihilate to $t\bar{t}$ directly or through cascade decays of Z' and the secondary or final state cosmic rays can be light the SM charged particles [83, 84], photons[85], neutrinos, protons, antiprotons [84] and recently considered Inverse Compton gamma rays [86–88]. We consider the most recent DM indirect detection search of energetic gamma rays results from Fermi Large Area Telescope (Fermi-LAT) [29], which present null results of 6 years gamma ray observation data from the dwarf spheroidal satellite galaxies (dSphs) of the Milky Way.

However, the lack of a significant detection signal can provide a constraint on the DM self-annihilation cross section $\langle\sigma v\rangle$. Fermi-LAT presents the upper limits on the $b\bar{b}$ annihilation cross section from the combined analysis of 15 dSphs. However, the limit is only strong for $m_{\chi} < 100$ GeV where the major annihilation channel is a Z' pair final state which can

further cascade decay to $b\bar{b}b\bar{b}$ [89, 90]. Indirect detection will not meaningfully constrain the parameter space in Figure 2.12 by the current Fermi-LAT limits.

2.4 Direct Detection

If DM interacts with the SM particles, this can lead to recoil of atomic nuclei in the direct detection experiments that produce detectable signals [26–28]. However, the null DM direct detection experimental results gives us constraints on the parameter space. The DM scattering with nucleons in the top-philic model of 2.2 is loop-induced by the $Z - Z'$ kinetic mixing ϵ via top-loop shown in Figure 2.13(a) and after integrating out Z' and tops in Figure 2.13(b) for the non-relativistic limit. The kinetic mixing coefficient ϵ can be further related to UV physics as follows [54, 56]:

$$\epsilon = \frac{1}{4\pi^2} [g_\chi g_t^{Z'} g_t^Z \log(\frac{m_{Z'}^2}{m_t^2})] \sim \mathcal{O}(10^{-4}) \times [g_\chi g_t^{Z'} \log(\frac{m_{Z'}}{m_t})] \quad (2.18)$$

which leads to the effective operator:

$$\mathcal{L}_{eff} = \frac{\epsilon g_\chi g_t \bar{\chi} \gamma^\mu \gamma^5 \chi \bar{q} \gamma^\mu \gamma^5 q}{m_{Z'}^2}, \quad q = u, d, s \quad (2.19)$$

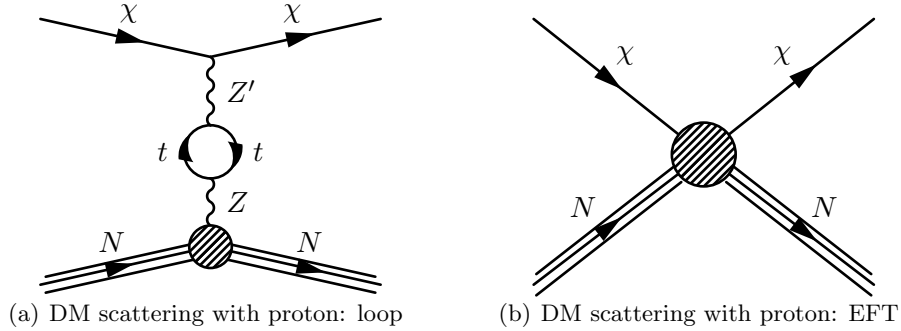


FIGURE 2.13: The direct detection scattering of DM with proton and neutron in the nucleons of targets in the detectors. (a): the kinetic mixing of $Z' - Z$ through a top-loop (b): DM scattering process is EFT at the detector energy scale.

However, the loop-induced effective operator described neglects complete gauge coupling running which runs through two EFTs, one is the low energy scale (below EW) EFT and another one is loop-induced $Z' - Z$ mixing effective operator scale. Since DM-nuclear scattering needs an understanding of nuclear matrix element, this requires matching of the two energy scales. In other words, RG flow of the gauge coupling g_t must run from the high

energy scale $\mathcal{O}(m_{Z'})$ down to the detector nuclear recoil energy scale ($\mu_N \sim \text{GeV}$) [41, 42]. Here we apply the package *RunDM* [42] to evolve RG running effect and calculate the non-relativistic (NR) DM-nucleon matrix element *NR Ops* [91] which uses the current LUX and future LZ projected limits [26, 27, 92].

RunDM uses Lagrangian:

$$\mathcal{L}_{\chi N}^{\mu N} = -\frac{1}{m_{Z'}^2} g_\chi \bar{\chi} \gamma_\mu \gamma^5 \chi \underbrace{(\mathcal{G}_v^N \bar{N} \gamma^\mu N + \mathcal{G}_a^N \bar{N} \gamma^\mu \gamma^5 N)}_{\text{RunDM}} \quad (2.20)$$

where N is for nucleons including protons (p) and neutrons (n) and the couplings \mathcal{G}^N here are the sum of quarks couplings within the nucleon:

$$\begin{aligned} \mathcal{G}_v^p &= 2\mathcal{G}_v^u + \mathcal{G}_v^d \\ \mathcal{G}_v^n &= \mathcal{G}_v^u + 2\mathcal{G}_v^d \\ \mathcal{G}_a^N &= \sum_{q=u,d,s} \mathcal{G}_a^q \Delta_q^N \end{aligned} \quad (2.21)$$

the axial vector charges Δ_q^N are the light quark contribution to the spin of the nucleon N . The details of running \mathcal{G} calculations are in [42] and here we highlight the couplings relevant for our model:

$$\begin{aligned} \mathcal{G}_v^u &\simeq \frac{g_t \alpha_t}{2\pi} (3 - 8s_{\theta_w}^2) \log\left(\frac{m_{Z'}}{m_Z}\right) \\ \mathcal{G}_v^d &\simeq -\frac{g_t \alpha_t}{2\pi} (3 - 4s_{\theta_w}^2) \log\left(\frac{m_{Z'}}{m_Z}\right) \\ \mathcal{G}_a^u &\simeq -\mathcal{G}_a^d \simeq -\mathcal{G}_a^s \simeq -\frac{3g_t \alpha_t}{2\pi} (3 - 4s_{\theta_w}^2) \log\left(\frac{m_{Z'}}{m_Z}\right) \end{aligned} \quad (2.22)$$

DM-nucleon matrix elements are expressed in the above effective operator in terms of NR operators and coefficients of NR effective theory:

$$\begin{aligned} \mathcal{M}_{\chi N} &\equiv \langle \chi N | \mathcal{L}_{\chi N}^{\mu N} | \chi N \rangle \\ &= \frac{1}{m_{Z'}^2} \langle g_\chi \mathcal{G}_v^N \bar{\chi} \gamma^\mu \gamma^5 \chi N \gamma^\mu N + g_\chi \mathcal{G}_a^N \bar{\chi} \gamma^\mu \gamma^5 \chi N \gamma^\mu \gamma^5 N \rangle \\ &\simeq \sum_i c_{\chi,i}^N \mathcal{O}_i^{NR} \\ &= \frac{8g_\chi m_\chi^2}{m_{Z'}^2} \{ \mathcal{G}_v^N [M_N(\vec{s}_\chi \cdot \vec{v}^\perp) + \vec{s}_\chi \cdot (\vec{s}_N \times \vec{q}_R)] - 2\mathcal{G}_a^N M_N(\vec{s}_\chi \cdot \vec{s}_N) \} \end{aligned} \quad (2.23)$$

where \vec{v} is DM-nucleon relative velocity, \vec{s}_χ and \vec{s}_N are DM spin and nucleon spin respectively, \vec{q}_R is the nuclear recoil momentum, M_N is the nucleon mass and the transverse velocity is $\vec{v}^\perp \equiv \vec{v} + \frac{\vec{q}_R}{\mu_{\chi N}}$ with the reduce mass of DM-nucleon system $\mu_{\chi N} = \frac{m_\chi M_N}{m_\chi + M_N}$. After integrating the differential DM-nuclei cross section over the nuclear recoil energy with correct nuclear response function [41], we have the spin-dependence cross section(SD) and the vector coupling \mathcal{G}_v contribution is suppressed by the DM velocity ($\sim 10^{-3}c$) and recoil momentum:

$$\sigma_{SD}^{\chi N} = \frac{3\mu_{\chi N}}{\pi} \frac{(g_\chi \mathcal{G}_a^N)^2}{m_{Z'}^4} \quad (2.24)$$

We take Eq. (2.24) and scan over the couplings and masses of Z' and DM to obtain the limits in Figure 2.12 using RunDM and NROps for the current LUX SD limit [26] and the LZ-projected limit [26] in Figure 2.14

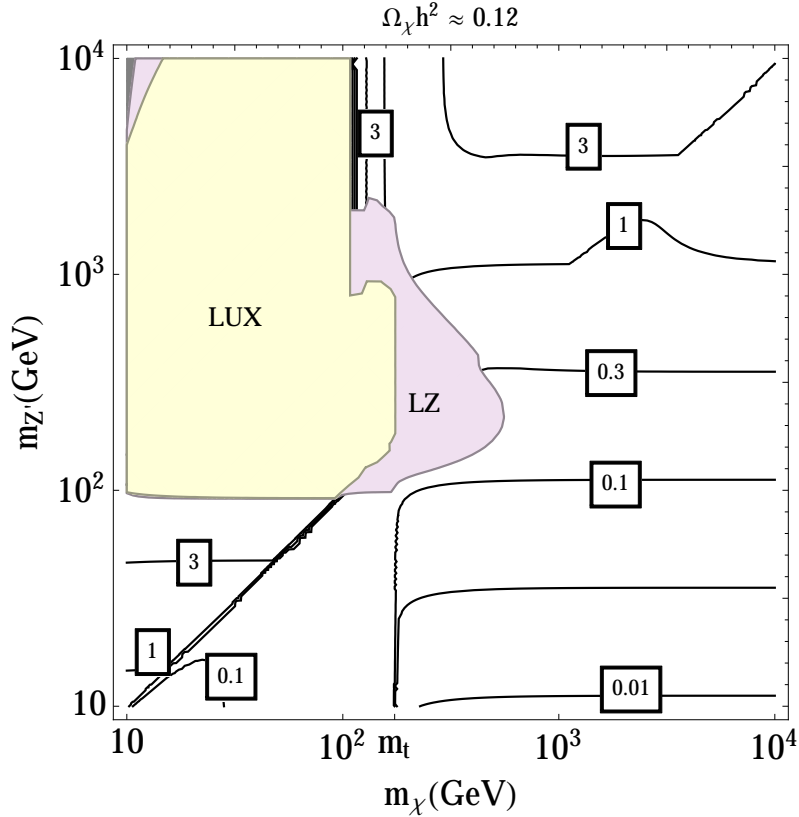


FIGURE 2.14: The RED REGION shows the LZ projected limit on SD direct detection and the YALLOW REGION is the current LUX SD limit. The box framed numbers are the couplings $g_\chi = g_t$ of relic density $\Omega_\chi h^2 \approx 0.12$ before running down the nuclear EFT. The excluded parameters mainly happen in the larger coupling region when DM annihilation channel is dominated by $b\bar{b}$.

The summary of the top-philic vector portal model taking into account the collider study, relic density, in-direct and direct detection is shown in Figure 2.14, observe the allow

parameter space.

2.5 Mono-jet v.s. Mono-photon in t_R -philic Z' Models

In this section, we develop a phenomenological method of addressing the top-philic coupling Z' ambiguity raised from Eq. (2.2). In other words, we consider what kind of collider signals can indicate that Z' only couples to t_R (and not Q_L) as required in a top-philic scenario.

DM signals can also appear as the missing transverse energy with a high energetic photon [93] at the LHC and the signal is relatively weaker than mono-jet searches, however, the ratio of mono-photon and mono-jet events can distinguish the flavors of loop fermions. Specifically, we investigate when the ratio of production cross section of mono-jet to mono-photon with DM can be inferred by the ratio of $\gamma^\mu\gamma^5$ to γ^μ couplings as shown in Figure 2.15. The γ^μ coupling part of Z' contributes the box-diagrams solely whereas $\gamma^\mu\gamma^5$ coupling contributions are mainly from the triangular diagram. From now on, we will refer \square as the box loop diagram and \triangle as the triangular loop diagram. Below describes the analytical relation of cross section between $\gamma^\mu\gamma^5$ and γ^μ and mono-jet and mono-photon as well:

$$\frac{\sigma_{t_R}^{j,\gamma^\mu\gamma^5}}{\sigma_{t_R}^{j,\gamma^\mu}} \equiv F_{t_R}^j(p_t) = \frac{\sigma_{t_R}^{j\triangle}}{\sigma_{t_R}^{j\square}} \quad (2.25)$$

$$\frac{\sigma_{t_R}^j}{\sigma_{t_R}^\gamma} \equiv F_{t_R}^\gamma(p_t) = \frac{\sigma_{t_R}^{j\triangle} + \sigma_{t_R}^{j\square}}{\sigma_{t_R}^{\gamma\square}} \quad (2.26)$$

where the jet/photon transverse momentum (p_t) kinetics factor $F_{j/\gamma}(p_t)$ is the consequence of different channels.

2.5.1 Mono- j /Mono- γ Complementarity

On the other hand, the mono-photon only has the box diagram. Here we neglect the photon propagator contribution in the mono-photon channel (from the quark-quark initial state). The mono-jet and mono-photon cross section ratio are presented in Eq. (2.26).

Here we simulate mono-jet signals with MadGraph 5 and present the cross section with respect to different transverse momentum of the jet in Figure 2.16 LEFT by setting $g_t =$

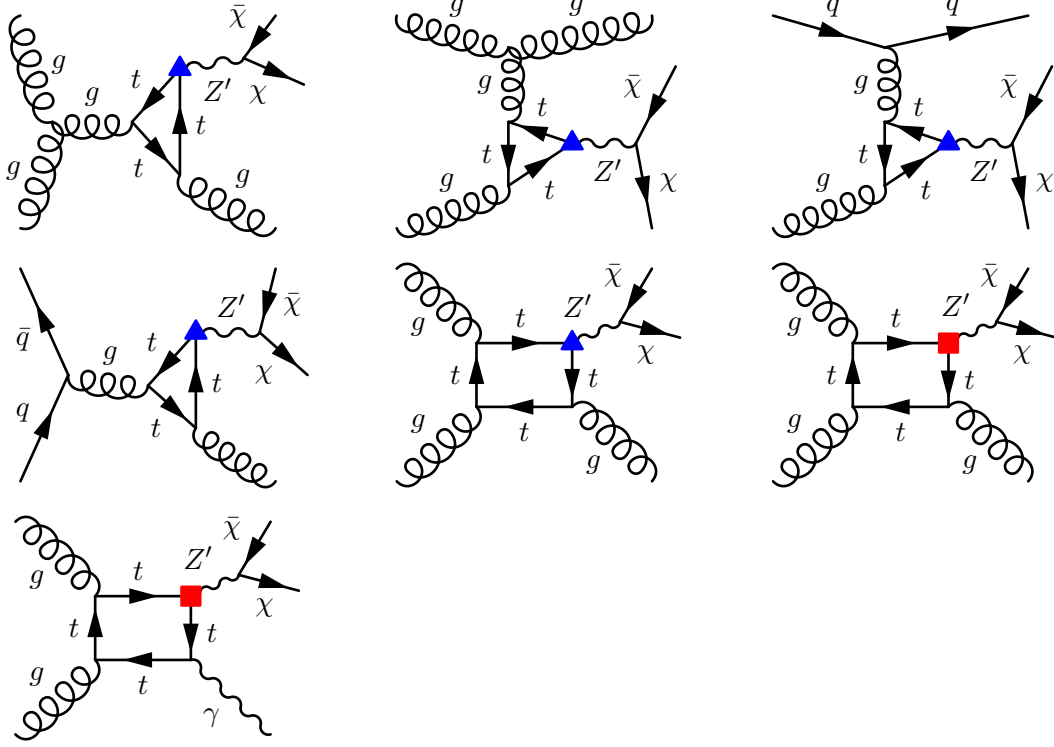


FIGURE 2.15: The diagrams relevant to mono-jet and mono-photon due to Z' coupled to t_R only. The RED BOX vertex is the γ^μ coupling of Z' and the BLUE TRIANGULAR vertex is the $\gamma^\mu \gamma^5$ vector coupling of Z' .

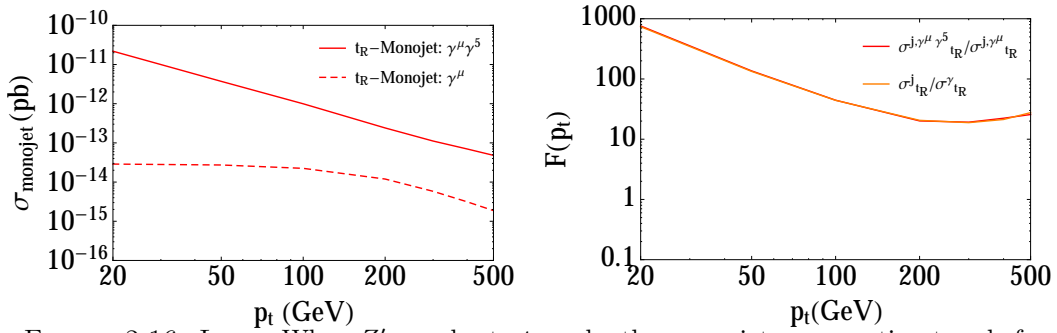


FIGURE 2.16: LEFT: When Z' couples to t_R only, the mono-jet cross section trends for the γ^μ and $\gamma^\mu \gamma^5$ couplings with respect to the transverse momentum of the jet. RIGHT: The ratio of the cross-section for the mono-jet vs mono-photon and $\gamma^\mu \gamma^5$ vs γ^μ is inferred by the kinetic factor $F(p_t)$. Here $m_{Z'} = 20 \text{ TeV}$, $g_{Vt} = g_{At} = g_{V\chi} = 0.1$ and the kinetic factor $F(p_t)$ is derived by $\frac{\sigma_{\text{mono-jet}}}{\sigma_{\text{mono-photon}}} \times \frac{\alpha_{EM}}{\alpha_S}$ for the mono-jet vs mono-photon line and $\frac{\sigma_{\text{axial}}}{\sigma_{\text{vector}}}$ for $\gamma^\mu \gamma^5$ vs γ^μ line. Here we only consider light DM ($m_\chi = 1 \text{ GeV}$) and Z' only axially couples to DM.

$g_\chi = 0.1$, $m_{Z'} = 20$ TeV and $m_\chi = 1$ GeV. Within the chosen parameters, the cross section is determined by the loop structure and p_t of the jet or photon. As a result, the mono-jet channel receives a contribution from the $\gamma^\mu \gamma^5$ coupling because the jet from the triangular loop is the initial state radiation (ISR) jet and the jet from the γ^μ coupling is box loop induced. The mono-photon is solely box-loop induced. Thus Eq. (2.26) becomes:

$$\frac{\sigma_{t_R}^j}{\sigma_{t_R}^\gamma} = \frac{\sigma_{t_R}^{j\Delta} + \sigma_{t_R}^{j\Box}}{\sigma_{t_R}^{\gamma\Box}} \simeq \frac{\sigma_{t_R}^{j\Delta}}{\sigma_{t_R}^{\gamma\Box}} = \frac{\alpha_s}{\alpha_{em}} \times F_{t_R}^j(p_t) \quad (2.27)$$

where $\frac{\alpha_s}{\alpha_{em}} \times F_{t_R}^j(p_t) = F_{t_R}^\gamma(p_t)$. This implies the ratio of mono-jet to mono-photon is proportional to ratio of the axial vector ($\gamma^\mu \gamma^5$) to vector (γ^μ) contributions, as shown in Figure 2.16 RIGHT .

2.5.2 The Inverse Problem

Since both *left-handed* t_L and *right-handed* t_R have $\gamma^\mu \gamma^5$ and $\gamma^\mu \gamma^5$ couplings but up to a sign flip for $\gamma^\mu \gamma^5$ coupling, this leads to a sign degeneracy on the cross sections discussed above. However, if Z' only couples to the third generation SU(2) doublet Q_L , then the quark neutral current part in Eq. (2.2) is:

$$\mathcal{L} \equiv \bar{Q}_L (g_{QL} (\gamma^\mu - \gamma^\mu \gamma^5)) Q_L Z'_\mu \quad (2.28)$$

$$= \bar{t}_L (g_{QL} (\gamma^\mu - \gamma^\mu \gamma^5)) t_L Z'_\mu + \bar{b}_L (g_{QL} (\gamma^\mu - \gamma^\mu \gamma^5)) b_L Z'_\mu \quad (2.29)$$

and this gives us the additional tree level diagrams from bottom quark PDF at LHC in Figure 2.17.

Consequently the ambiguity can be broken due to both the tree level contributions and the triangular loop from the $\gamma^\mu \gamma^5$ coupling which is comparable to the tree level contributions. Thus Eq. (2.25), Eq. (2.26) and Eq. (2.27) are changed to be:

$$\frac{\sigma_{Q_L}^{j, \gamma^\mu \gamma^5}}{\sigma_{Q_L}^{j, \gamma^\mu}} \equiv F_{Q_L}^j(p_t) = \frac{\sigma_{tree}^{j, \gamma^\mu \gamma^5} + \sigma_{Q_L}^{j\Delta}}{\sigma_{tree}^{j, \gamma^\mu} + \sigma_{Q_L}^{j\Box}} \simeq \frac{\sigma_{tree}^{j, \gamma^\mu \gamma^5} + \sigma_{Q_L}^{j\Delta}}{\sigma_{tree}^{j, \gamma^\mu}} \sim 1 + \frac{\sigma_{Q_L}^{j\Delta}}{\sigma_{tree}^{j, \gamma^\mu}} \quad (2.30)$$

$$\frac{\sigma_{Q_L}^j}{\sigma_{Q_L}^\gamma} \equiv F_{Q_L}^\gamma(p_t) = \frac{\sigma_{tree}^j + \sigma_{Q_L}^{j\Delta} + \sigma_{Q_L}^{j\Box}}{\sigma_{tree}^\gamma + \sigma_{Q_L}^{\gamma\Box}} \simeq \frac{\sigma_{tree}^j + \sigma_{Q_L}^{j\Delta}}{\sigma_{tree}^\gamma} \sim \frac{\alpha_s}{\alpha_{em}} (1 + \frac{\sigma_{Q_L}^{j\Delta}}{\sigma_{tree}^j}) \quad (2.31)$$

and the simulations are shown in Figure 2.19. The rapidity and $F(p_t)$ of mono-jet for t_R only and Q_L only are shown in 2.20.

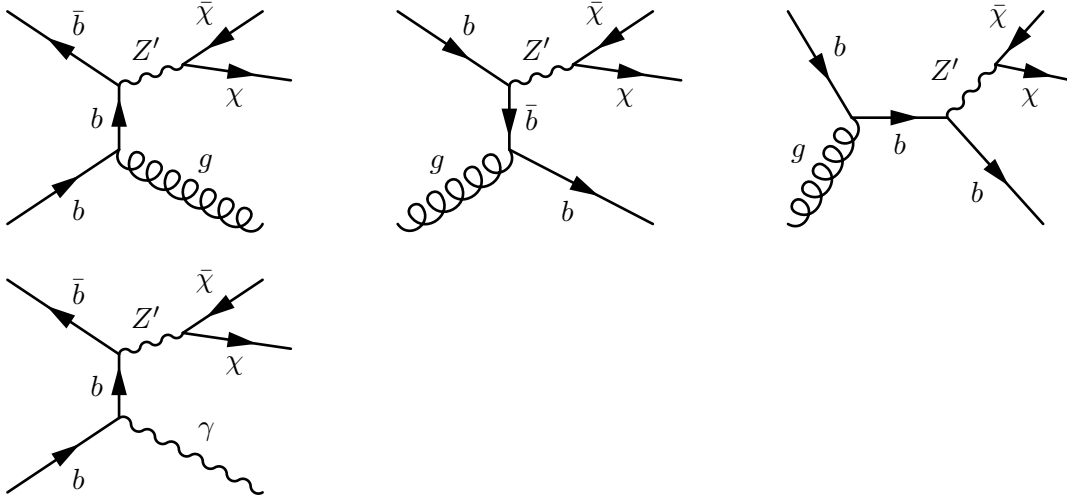


FIGURE 2.17: The additional tree diagrams relevant to mono-jets and mono-photons due to Z' coupled to Q_L only while the loop diagrams are the same as those for t_R only.

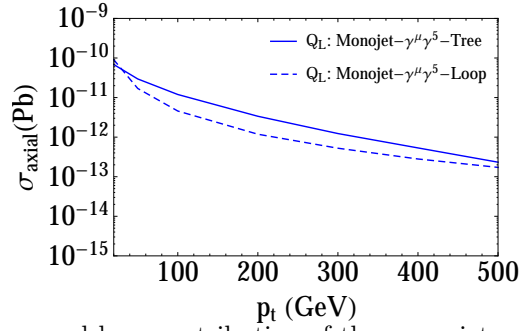


FIGURE 2.18: The tree and loop contribution of the mono-jet cross section in terms of p_t for the axial vector coupling in Q_L -philic scenario. $m_{Z'} = 20$ TeV, $g_{Q_L} = g_\chi = 0.1$ and $m_\chi = 1$ GeV

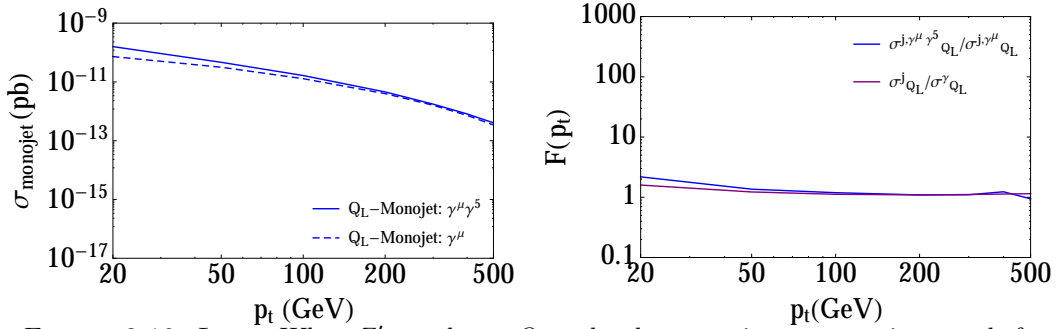


FIGURE 2.19: LEFT: When Z' couples to Q_L only, the mono-jet cross section trends for the γ^μ and $\gamma^\mu \gamma^5$ couplings with respect to the transverse momentum of the jet. RIGHT: The ratio of the cross-section for the mono-jet vs mono-photon and $\gamma^\mu \gamma^5$ vs γ^μ is inferred by the kinetic factor $F(p_t)$. Here $m_{Z'} = 20$ TeV, $g_{Q_L} = g_\chi = 0.1$ and the kinetic factor $F(p_t)$ is derived by $\frac{\sigma_{mono-jet}}{\sigma_{mono-photon}} \times \frac{\sigma_{tree}^\gamma}{\sigma_{tree}^\gamma}$ for the mono-jet vs mono-photon line and $\frac{\sigma_{axial}}{\sigma_{vector}}$ for $\gamma^\mu \gamma^5$ vs γ^μ line. $m_{Z'} = 20$ TeV, $g_{Q_L} = g_\chi = 0.1$ and $m_\chi = 1$ GeV

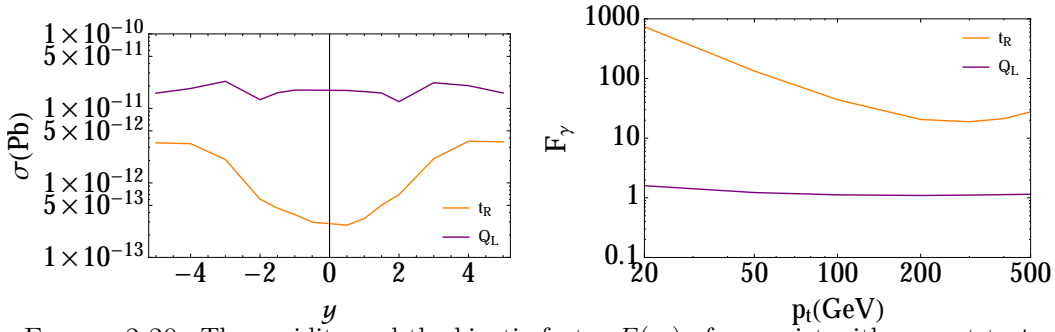


FIGURE 2.20: The rapidity and the kinetic factor $F(p_t)$ of mono-jet with respect to t_R only and Q_L only.

The kinetic factors of Q_L -philic have different behaviors in the case of top-philic. Moreover, the loop contribution is comparable to the tree-level contribution in Q_L -philic model whereas there is only loop diagrams in top-philic model. Here all the productions are generated without applying the LHC selection rules.

In order to distinguish the difference arisen from the chirality, for example, $F_\gamma(t_R) = \sigma_j/\sigma_\gamma|_{t_R} \approx 100$ at 50 GeV p_t cut and $F_\gamma(Q_L) \approx 1$

$$\frac{F_\gamma(t_R)}{F_\gamma(Q_L)} \approx 100 \quad (2.32)$$

$$\rightarrow \frac{\sigma_j/\sigma_\gamma|_{t_R}}{\sigma_j/\sigma_\gamma|_{Q_L}} \approx 100 \quad (2.33)$$

$$\rightarrow \sigma_j/\sigma_\gamma|_{t_R} \approx 100 \text{ and } \sigma_j/\sigma_\gamma|_{Q_L} \approx 1 \quad (2.34)$$

Therefore, Q_L -philic model is valid only if the ratio for the signals of mono-jet and mono-photon are $\mathcal{O}(1)$ otherwise the signals might be from the top-philic model for the given luminosity and selection rules.

2.6 UV Complete Theory and Mass Gereneration

So far we have discussed top-philic simplified model in Eq. (2.2) without considering the UV completeness. However, the sensitivity of UV theory will affect some of the above discussion. For example, the loop induced operators $\mathcal{O}_{Z'bb}$ and $\mathcal{O}_{Z'ZH}$ should be considered for the behavior of UV complete theory. Here we extend Eq. (2.2) and discuss the mass generation of the SM top quark and DM.

2.6.1 Top Mass Generation and Mixing

There are several scenarios to generate the mass term of top-philic model, for example, we can introduce a $U(1)'$ charged private Higgs H_t for the top specially [94], however, which leads $m_Z \sim \sqrt{v_{SM}^2 + \langle H_t \rangle^2} \sim 91 \text{ GeV}$, but for $m_{Z'} \sim \langle H_t \rangle$, the mass Z' becomes EW scale from the Z boson mass constraint.

Here we discuss a EFT theory and a UV complete model which is outlined in [53] related to the top partner in little Higgs model [95, 96]. We will not discuss the quadratically divergent cancellation with little Higgs model.

2.6.1.1 EFT

A Froggatt-Nielsen [97] effective operator by integrating out heavy chiral top partners as follows:

$$\mathcal{L}_{FN} = \frac{y_t}{\Lambda_1} S_1 H^\dagger \bar{Q}_L t_R \rightarrow \frac{y_t}{\Lambda_1} \langle S_1 \rangle \langle H \rangle \bar{t}_L t_R \equiv m_t \bar{t}_L t_R \quad (2.35)$$

where the SM singlet scalar S_1 carrying $U(1)'$ charge to make Eq. (2.35) gauge invariant. Specifically, we will discuss the UV completion model [53] in the next subsection. Note that this spectrum is anomaly free and more details will be discussed in *Chapter 3* and *4*.

The mass term for the physical top can be generated via a dimension five operator of Eq. (2.35) after integrating out the heavy eigenstate T , as illustrated in Figure 2.21. In the decoupling limit $m_t \simeq y_t \langle H \rangle / \sqrt{2} \approx 172 \text{ GeV}$ and $m_T \simeq \langle S_1 \rangle$.

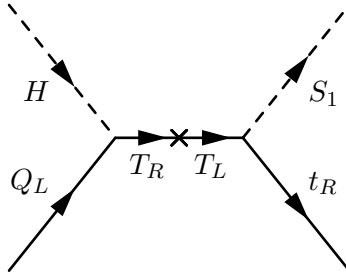


FIGURE 2.21: The dimension-5 effective operator $\frac{1}{\Lambda_1} S_1 H^\dagger \bar{Q}_L t_R$ raises by integrating out heavy fermion T_L and T_R .

2.6.1.2 UV Complete Model

Here the UV complete model is outlined in [53]. In this model, the SM top is neutral under $U(1)'$ and the top partners $\tilde{T}_{L,R}$ are $U(1)'$ charged vectorially therefore it is anomaly free. The extra scalar \tilde{S}_1 is needed to make the new yukawa terms gauge invariant:

Field	$SU(3)$	$SU(2)$	$U(1)_Y$	$U(1)'$
\tilde{Q}_L	3	2	1/3	0
\tilde{t}_R	3	1	4/3	0
H	1	2	2	0
\tilde{T}_L	3	1	4/3	1
\tilde{T}_R	3	1	4/3	1
S_1	1	1	0	1

TABLE 2.2: The gauge charges assignments of UV complete top-philic model.

The $\tilde{t} - \tilde{T}$ mass mixing behavior:

$$\mathcal{L}_{mass} \equiv y_t H^\dagger \tilde{Q}_L \tilde{t}_R + \tilde{m}_T \tilde{T}_L \tilde{T}_R + y_T \tilde{S}_1 \tilde{T}_L \tilde{t}_R \quad (2.36)$$

$$\rightarrow \tilde{m}_t \tilde{t}_L \tilde{t}_R + \tilde{m}_T \tilde{T}_L \tilde{T}_R + x \tilde{T}_L \tilde{t}_R \quad (2.37)$$

where $x \equiv y_T \langle S_1 \rangle$. The mass matrix becomes

$$\mathcal{M}_{\tilde{t}, \tilde{T}} \equiv \begin{pmatrix} \tilde{t}_{R,L} & \tilde{T}_{R,L} \end{pmatrix} \begin{pmatrix} \tilde{m}_t & x \\ 0 & \tilde{m}_T \end{pmatrix} \begin{pmatrix} \tilde{t}_{R,L} \\ \tilde{T}_{R,L} \end{pmatrix} \quad (2.38)$$

and we rotate $\mathcal{M}_{\tilde{t}, \tilde{T}}$ with an unitary operator \mathcal{U} to be $\mathcal{M}_{t, T}$

$$\mathcal{M}_{t, T} \equiv \begin{pmatrix} t_{R,L} & T_{R,L} \end{pmatrix} \begin{pmatrix} m_t & 0 \\ 0 & m_T \end{pmatrix} \begin{pmatrix} t_{R,L} \\ T_{R,L} \end{pmatrix} \quad (2.39)$$

and \mathcal{U} is defined

$$\begin{pmatrix} t_{R,L} \\ T_{R,L} \end{pmatrix} \equiv \mathcal{U} \begin{pmatrix} \tilde{t}_{R,L} \\ \tilde{T}_{R,L} \end{pmatrix} = \begin{pmatrix} \cos \theta_{R,L} & -\sin \theta_{R,L} \\ \sin \theta_{R,L} & \cos \theta_{R,L} \end{pmatrix} \begin{pmatrix} \tilde{t}_{R,L} \\ \tilde{T}_{R,L} \end{pmatrix} \quad (2.40)$$

The eigenvalues of Eq. (2.39) are

$$m_t = \sqrt{(\tilde{m}_t^2 + \tilde{m}_T^2 + x^2 - \Delta)/2} \quad (2.41)$$

$$m_T = \sqrt{(\tilde{m}_t^2 + \tilde{m}_T^2 + x^2 + \Delta)/2} \quad (2.42)$$

and the mass splitting parameter Δ

$$\Delta \equiv \sqrt{(\tilde{m}_t^2 + \tilde{m}_T^2 + x^2)^2 - 4(\tilde{m}_t \tilde{m}_T)^2}. \quad (2.43)$$

The rotation angles in Eq.(2.40) are

$$\tan \theta_L = \frac{\tilde{m}_t^2 - \tilde{m}_T^2 + x^2 + \Delta}{2x\tilde{m}_T} \quad (2.44)$$

$$\tan \theta_R = \frac{\tilde{m}_t^2 + \tilde{m}_T^2 - x^2 + \Delta}{2x\tilde{m}_t} \quad (2.45)$$

The mixing angles are infinitesimal $\sin \theta_{R, L} \ll 1$ in the limit of $\tilde{m}_t = m_t \approx 172\text{GeV}$ and the heavier eigenstate of Eq. (2.39) has the mass scale as $\langle S_1 \rangle$.

Now the interactions among $t - T$ becomes

$$\begin{aligned} \mathcal{L} = & i \bar{t} \not{D}_t t + i \bar{T} \not{D}_T T + \frac{g}{\sqrt{2}} (s_L \bar{T} - c_L \bar{t}) \gamma^\mu W_\mu P_L b + h.c \\ & + \bar{T} \gamma^\mu Z'_\mu g_{Z'} (c_L s_L P_L + c_R s_R P_R) t + h.c \\ & + c_L s_L [g_{\tilde{t}_R}^Z - g_{\tilde{t}_L}^Z] \bar{T} \gamma^\mu Z_\mu P_L t + h.c \\ & + y_t c_L c_R H \bar{t} t + y_t s_L s_R H \bar{T} T - y_t H \bar{t} (s_R c_L P_R + s_L c_R P_L) T + h.c \\ & - \lambda_1 s_L c_R S_1 \bar{t} t + \lambda_1 c_L s_R S_1 \bar{T} T + \lambda_1 S_1 \bar{t} (s_L s_R P_R - c_L c_R P_L) T + h.c \end{aligned} \quad (2.46)$$

where $c_{L, R}$ and $s_{L, R}$ are short hand for $\cos \theta_{L, R}$ and $\sin \theta_{L, R}$ respectively and the covariant derivatives are

$$D_{t\mu} = \partial_\mu - i \left[(g_{\tilde{t}_R}^Z s_L^2 + g_{\tilde{t}_L}^Z c_L^2) P_L + g_{\tilde{t}_R}^Z P_R \right] Z_\mu - i g_{Z'} (s_R^2 P_R + s_L^2 P_L) Z'_\mu - i g_{\tilde{t}_R} A_\mu \quad (2.47)$$

and

$$D_{T\mu} = \partial_\mu - i \left[(g_{\tilde{t}_R}^Z c_L^2 + g_{\tilde{t}_L}^Z s_L^2) P_L + g_{\tilde{t}_R}^Z P_R \right] Z_\mu - i g_{Z'} (c_R^2 P_R + c_L^2 P_L) Z'_\mu - i g_{\tilde{t}_R} A_\mu \quad (2.48)$$

where $g = e/\sin\theta_w$, $g_{\tilde{t}_R} = 2e/3$, and $g_{\tilde{t}_{R/L}}^Z = e\cos\theta_w^{-1}\sin\theta_w^{-1}(T_3 - (2e/3)\sin^2\theta_w)$ are the regular the SM couplings.

2.6.2 Electroweak Precision and LHC Constraints on Top Quark Partner Fermion

As shown in Eq. (2.47), there are additional BSM mixing terms of Z-T-t and W-T-b interaction terms, therefore, EW interactions might be modified by those non-zero interactions. We discuss the limit of the mixing effect $s_{L,R}$ in Eq. (2.40) and the mass of the partner of top, i.e. m_T by considering the EW oblique Peskin-Takeuchi parameters S, T, U [18]. It was shown and performed that ΔS and ΔU are very small in [54, 98, 99] when $m_T > m_t > m_Z$ in which case:

$$\begin{aligned}\Delta T &= T_{SM}[-(1 + C_L^2) + rs_L^2 + 2c_L^2 \frac{r}{r-1} \log(r)] \\ \Delta S &= -\frac{N_C}{18\pi} s_L^2 \{ \log(r) + c_L^2 [\frac{5(r^2+1) - 22r}{(r-1)^2} + \frac{3(r+1)(r^2-4r+1)}{(1-3)^2} \log(r)] \} \simeq 0 \\ \Delta U &= \Delta S + \frac{N_C}{9\pi} s_L^2 \log(r) \simeq 0\end{aligned}\tag{2.49}$$

and $r \equiv \frac{m_T^2}{m_t^2}$, $N_C = 3$ and $T_{SM} = \frac{N_C}{16\pi} \frac{1}{\sin\theta_w} \frac{m_t}{m_W^2} \simeq 1.19$. We present the current SU(2) singlet vector-like top quark partner mass lower limit 890 GeV from ATLAS search of vector-like top partner in $Zt + X$ channel [100] with the $\Delta T \lesssim 0.14(0.10)$ at 95 (68) % CLs limit in Figure (2.22) which indicates $m_T \lesssim 3$ TeV when $s_L \approx 0.1$ and $s_L \lesssim 0.15$ for $m_T \gtrsim 890$ TeV.

The loop function modification including $H \rightarrow gg$ and $H \rightarrow \gamma\gamma$ for both top and top partner for Higgs measurements are relatively small since the Higgs-top coupling in Eq. (2.47) is still the SM-like when top partner mass is decouple $m_T \gg m_t$ and also due to the $s_{L,R}$ suppression.

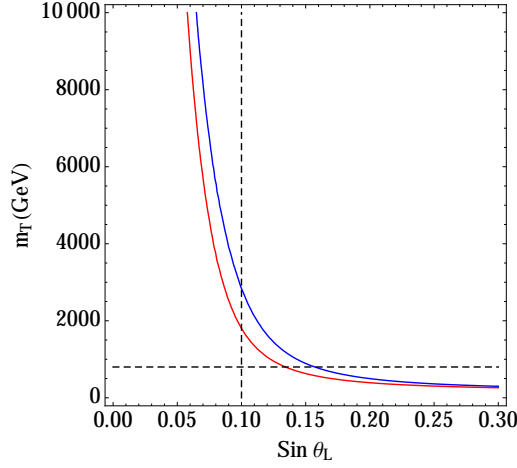


FIGURE 2.22: The BLUE and RED lines are the 95(68)% CLs limits on ΔT and the DASHED line is the current lower mass limit for m_T from $T \rightarrow Z + t$ searching channel of vector-like top partner fermion at ATLAS.

2.6.3 Kinetic and Mass Mixing of Z - Z'

The kinetic mixing and mass mixing effect between Z and Z' has been discussed in *Chapter 1* and here we focus the constraints of EWPT from the loop-induced mixing:

$$\begin{aligned} \mathcal{L}_{mixing} = & -\frac{1}{4}\hat{B}^{\mu\nu}\hat{B}_{\mu\nu} - \frac{1}{4}\hat{Z}'^{\mu\nu}\hat{Z}'_{\mu\nu} + \frac{1}{2}m_Z^2\hat{Z}^\mu\hat{Z}_\mu + \frac{1}{2}m_{Z'}^2\hat{Z}'^\mu\hat{Z}'_\mu \\ & - \frac{1}{2}\sin\epsilon\hat{B}^{\mu\nu}\hat{Z}'_{\mu\nu} + \delta m^2\hat{Z}^\mu\hat{Z}'_\mu \end{aligned} \quad (2.50)$$

where the hatted field contents are the canonical gauge interaction fields with mixing effect and the mass mixing term here is top-loop induced [56]

$$\epsilon \approx \frac{2}{3} \frac{N_c g_t g}{(4\pi)^2} \log \frac{\Lambda^2}{m_t^2} \quad (2.51)$$

$$\delta m^2 \approx \frac{1}{2} m_t^2 \frac{N_c g_t g'}{(4\pi)^2} \log \frac{\Lambda^2}{m_t^2} \quad (2.52)$$

We estimate the mixing parameter by considering $\Lambda \approx 1$ TeV when $m_{Z'} \lesssim 1$ TeV and $\Lambda \approx m_{Z'}$ when $m_{Z'} \gtrsim 1$ TeV. The resulting the SM neutral current after applying rotation matrices can be expressed with EWPT parameters in mass eigenstate basis:

$$\mathcal{L}_{Zff} = -\frac{e}{2s_W c_W} \left(1 + \frac{\alpha T}{2}\right) Z_\mu \bar{f} \gamma^\mu \left(\left(T_3^f - 2Q^f \left(s_W^2 + \frac{\alpha S - 4c_W^2 s_W^2 \alpha T}{4(c_W^2 - s_W^2)} \right) \right) - T_3^f \gamma^5 \right) f \quad (2.53)$$

where the Z is the SM neutral boson and c_W , s_W are cosine and sine function of θ_W .

$$S = \frac{4}{\alpha} c_W^2 s_W \xi (\epsilon - s_W \xi) \quad (2.54)$$

$$T = \frac{\xi^2}{\alpha} \left(\frac{m_{Z'}^2}{m_Z^2} - 2 \right) + 2s_W \xi \epsilon \quad (2.55)$$

with

$$t_{2\xi} = \frac{-2c_\epsilon(\delta m^2 + m_Z^2 s_W s_\epsilon)}{m_{Z'}^2 - m_Z^2 c_\epsilon^2 + m_Z^2 s_W^2 s_\epsilon^2 + 2\delta m^2 s_W s_\epsilon}. \quad (2.56)$$

We plot the S and T parameters with respect to $m_{Z'}$ region in our relic density parameter and set up the upper limit of g_t in Figure 2.23³

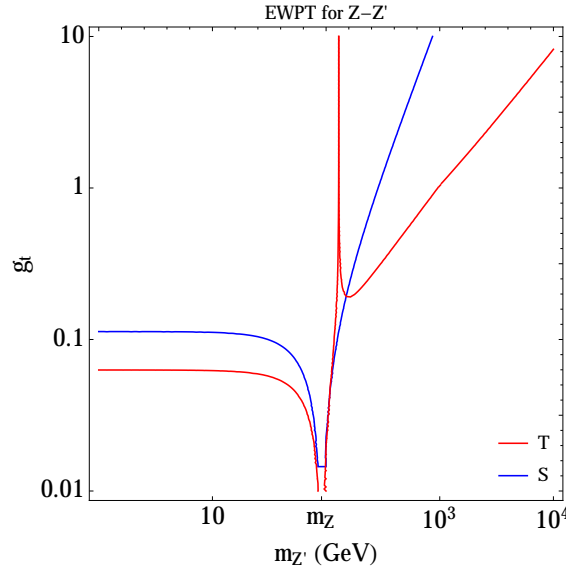


FIGURE 2.23: The BLUE and RED contours are 90 % CLs limits on g_t for EWPT S and T parameters for $m_{Z'}$ from 1 GeV to 1 TeV. As we can see, T has stronger bound than S . When $m_{Z'} < \mathcal{O}(10^2)$ GeV, $g_t \lesssim \mathcal{O}(0.1)$ and $g_t \sim \mathcal{O}(1)$ when $m_{Z'} > \mathcal{O}(10^2)$ GeV.

Finally, we observe that the parameter space including all theory and experiment constraints in Figure 2.24 has the following excluded regions:

1. When $m_\chi > m_t$, the excluded area is when $m_{Z'} \sim \mathcal{O}(m_Z)$.
2. When $m_\chi < m_t$, all $m_{Z'}$ region is excluded by direct detection and EWPT expect.

³There is a marginal improvement by considering the di-lepton resonance limits. [56, 101, 102]

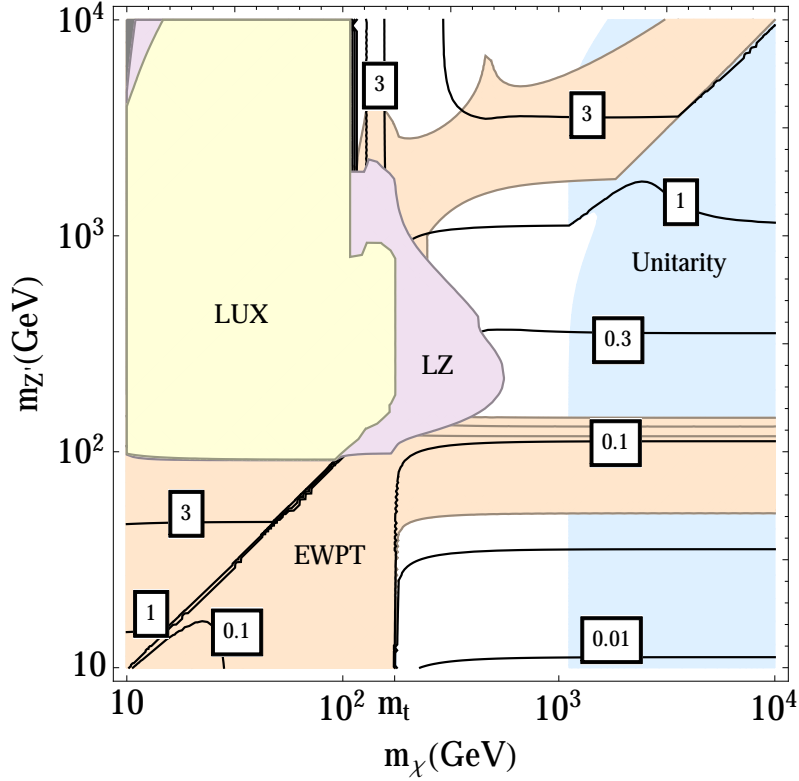


FIGURE 2.24: The contours show the value of $g_t = g_\chi$ to make $\Omega_\chi h^2 \approx 0.12$ and the framed-boxes show values of $g_t = g_\chi$. The GRAY region is when couplings reach non-perturbative coupling region. The YELLOW and RED regions are the current LUX and projected LZ direct detection limits respectively. The ORANGE REGION is the EWPT limit from T parameter of Z - Z' mixing. The BLUE REGION indicates the unitarity constraint $m_{Z'} \gtrsim g_f m_f$ where f is either top or DM.

2.6.4 Majorana Dark Matter and Scalar Portal Model

So far, our DM candidate is $U(1)'$ charged Dirac fermion and we mainly focus on *axial vector* coupling to Z' which indeed can be extended to Majorana fermionic DM since Majorana only has axial vector coupling to Z' due to its charge conjugation feature. We will specify a simplified top-philic Majorana DM model.

In the previous discussions, we are using the pair of Dirac fields χ_L and χ_R to describe our DM field. Economically, we can use only one χ_L and its own charge conjugate to describe the Majorana DM. We assume an $U(1)'$ charged Weyl spinor χ_L and its charged conjugate $\epsilon\chi_L^* \equiv \chi_R'$ where ϵ is the Levi-Civita matrix (or simply $i\tau_2$). Then the four-component fermion χ is composed from χ_L and χ_R'

$$\chi \equiv \chi_L + \chi_R' = \begin{pmatrix} \chi_L \\ \chi_R' \end{pmatrix} = \chi_L + \epsilon\chi_L^* = \begin{pmatrix} \chi_L \\ \epsilon\chi_L^* \end{pmatrix} \quad (2.57)$$

which is a Majorana fermion

$$\chi^c \equiv \mathcal{C}\bar{\chi}^T = \mathcal{C} \begin{pmatrix} -\epsilon\chi_L \\ \chi_L^* \end{pmatrix} = \begin{pmatrix} \epsilon & 0 \\ 0 & \epsilon \end{pmatrix} \begin{pmatrix} -\epsilon\chi_L \\ \chi_L^* \end{pmatrix} = \begin{pmatrix} \chi_L \\ \epsilon\chi_L^* \end{pmatrix} = \chi \quad (2.58)$$

And its mass comes from the Yukawa term with a charged scalar S :

$$\mathcal{L}_{mass} = \lambda_{DM} S \chi_L^T \epsilon \chi_L + \text{h.c.} = \lambda_{DM} S \bar{\chi}'_R \chi_L + \text{h.c.} = \lambda_{DM} S \bar{\chi} \chi \quad (2.59)$$

where S carries $U(1)'$ charge to keep the mass term $U(1)'$ gauge invariant and the non-zero $\langle S \rangle$ gives mass to the Majorana χ mass and breaks $U'(1)$ symmetry spontaneously. We construct a Majorana DM χ which only has axial vector coupling to Z' . Now, Eq. (2.5) becomes

$$\mathcal{L} = \bar{t}(g_{tR}(\gamma^\mu + \gamma^\mu \gamma^5))tZ'_\mu + \frac{1}{2}\bar{\chi}(g_{\chi A}\gamma^\mu \gamma^5)\chi Z'_\mu + S\bar{\chi}\chi \quad (2.60)$$

which is a simplified top-philic Majorana DM model. Note that there is a factor of 1/2 difference in Z' axial vector interaction term compared to Eq. (2.5) due to Majorana condition $\chi^c = \chi$ which makes our previous results effected by this symmetric factor.

Since Majorana DM has scalar S interaction term in Eq. (2.60), this leads to a *Scalar and Vector Potral* Majorana DM simplified model [37, 103–105]. Meanwhile, with some specific $U(1)'$ charges assignment, there is a possible di-jet or di-photon scalar resonance search at LHC [106] when the mass term of exotics top partner in Eq. (2.36) becomes $m_T \bar{\tilde{T}}_L \tilde{T}_R = \lambda_T \langle S \rangle \bar{\tilde{T}}_L \tilde{T}_R$, i.e. the top partner gets mass from breaking $U(1)'$ as well. That means two searches of new physics can be linked by this scalar S illustrated in Figure 2.25(a) and 2.25(b).

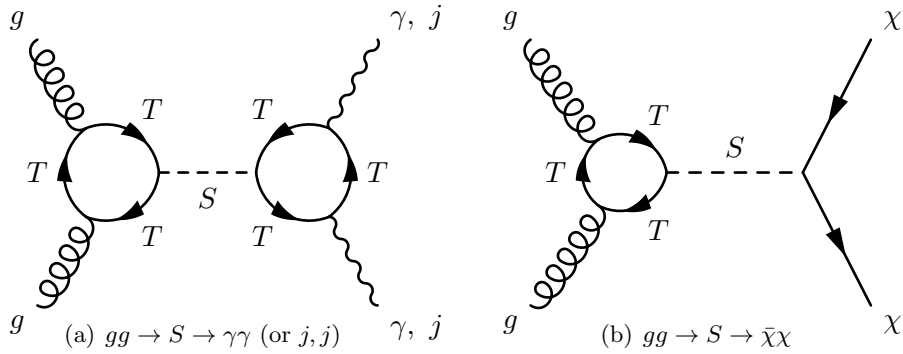


FIGURE 2.25: The di-photon or di-jet resonance of scalar S which is also the mediator of DM.

We can apply the mono-jet and $t\bar{t} + MET$ collider searches for the scalar mediator. However, this scalar portal DM model is beyond the scope of this work and we will not have further discussion.

2.7 Future Outlook and Discussion

In this work, we study top-philic vector portal DM models in a comprehensive manner. When the new gauge boson Z' only couples to right-handed quarks, the axial vector coupling contribution dominates the mono-jet search at the LHC. This leads to a non-suppress spin-dependent scattering cross section in DM direct detection experiments in the case that DM is axially coupled to Z' as well. We find the current LHC collider limits from both mono-jet and $t\bar{t} + MET$ are relatively weak for top-philic vector portal models. For the direct detection experiment and DM relic density studies, we study the details of the scattering cross section between the DM and the SM contents. We use the current LUX and future projected LZ limits to constrain the parameter space in which DM relic abundance $\Omega_{DM}h^2 \approx 0.12$ via DM freeze-out annihilation mechanism.

When gamma rays comes from DM annihilation in the galaxy which provides the indirect detection search of DM and the photon flux for specific spectra are linked with DM annihilation to a pair of top quarks. Since the $t\bar{t}$ annihilation channel mainly dominates in our DM relic abundance parameter space and the current Fermi-LAT limits has no impact on our parameter space in the case the correct DM relic density arises from freeze-out mechanism.

We present a new phenomenological method to break down the ambiguity caused by the chirality of top quark by introducing two kinetic factors:

- The first one is defined as the ratio of axial vector and vector cross sections of mono-jet for purely right-handed top-philic Z' .
- The second one is defined as the ratio of mono-jet and mono-photon to distinguish the difference between the right-handed top-philic and the third generation specific models.

In addition to the top-philic simplified model, we discuss a minimal UV complete model and the EWPT limits on the associated exotics. The EWPT for Z - Z' mixing sets up another sharp bound on our existing parameter space.

Chapter 3

ANOMALY CANCELLATION WITH AXIAL VECTOR Z'

3.1 Introduction

Couplings between chiral fermions f_L , f_R and a vector boson Z' associated to a $U(1)$ gauge symmetry are of the form

$$\bar{f} \not{D} f = \bar{f} \gamma_\mu \left(\partial^\mu - ig(q_{f_L} + q_{f_R}) \frac{1}{2} Z'^\mu - ig(q_{f_L} - q_{f_R}) \frac{\gamma_5}{2} Z'^\mu \right) f . \quad (3.1)$$

For the special case in which $q_{f_L} = -q_{f_R}$ the gauge boson is a pure axial vector. Many phenomenological studies contemplate a new axial vector which couples to Standard Model (SM) fermions. In particular, they are common in various scenarios for providing a portal between dark matter (DM) and SM states, e.g. [20, 69, 107, 108], partially because if either the DM or SM fermions couple only axially to the vector mediator, the direct detection cross section is either spin-dependent or suppressed by factors of the DM velocity or momentum exchange.

Charging the SM fermions under a new $U(1)'$, in the absence of additional chiral fermions, generically leads to the $U(1)'$ being anomalous. However, many studies neglect to specify the field content which would lead to an anomaly free theory [20, 66, 69, 108–110]. Notably, any anomalous set of fermions can be embedded into a larger set which is anomaly free and whose members carry only rational charges [23, 111]. Still, the associated extra

states are typically charged under the SM gauge group.¹ As we will argue, these new states can not be arbitrarily separated from the mass scale of the axial vector. Thus it is important to consider the UV theory since such states are in principle observable at collider experiments. While there are many occurrences of complete anomaly free models of Z' with general couplings in the literature [8], there is a lack of examples for pure axial vectors.² Thus it is of interest to find anomaly free spectra for different scenarios in which the SM fermions interact with a new axial vector.

We also note that new abelian gauge bosons are motivated from a GUT perspective, as large gauge groups naturally break to the Standard Model group supplemented with abelian factors. The breaking pattern may include $U(1)'$ factors and anomaly cancellation can be inherited from the matter content under the larger gauge group, as in the case of the **27** of E_6 under its axial subgroup $U(1)_\psi$ [8]. However, finding GUT completions for specific charge assignments can be challenging, and thus here we examine systematic ‘bottom-up’ methods of anomaly cancellation without references to GUTs. Moreover, the GUT structure adds extra states not involved in anomaly cancellation and, to avoid proton decay, the $U(1)'$ scale is restricted to be near the GUT scale. Without requiring gauge coupling unification, by contrast, there is greater freedom in cancelling anomalies with new chiral exotics.

This chapter and next chapter are structured as follows: In 3.2 we discuss the requirements for anomaly cancellation when the gauge structure of the SM is supplemented with a new $U(1)'$ factor, focusing on the case in which the $U(1)'$ gauge boson has only axial vector couplings to the SM fermions (and DM). In 3.3 we explore systematic methods for generating anomaly free models by adding new chiral fermions to the spectrum. Subsequently, we use these techniques to identify a number of anomaly free spectra for axial vector models of interest. For completeness we give some anomaly free models for the case of a pure vector Z' in 3.4. We also show alternative sets of anomaly free sets of fermions with axial vector Z' in 3.5 and we give an explicit example of the algebraic constructions of anomaly free spectra in 3.6.

¹ Cancellation mechanisms beyond new field content are available in extra dimensional gauge theories, most prominently the Green-Schwarz mechanism [112] and anomaly inflow [113]. For reviews see e.g. [114, 115]. Here we restrict our discussion to anomaly cancellation through new chiral fermions.

² Note that examples of axial vector models with anomaly cancelling exotics are presented in [107]; model ‘Axial-A’ is anomaly free, ‘Axial-B’ is anomalous, and ‘Axial-Leptophobic’ is anomaly free if one adds exotics ψ_R^l and ψ_L^e with $U(1)'$ charge zero.

In the next chapter 4.1 considers the model building requirements for giving mass to the SM and exotic fermions. In section 4.2 we ask at what scale the effective low energy description breaks down due to a loss of renormalisability, necessitating the introduction of new fermions, as well as the perturbativity bound on the $U(1)'$ coupling induced by the fermions. As one of the main motivations for these models is to use the axial vector as a portal to connect SM fermions and DM, section 4.3 considers the requirements for obtaining the observed DM relic density due to freeze-out via the axial vector, and the corresponding constraints from direct and indirect detection experiments and LHC searches. Section 4.4 presents some concluding remarks.

3.2 Gauge Anomalies and Axial Vectors

Noether's theorem implies that any gauge symmetries are conserved if and only if when their associated currents are conserved $\partial_\mu j^\mu = 0$ and in chiral gauge theories, unless the charges are appropriately arranged, anomalies from loop diagrams generically spoil gauge invariance:

$$\partial_\mu j^{\mu 5} \sim \mathcal{A}^{abc} = \text{Tr}[\gamma^5 t^a \{t^b, t^c\}] \neq 0. \quad (3.2)$$

where \mathcal{A} is the anomaly coefficient, γ^5 refers the chirality and t^i is the gauge representation. As is well known, SM anomaly conditions arise from triangle diagrams involving the following gauge interaction structures: $SU(2)^2 \times U(1)_Y$, $SU(3)^2 \times U(1)_Y$, $[\text{Gravity}]^2 \times U(1)_Y$, $U(1)_Y^3$.

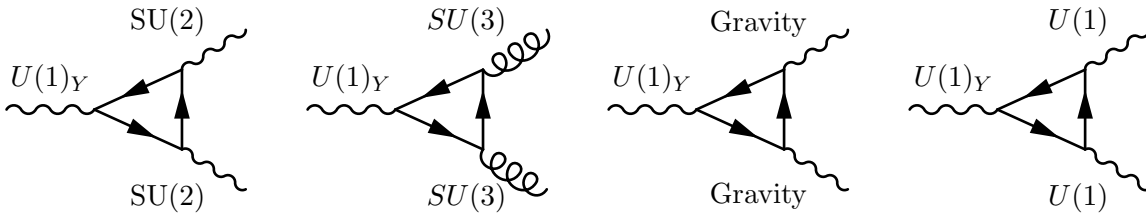


FIGURE 3.1: Anomaly Cancellation in SM.

The requirement that the anomaly coefficients satisfy $\mathcal{A} \propto \partial^\mu j_\mu = 0$ for each of the triangle diagrams above gives rise to the following four conditions, respectively:

$$\begin{aligned}
\mathcal{A}_{WWB} &:= \sum_{f_L/\text{w } SU(2)} C_2[f_L] d_3[f_L] Y[f_L] - \sum_{f_R/\text{w } SU(2)} C_2[f_R] d_3[f_R] Y[f_R] = 0 , \\
\mathcal{A}_{ggB} &:= \sum_{f_L/\text{w } SU(3)} C_2[f_L] d_2[f_L] Y[f_L] - \sum_{f_R/\text{w } SU(3)} C_2[f_R] d_2[f_R] Y[f_R] = 0 , \\
\mathcal{A}_{GGB} &:= \sum_{f_L} d_2[f_L] d_3[f_L] Y[f_L] - \sum_{f_R} d_2[f_R] d_3[f_R] Y[f_R] = 0 , \\
\mathcal{A}_{BBB} &:= \sum_{f_L} d_2[f_L] d_3[f_L] (Y[f_L])^3 - \sum_{f_R} d_2[f_R] d_3[f_R] (Y[f_R])^3 = 0 ,
\end{aligned} \tag{3.3}$$

where d_N and C_2 are the dimension and quadratic Casimir of a given representation under $SU(N)$, and Y is the hypercharge of a given state. The sums run over the left-handed (LH) and right-handed (RH) fermions respectively, and in the first/second condition the sum is restricted to representations of $SU(2)/SU(3)$ only. Note that the other triangle diagrams cancel trivially.

There is also the Witten anomaly [116] which places additional restrictions on field content transforming under groups which are equivalent to $Sp(N)$. In particular, an $SU(2)_L \cong Sp(1)$ gauge theory with an odd number of LH-fermion doublets (and no other $SU(2)$ -charged fermions) is inconsistent. However, as the SM is anomaly free and here we add fermions in vector-like pairs under the SM gauge group, or mimicking the SM generations, the Witten anomaly will not constrain our constructions. Furthermore, we restrict our field content to states with rational charges. This is motivated from charge quantisation considerations. In particular, this constraint plays a role in simple UV completions into larger GUT groups. While no theorems forbid irrational charges in field theories, they are disfavoured in UV completions to GUTs [117], and forbidden in quantum theories of gravity [118].

3.2.1 $U(1)'$ Anomaly Conditions

An extension of the SM gauge symmetry by an abelian factor, $SU(3) \times SU(2)_L \times U(1)_Y \times U(1)'$, introduces further anomaly conditions in addition to those of eq. (3.3). The vanishing of these new anomalies constrains the charges z of states transforming under $U(1)'$,

including any new fermions [119]. First there are the four analogues to those involving $U(1)_Y$, namely,

$$SU(2)^2 \times U(1)', \quad SU(3)^2 \times U(1)', \quad [\text{Gravity}]^2 \times U(1)', \quad U(1)'^3.$$

The coefficients $\mathcal{A}_{WWZ'}$, $\mathcal{A}_{ggZ'}$, $\mathcal{A}_{GGZ'}$, and $\mathcal{A}_{Z'Z'Z'}$ are direct analogues of eq. (3.3) except with Y replaced by z . Two further anomaly conditions arise from mixed $U(1)$ - $U(1)'$ diagrams

$$U(1)_Y \times U(1)'^2, \quad U(1)' \times U(1)_Y^2.$$

The associated anomalies vanish given the following conditions

$$\begin{aligned} \mathcal{A}_{Z'Z'B} &:= \sum_{f_L} d_2[f_L] d_3[f_L] Y[f_L] (z[f_L])^2 - \sum_{f_R} d_2[f_R] d_3[f_R] Y[f_R] (z[f_R])^2 = 0, \\ \mathcal{A}_{BBZ'} &:= \sum_{f_L} d_2[f_L] d_3[f_L] z[f_L] (Y[f_L])^2 - \sum_{f_R} d_2[f_R] d_3[f_R] z[f_R] (Y[f_R])^2 = 0. \end{aligned} \quad (3.4)$$

There could also be an $SU(3)^3$ anomaly with the addition of new chiral fermions. However, if the exotics are added in vector-like pairs under the SM group this vanishes automatically. In what follows, we will use the compact notation $z_X \equiv z[X]$ for a given field X .

3.2.2 Coloured Exotics and Anomaly Free $U(1)'$ Extensions

The case in which a $U(1)'$ gauge boson has only axial couplings to the SM fermions is distinguished as it implies:

$$z_q^{(i)} := z_Q^{(i)} = -z_u^{(i)} = -z_d^{(i)} \quad \text{and} \quad z_l^{(i)} := z_L^{(i)} = -z_e^{(i)}. \quad (3.5)$$

The index $i = 1, 2, 3$ denotes the SM generation. Furthermore, if DM states χ_L and χ_R are present and couple axially to the Z' , it follows that

$$z_{\text{DM}} := z_{\chi_L} = -z_{\chi_R}. \quad (3.6)$$

Interestingly, the anomaly condition for $SU(3)^2 \times U(1)'$ alone immediately yields some useful information. Consider an axial vector which couples to quarks, thus $z_q^{(i)} \neq 0$. In

the absence of new colored states the $SU(3)^2 \times U(1)'$ anomaly $\mathcal{A}_{ggZ'}$ is

$$\mathcal{A}_{ggZ'} = 2 \left(z_q^{(1)} + z_q^{(2)} + z_q^{(3)} \right) . \quad (3.7)$$

In the case that the $U(1)'$ charge assignments for the SM fermions are mirrored in each generation ($z_q^{(1)} = z_q^{(2)} = z_q^{(3)}$), or only one generation is charged under $U(1)'$ (for instance $z_q^{(1)} = z_q^{(2)} = 0$), then $\mathcal{A}_{ggZ'}$ will not vanish unless new colored chiral fermions are introduced. Notably, the constraints from collider searches for colored exotics are substantially more stringent than for uncolored states. In the absence of new colored fermions the anomaly condition of eq. (3.7) enforces

$$z_q^{(1)} + z_q^{(2)} + z_q^{(3)} = 0 , \quad (3.8)$$

which requires different $U(1)'$ charges between generations of SM quarks. Allowing the $U(1)'$ charge assignments to differ between different generations introduces substantial freedom. In what follows we restrict ourselves to the cases where either the $U(1)'$ charges are replicated in the generation structure, or only one generation is charged under the $U(1)'$.

It is worth noting that in the pure vector case this anomaly cancels trivially, as when $z_Q^{(i)} = z_u^{(i)} = z_d^{(i)}$, $\mathcal{A}_{ggV} = 0$ automatically without new colored states. In 3.6 we present some anomaly free models for the pure vector case, to illustrate that anomaly cancellation is typically much simpler in this scenario.

3.3 Construction of Anomaly-Free Axial Vector Models

To calculate the anomaly coefficients one sums over all loops of chiral fermions, cf. eq. (3.3), including any chiral fermion exotics. Anomaly cancellation generically requires, and constrains, new exotic field content. For certain choices the exotic fermions automatically preserves the anomaly cancellation of the SM group. For instance, the exotics can mirror the SM fermion $U(1)'$ charges in order to cancel anomalies (Section 3.3.1). Alternatively, the exotics can constitute vector-like pairs under the SM gauge group, but have chiral charges under $U(1)'$ (Sections 3.3.2 and 3.3.3). Moreover, with appropriate charges and

Field Name	$U(1)_Y$	$SU(2)_L$	$SU(3)$
$Q_L^i, Q'_{L,R}$	1/3	2	3
$u_R^i, u'_{L,R}$	4/3	1	3
$d_R^i, d'_{L,R}$	-2/3	1	3
$L_L^i, L'_{L,R}$	-1	2	1
$e_R^i, e'_{L,R}$	-2	1	1
$\nu_R, \chi_{L,R}$	0	1	1
H	1	2	1

TABLE 3.1: The representation structure of the SM states, along with fermion exotics in matching representations. Here we assume the dark matter χ is a SM singlet; the ν_R entry indicates other singlets which do not constitute the dark matter. For the SM fields the index i indicates the generation structure ($i = 1, 2, 3$), there could also be multiple copies of any given exotic. The notation permits for an index z for a $U(1)'$ charge and we will give anomaly free assignments for z .

representations one can cancel anomalies arising from diagrams involving the $U(1)'$ gauge bosons.

While, in principle, one can introduce exotics in a variety of representations to arrange for anomaly cancellation, the most straightforward approach is to restrict the new field content to the fundamental representations of the SM group. Thus we restrict our analysis to the case that the exotics emulate the SM fermions, including hypercharge assignments (although this could be relaxed). We denote the new exotics as *primed* versions of their SM counterparts, and list them in Table 3.1. In this section we will outline manners to systematically construct anomaly free sets of fermions. These techniques will be subsequently used in the construction of a selection of motivated scenarios of axial vector extensions of the SM.

3.3.1 Mirror Constructions

In the case that the new exotics mirror the SM fields there is a simple manner to cancel any anomalies involving $U(1)'$ gauge bosons which we outline below. However, as we discuss in Section 4.1, this model requires a doubling of the exotics, or a non-minimal scalar sector in order to give masses to the anomaly cancelling fermions.

Each generation of the SM is an anomaly free set. However, if the SM fields are charged under the $U(1)'$, this introduces new anomaly contributions. Notably, anomaly cancellation is automatic if for every SM fermion an exotic in the same representation of $SU(2)$ and $SU(3)$ is introduced which either *i*). has the same $U(1)_Y$ and $U(1)'$ charges but opposite chirality, or *ii*). with matching chirality, but opposite $U(1)_Y$ and $U(1)'$ charges. For instance, suppose that Q_L carries $U(1)'$ charge z_q , which we denote as $(3, 2)_{\frac{1}{3}, z_q}$, one might add either a LH exotic in the representation $(3, 2)_{-\frac{1}{3}, -z_q}$ or a RH exotic in $(3, 2)_{\frac{1}{3}, z_q}$. We call this approach the *mirror construction* for generating anomaly free sets of fermions.

For each SM fermion, one adds a corresponding exotic. Therefore the mirror construction ensures that anomaly cancellation occurs state by state, and thus generation by generation. In the case that one adds opposite chirality mirror partners, then each exotic forms a vector-like pair with one of the SM fermions. If additional SM singlet states charged under $U(1)'$ are also introduced, such as DM fields χ_L and χ_R , the contributions from these states can be cancelled via the addition of RH neutrino states ν_R with appropriate $U(1)'$ charges. Note that SM fermions that do not carry $U(1)'$ charges must still have exotic partners (with $U(1)'$ charge zero) to cancel the anomalies of the SM gauge group, unless the set of states uncharged under $U(1)'$ have the correct representations to fill out a full SM generation.

If only certain SM fermions carry $U(1)'$ charges, such as a single generation, then such mirror constructions have relatively minimal fermion spectra. However, if all or many SM fermions carry $U(1)'$ charges then, it implies the introduction of a large number of exotics. Note that there are generically flavor constraints on non-universal Z' models, which are somewhat alleviated in the case that the first two generations have the same $U(1)'$ charge [120].

In the rightmost two columns of Table 3.2 we show two examples in which a single SM generation is charged under $U(1)'$ and the anomalies are cancelled through mirror exotics. In the remainder of this section we consider more general algebraic approaches which can present smaller anomaly free sets of fermions.

3.3.2 An Algebraic Construction

Requiring anomaly cancellation gives a set of equations, which for a definite set of charges can be solved directly. Specifically, consider the case that the SM gauge group is extended by a $U(1)'$ factor, with no additional states except for those required to cancel anomalies and that all of the SM fermions couple to the gauge boson with only axial vector couplings, thus the charges satisfy eq. (3.5). Further, we assume the charges are the same for each generation: $z_q^{(1)} = z_q^{(2)} = z_q^{(3)}$ (similarly for leptons). To simplify the Higgs sector required to give Yukawa couplings to the SM fermions (as we discuss in Section 4.1.1) we also take $z_q^{(i)} = z_l^{(i)}$, for all generations i . We refer to this scenario as ‘Model #1’ in later sections. To emphasize the relation between charges we write $z_{\text{SM}} := z_q = z_l$.

Field	#1	#2	#3	#4	#5	#6
$z[Q_L]$	1	1	1	0	1	1
$z[u_R]$	-1	-1	-1	0	-1	-1
$z[d_R]$	-1	-1	-1	0	-1	-1
$z[L_L]$	1	1	0	1	1	0
$z[e_R]$	-1	-1	0	-1	-1	0
$z[\chi_L]$	-	9	9	-9/4	1	1
$z[\chi_R]$	-	-9	-9	9/4	-1	-1
$z[Q'_L]$	1	1	1	-	-	-
$z[Q'_R]$	3	-1	0	-	1	1
$z[u'_L]$	-3	-2	-2	-2	-1	-1
$z[u'_R]$	4	3	-1	5/2	-	-
$z[d'_L]$	3	-6	-2	2	-1	-1
$z[d'_R]$	4	5	11	-5/2	-	-
$z[L'_L]$	-9	-82/3	-49/12	-157/48	-	-
$z[L'_R]$	-3	-28/3	95/12	-13/48	1	0
$z[e'_L]$	-13	-100/3	103/6	-85/24	-1	0
$z[e'_R]$	-16	-127/3	67/6	-121/24	-	-
$z[\nu_R]$	-	-	-	-	1	1
$N[\nu_R]$	-	-	-	-	2	2
b_{m_z}	45	207	198	153/8	17	14
$b_{m_z} + b_M$	860	15038/3	14065/12	90697/192	34	28
$\mathcal{A}_{Z'Z'Z'}^{\text{SM}} + \mathcal{A}_{Z'Z'Z'}^{\text{DM}}$	45	45+1458	36+1458	9 - 729/32	15+2	12+2

TABLE 3.2: Charge assignments $z[f]$ and multiplicities $N[f]$ of states which give anomaly free spectra. For Models #1-#4 the $U(1)'$ charges are mirrored in each SM generation. In Models #5-#6, only one generation carries $U(1)'$ charge. A dash ‘-’ indicates that the corresponding state is absent in a given model. See Table 3.1 for representations and charge assignments of states under the SM gauge group. We also give b_{m_z} and $(\mathcal{A}_{Z'Z'Z'}^{\text{SM}} + \mathcal{A}_{Z'Z'Z'}^{\text{DM}})$, the β -function and $U(1)^3$ anomaly contributions from the SM fermions plus DM, and b_M the exotics β -function contribution, which are referenced in Section 4.2.

We will assume that the anomaly cancelling exotic fermions form a single full generation of vector-like fermions under the SM group $Q'_L, Q'_R, u'_L, u'_R, d'_L, d'_R, l'_L, l'_R, e'_L, e'_R$, which mimic their SM namesakes (see Table 3.1 for definitions of the representations). That this set of fermions is vector-like under the SM group implies that the SM chiral anomalies and the Witten anomaly are resolved automatically. Interestingly in this case the equations which ensure anomaly cancellation can be solved directly to arrive at a general, unique set of seven conditions which generically determine anomaly free sets of fermions with rational charges:³

$$\begin{aligned}
z_{Q'_R} &= z_{Q'_L} + 2z_{\text{SM}}, & z_{u'_R} &= 7z_{\text{SM}} + z_{u'_L}, \\
z_{d'_R} &= z_{d'_L} + z_{\text{SM}}, & z_{l'_R} &= z_{l'_L} + 6z_{\text{SM}}, \\
z_{e'_L} &= \frac{1}{3}(z_{d'_L} + 6z_{l'_L} - 2z_{Q'_L} - 28z_{\text{SM}} - 14z_{u'_L}), & z_{e_{R'}} &= z_{e_{L'}} - 3z_{\text{SM}} \\
z_{L'_L} &= \frac{1}{\Omega} \left(-8z_{d'_L}^2 - 4z_{d'_L} z_{Q'_L} - 32z_{Q'_L}^2 - 74z_{d'_L} z_{\text{SM}} + 58z_{Q'_L} z_{\text{SM}} \right. \\
&\quad \left. - 404z_{\text{SM}}^2 - 28z_{d'_L} z_{u'_L} + 56z_{Q'_L} z_{u'_L} + 469z_{\text{SM}} z_{u'_L} + 133z_{u'_L}^2 \right),
\end{aligned} \tag{3.9}$$

with $\Omega = 606z_{\text{SM}} + 168z_{u'_L} - 12z_{d'_L} + 24z_{Q'_L} \neq 0$.

The above set of equations uniquely characterizes the solution set. Since the charges are all related through anomaly cancellation, fixing a subset of the charges determines the remaining charges; e.g. taking $z_{\text{SM}} = z_{Q'_L} = 1$ and $z_{u'_L} = -z_{d'_L} = -3$ one obtains that for anomaly cancellation the other charges are required to be

$$\begin{aligned}
z_{Q'_R} &= 3, & z_{u'_R} &= 4, & z_{d'_R} &= 4, \\
z_{L'_L} &= -9, & z_{L'_R} &= -3, & z_{e'_L} &= -13, & z_{e'_R} &= -16.
\end{aligned} \tag{3.10}$$

If any LH-RH pair obtains the same $U(1)'$ charge, the states are redundant for anomaly cancellation, and thus can be removed from the model if desired.

For models which also include fermion DM χ_L and χ_R with $U(1)'$ charges which also have only axial couplings to the $U(1)'$ gauge boson, the situation is somewhat different. The additional freedom, due to the undetermined charge assignment of z_{DM} , means that

³Other possible solution sets generically yield irrational charges, which are theoretically disfavoured [117, 118].

solving the conditions for anomaly cancellation with a single full generation of SM-vector-like fermions leads to six sets of solutions which each provide anomaly free spectra with rational charges. This is in contrast to the unique set found without the inclusion of DM. In this case, if one removes the u'_L and u'_R exotics (or make them vector-like under $U(1)'$ such that $z_{u'_L} = z_{u'_R}$) then again there is a unique set of equations which determine the anomaly free sets of fermions. However, it is useful to use a full generation of SM-vector-like fermions as this makes it easier to find anomaly free models with simpler charge assignments, avoiding fractional charges with large numerators and denominators. For brevity, we neglect to give the sets of equations which ensure anomaly cancellation with the addition of DM, but these can readily be derived using *Mathematica* [121] or an analogous equation solver.

3.3.3 General Algebraic Constructions

A more general approach to finding anomaly free sets of fermions with arbitrary charges was outlined in the work of Batra, Dobrescu and Spivak [23], providing algebraic expressions for the $U(1)'$ charge assignments of the exotics and multiplicities of the SM singlets, as a function of the $U(1)'$ charges of the SM fermions. Indeed, using this method one can systematically embed any anomalous set of fermions into a larger theory which is anomaly free and where the fermions carry only rational charges.

To systematically find anomaly free spectra for SM fermions with arbitrary charges under $U(1)'$, one should introduce at least one chiral pair of states transforming under $SU(3)$, one chiral pair transforming under $SU(2)$ and one chiral pair charged under hypercharge. This set of exotics provides sufficient freedom to cancel the anomalies arising from the diagrams between mixed $U(1)'$ and SM gauge bosons. Following [23], we introduce pairs of exotics $d'_L, d'_R, L'_L, L'_R, e'_L, e'_R$, which are vector-like under the SM group. (Note that, unlike the previous sections, we do not introduce Q' or u' exotics here.)

Firstly, from the requirement of vanishing anomalies for the three diagrams involving two SM gauge bosons ($U(1)_Y^2 \times U(1)', SU(2)^2 \times U(1)', SU(3)^2 \times U(1)'$), one can readily obtain equations for the difference between the charges of the LH and RH exotics, i.e. $(z_{d'_L} - z_{d'_R}), (z_{L'_L} - z_{L'_R}), (z_{e'_L} - z_{e'_R})$. The next step in the construction is to posit a basis for the sum of the exotic charges in terms of a linear combination of the $U(1)'$ charges of the SM

fields:

$$(z_{X'_L} + z_{X'_R}) = C_1^X z_q + C_2^X z_{\text{DM}} + C_3^X z_l \quad \text{for } X = d, L, e. \quad (3.11)$$

Given the difference of the charges of the LH and RH exotics, and the above form of the sum of these charges, one can take linear combinations of these equations to obtain expressions for the $U(1)'$ charges of each of the exotics in terms of the SM charges and the constants C_i^X . Then demanding the vanishing of the $U(1)'^2 \times U(1)_Y$ anomaly for arbitrary SM $U(1)'$ charge assignments leads to relations between the various constants C_i^X . This typically leaves a number of constants undetermined.

It remains to arrange for the $[\text{Gravity}]^2 \times U(1)'$, and $U(1)^3$ anomalies to vanish. We assume the spectrum contains two types of RH neutrinos $N_1 \times \nu_R^{(1)}$ and $N_2 \times \nu_R^{(2)}$ which are SM singlets with $U(1)'$ charges $z[\nu_R^{(1)}] = -1$ and $z[\nu_R^{(2)}] = 2$, and N_α indicate the number of copies of these states. Then insisting that the two remaining anomalies vanish, one obtains an equation for multiplicities N_α of the RH neutrinos states. If $N_\alpha < 0$ this implies that $|N_\alpha|$ RH (or LH) SM singlets with charge $z[-\nu_R^{(\alpha)}]$ (with charge $z[\nu_R^{(\alpha)}]$) are required.

Then fixing the SM charges and the undetermined C_i^X , any choice which yields integer values for N_1 and N_2 gives a consistent anomaly free fermion spectrum. This commonly leads to high multiplicities N_1 and N_2 . However, following the procedures outlined in [23], the number of SM singlets can often be replaced with a smaller set of RH neutrinos with larger $U(1)'$ charges. 3.5 gives anomaly free sets of fermions for various models which are derived via an application of the method of [23]. Additionally, in 3.4 we present an explicit derivation using this method.

3.3.4 A Selection of Axial Vector Models

There are many scenarios involving axial vectors which could be of interest. Here, we highlight a number of motivated extensions of the SM here and construct anomaly free spectra which realise these scenarios. Specifically, we will consider the following cases:

- **Model #1:** The simplest scenario is the extension of the SM gauge group with an additional $U(1)'$ factor, where all of the SM fermions couple axially to the Z' , and

the $U(1)'$ charge assignments of the SM fermions are replicated in the generation structure.⁴

- **Model #2:** A minimal extension of Model #1 is to include chiral fermion DM states which are SM singlets, and also couple axially to the gauge boson of $U(1)'$. We shall also assume the scenario of fermion DM charged under $U(1)'$ in Models #3-#6.
- **Model #3:** A slight modification to Model #2 is the case the axial vector has no tree level couplings to leptons by enforcing $z_l = 0$, thus yielding a leptophobic axial vector.
- **Model #4:** Conversely, one might consider a leptophilic case with $z_l \neq 0$ and $z_q = 0$.
- **Model #5:** Not all SM generations need be charged under $U(1)'$ and we consider the case that only a single generation (1G) has $U(1)'$ charges. For example $z_q^{(1)} = z_l^{(1)} = z_q^{(2)} = z_l^{(2)} = 0$.
- **Model #6:** Moreover, it could be that only a small subset of SM fermions carry $U(1)'$ charge. Specifically, we consider the case that only $z_Q^{(3)} = -z_u^{(3)} = -z_d^{(3)} \neq 0$, with all other SM fields neutral under $U(1)'$. This realises a single generation leptophobic model.

A summary of the above models is given in Table 3.3. In Table 3.2 we present anomaly free sets of fermions which realise Models #1-#6 outlined above. The anomaly free sets presented for Models #1-#4 are generated via the method of Section 3.3.2, while the spectra for Models #5 & #6 come from the mirror construction, as discussed in Section 3.3.1. Alternative anomaly free sets for Models #1-#6 which eliminate some of the colored exotics at the price of introducing RH neutrinos, as discussed in Section 3.3.3, are given in 3.5.

3.4 A Selection of Anomaly Free Vector Models

We provide Table 3.4 of the charge assignments which lead to anomaly cancellation for the case of pure vector couplings to the SM fermions (and dark matter), for analogues of Models #1-#6. This is given both for completeness and to demonstrate that the axial vector case typically requires far more exotics in order to arrange for anomaly cancellation

⁴Model #1 is also relevant when including scalar DM or fermion DM with vector couplings to Z' .

Name	n_G	Lepto-phobic/philic?
#1. Universal Model	3	X
#2. /w DM Model	3	X
#3. L -phobic Model	3	Leptophobic
#4. L -philic Model	3	Leptophilic
#5. 1G-Model	1	N/A
#6. t - b -Model	1	Leptophobic

TABLE 3.3: Summary of the models we study. n_G is the number of SM generations charged under $U(1)'$.

compared to the vector case. This also highlights that there is no need of colored exotics in the pure vector case.

Field	#1V	#2V	#3V	#4V	#5V	#6V
$z[Q_L]$	1	1	1	0	1	1
$z[u_R]$	1	1	1	0	1	1
$z[d_R]$	1	1	1	0	1	1
$z[L_L]$	1	1	0	1	1	0
$z[e_R]$	1	1	0	1	1	0
$z[\chi_L]$	-	1	1	1	1	1
$z[\chi_R]$	-	-1	-1	-1	-1	-1
$z[L'_L]$	-1	-6	-4	-1	-2	-1
$z[L'_R]$	11	6	5	2	2	2
$z[e'_L]$	11	6	5	2	2	2
$z[e'_R]$	-1	-6	-4	-1	-2	-1
$z[\nu_R^{(1)}]$	1	-1	1	1	1	1
$z[\nu_R^{(2)}]$	2	2	-4	-2	-2	-2
$z[\nu_R^{(3)}]$	-3	-5	-5	-	-	-
$z[\nu_R^{(4)}]$	-7	-7	-	-	-	-
$z[\nu_R^{(5)}]$	-10	-	-	-	-	-
$N[\nu_R^{(1)}]$	1	7	2	4	3	1
$N[\nu_R^{(2)}]$	5	6	1	1	2	1
$N[\nu_R^{(3)}]$	1	1	1	-	-	-
$N[\nu_R^{(4)}]$	1	1	-	-	-	-
$N[\nu_R^{(5)}]$	1	-	-	-	-	-

TABLE 3.4: Similar to Table 3.2, charge assignments for Models #1-#6 but for the case of a gauge boson with pure vector couplings to states (as can be seen from the charge assignments).

3.5 An Alternative Set of Anomaly Free Axial Vector Models

In this appendix we give alternative anomaly free sets of fermions for the case in which the SM fermions (and dark matter) have only axial vector coupling with a new $U(1)'$ gauge boson. These charges assignments are derived using the method of [23], see Section 3.3.3. While some colored exotics are removed, the price is the introduction of a multitude of RH neutrinos:

Field	#1b	#2b	#3b	#4b	#5b	#6b
$z[Q_L]$	1	1	1	0	1	1
$z[u_R]$	-1	-1	-1	0	-1	-1
$z[d_R]$	-1	-1	-1	0	-1	-1
$z[L_L]$	1	1	0	1	1	0
$z[e_R]$	-1	-1	0	-1	-1	0
$z[\chi_L]$	-	1	1	1	1	1
$z[\chi_R]$	-	-1	-1	-1	-1	-1
$z[d'_L]$	-6	-6	-6	-	-2	-2
$z[d'_R]$	6	6	6	-	2	2
$z[L'_L]$	-6	-6	1	1	-2	-1
$z[L'_R]$	6	6	10	4	2	2
$z[e'_L]$	-	-	18	-4	-	2
$z[e'_R]$	-	-	15	-1	-	1
$z[\nu_R^{(1)}]$	2	2	1	-1	1	1
$z[\nu_R^{(2)}]$	-3	-3	-2	2	-4	2
$z[\nu_R^{(3)}]$	-5	-5	-4	-6	-	-3
$z[\nu_R^{(4)}]$	-10	-10	-9	-	-	-
$z[\nu_R^{(5)}]$	-	1	-	-	-	-
$N[\nu_R^{(1)}]$	8	8	2	2	1	1
$N[\nu_R^{(2)}]$	2	2	1	5	1	1
$N[\nu_R^{(3)}]$	1	1	1	1	-	2
$N[\nu_R^{(4)}]$	2	2	1	-	-	-
$N[\nu_R^{(5)}]$	-	2	-	-	-	-

TABLE 3.5: Similar to Table 3.2, alternative charge assignments $z[f]$ and multiplicities $N[f]$ of states which give anomaly free spectra for Models #1-#6 derived using the method of [23].

3.6 Algebraic Construction of Axial Vector Examples

Next we give a worked example of the algebraic construction of [23] discussed in Section 3.3.3 and 3.5. We consider the scenario in which there are n_G generations charged under $U(1)'$, each generation with identical charge assignments, such that the SM fermions have axial couplings to the new vector boson, and we include chiral fermion DM states which also couple axially to the $U(1)'$ gauge boson. Following [23], the requirement that the anomaly cancellation occurs for $U(1)_Y^2 \times U(1)'$, $SU(2)^2 \times U(1)'$, and $SU(3)^2 \times U(1)'$ implies

$$(z_{d'_L} - z_{d'_R}) = -4n_G z_q, \quad (z_{L'_L} - z_{L'_R}) = -n_G(z_l + 3z_q), \quad (z_{e'_L} - z_{e'_R}) = n_G(z_q - z_l) .$$

Taking the sum of the LH and RH charges to be a linear combination of the $U(1)'$ charges of the SM fields $(z_{X'_L} + z_{X'_R}) = C_1^X z_q + C_2^X z_{\text{DM}} + C_3^X z_l$, for $X = d, L, e$ and where the C_i^X are arbitrary integers, it follows that the charges of the exotics can be expressed in terms of the $U(1)'$ charges of the SM fields

$$\begin{aligned} z_{d'_L} &= \frac{1}{2} \left[-C_2^L z_{\text{DM}} + C_3^d(z_l - 9z_q) - 2C_1^e z_q - 4n_G z_q \right] \\ z_{d'_R} &= \frac{1}{2} \left[-C_2^L z_{\text{DM}} + C_3^d(z_l - 9z_q) - 2C_1^e z_q + 4n_G z_q \right] \\ z_{L'_L} &= \frac{1}{2} \left[C_2^L z_{\text{DM}} + C_1^e(3z_q - z_l) - 4C_3^d(z_l - 3z_q) - n_G(3z_q + z_l) \right] \\ z_{L'_R} &= \frac{1}{2} \left[C_2^L z_{\text{DM}} + C_1^e(3z_q - z_l) - 4C_3^d(z_l - 3z_q) + n_G(3z_q + z_l) \right] \\ z_{e'_L} &= \frac{1}{2} \left[-C_2^L z_{\text{DM}} + 4C_3^d z_l + C_1^e(z_q + z_l) - n_G(z_l - z_q) \right] \\ z_{e'_R} &= \frac{1}{2} \left[-C_2^L z_{\text{DM}} + 4C_3^d z_l + C_1^e(z_q + z_l) + n_G(z_l - z_q) \right] . \end{aligned} \tag{3.12}$$

Note that those C_i^X absent in the above have been fixed by anomaly cancellation conditions.⁵ Finally, the multiplicities N_α (for $\alpha = 1, 2$) of the SM singlet RH-fermions $\nu_R^{(\alpha)}$

⁵This fixes six constants: $C_2^d = C_2^e = -C_2^L$ and $C_1^L = 3C_3^e = -3C_3^L = 3(4C_3^d + C_1^e)$ and $C_1^d = -2C_1^e - 9C_3^d$.

required by anomaly cancellation are given by

$$\begin{aligned}
N_1 &= \frac{1}{3} \left(3n_G z_l^3 - 12n_G z_l + 12n_G z_q^3 - 48n_G z_q + 3z_{d_L}^3 - 12z_{d_L} + 2z_{\text{DM}}^3 - 8z_{\text{DM}} \right. \\
&\quad \left. - 3z_{d_R}^3 + 12z_{d_R} + z_{e_L}^3 - 4z_{e_L} - z_{e_R}^3 + 4z_{e_R} + 2z_{L_L}^3 - 8z_{L_L} - 2z_{L_R}^3 + 8z_{L_R} \right) \\
N_2 &= \frac{1}{2} \left(N_1 + 2z_{\text{DM}} + 3n_G z_l + 12n_G z_q + 3z_{d_L} - 3z_{d_R} + z_{e_L} - z_{e_R} + 2z_{L_L} - 2z_{L_R} \right).
\end{aligned} \tag{3.13}$$

Anomaly-free spectra can be found by choosing $U(1)'$ charges for the SM fermions (provided $N_1, N_2 \in \mathbb{Z}$), but are not unique and may not be the most minimal. Specifically, one obtains Model #2b for

$$n_G = 3, \quad z_{\text{DM}} = z_l = z_q = 1, \quad C_2^L = -2C_3^d = \frac{2}{3} C_1^e. \tag{3.14}$$

The above parameter values leads to $N_1 = -687$ and $N_2 = -350$ but these can be manipulated to obtain the set of RH neutrinos in Table 4.1 using the method described in [23].

Chapter 4

AXIAL VECTOR Z' MODELS

4.1 Mass Generation

In this chapter, we follow the previous discussion of axial-vector models and then consider what form of scalar sector is required to give masses to the SM and exotic fermions for the axial vector models outlined in the previous section. These considerations are often absent in phenomenological studies, but regularly require non-trivial model building. We do not attempt to be comprehensive, but rather make some general remarks.

4.1.1 Mass Generation for Standard Model Fermions

If all SM fermions couple axially to $U(1)'$, then gauge invariance forbids a full set of SM Yukawa couplings from a single Higgs. The reason is that the $U(1)'$ charge of the bilinears is $z[\bar{Q}_L u_R] = z[\bar{Q}_L d_R] = 2z_q$ for axial vector couplings. To form a gauge invariant operator $H^\dagger \bar{Q}_L u_R$ requires $z[H^\dagger] = -2z_q$, but this forbids the Yukawa couplings for the down-quarks and leptons since in the SM these involve the conjugate field. This difference in SM fermion bilinears is even more apparent if only some generations are charged under $U(1)'$. Finally, electroweak precision data also constrains the $U(1)'$ charge of the SM Higgs because of the induced Z - Z' mixing. The remaining mass terms could still arise via renormalisable terms involving additional Higgses, as in a Type II Two Higgs Doublet Model [122], or due to higher dimension operators. Perhaps the simplest manner to give masses to all of the SM fermions is for the Higgs to be uncharged under $U(1)'$ and introduce a scalar S which is charged under $U(1)'$, but is a SM singlet, such that there

are dimension five effective operators for the remaining SM fermions: $(1/\Lambda_*)SH^\dagger\bar{Q}_L u_R$, etc. This operator is generated by physics integrated out at the scale Λ_* , and the theory must UV complete to a renormalisable Lagrangian at energies approaching Λ_* . This is reminiscent of the Froggatt-Nielsen mechanism [97].

Since S is a SM singlet, gauge invariant dimension five operators can be formed using S and S^\dagger , which give mass terms to all SM fermions once S acquires a VEV $\langle S \rangle$. The $\langle S \rangle$ breaks the $U(1)'$, and thus the fermion masses are connected to the axial vector mass. This scenario is no longer UV complete, and one expects additional states to enter at the scale which generates the higher dimension operators, which could be near the TeV scale. For mass terms induced due to $\langle S \rangle^n$ this yields effective Yukawa couplings of order $(\langle S \rangle/\Lambda_*)^n$. However, a good effective field theory (EFT) requires $\langle S \rangle \lesssim \Lambda_*$, and thus it is challenging to obtain $\mathcal{O}(1)$ Yukawa couplings via high dimension operators. Hence, from a model building stance, the use of high dimension operators to generate the top Yukawa is disfavoured.

In an EFT with a Z' , where the scalar S responsible for breaking $U(1)'$ has been integrated out, the VEV of this scalar $\langle S \rangle \equiv v'$ introduces an order parameter, which acts as a cutoff of the EFT. The VEV responsible for breaking $U(1)'$ generates the Z' mass $m_{Z'} \simeq g'v'$, and the mass of the associated scalar is parametrically $m_S \sim \lambda_S v'$, where λ_S is the S quartic coupling. Unitarity of the EFT describing the light SM fermions f , DM, and Z' requires that $m_f, m_{\text{DM}} \lesssim \frac{m_{Z'}}{g'} \simeq v'$ and the bosons should satisfy $m_{Z'}, m_S \lesssim v'$; see e.g. [20] for further discussion. For example, giving the top a $U(1)'$ coupling $g' \sim 1$ would imply a lower bound on the Z' mass of $m_{Z'} \gtrsim 175$ GeV. This bound is stronger for heavy DM states

$$m_{Z'} \gtrsim 1 \text{ TeV} \left(\frac{g'}{1} \right) \left(\frac{m_{\text{DM}}}{1 \text{ TeV}} \right) . \quad (4.1)$$

4.1.2 Mass Generation for Pairs of Exotic Fermions

Anomaly cancellation in models with axial vector Z' requires an array of exotics with chiral charge under $U(1)'$, and, as can be seen from Table 3.2, the pattern of $U(1)'$ charge assignments of these exotics is often complicated. As such these new fermions can not typically be given dimension four Yukawa couplings involving the Standard Model Higgs. The simplest manner to give masses to the exotic fermions is through the introduction

of *exotic Higgses*, new SM singlet scalars charged under $U(1)'$ which acquire VEVs, and give masses to the various exotics via renormalisable interactions. In the case where the exotics come in pairs that are vector-like under the SM, they may acquire masses through renormalisable interactions involving the exotic Higgses. Due to the different $U(1)'$ charges of the new fermions, this generally requires one exotic Higgs for each exotic fermion pair. In addition to the LH-RH mass bilinears (e.g. $\bar{Q}'_L Q'_R$), the exotics could also have chiral mass bilinears (e.g. $\bar{Q}'_L u'_R$). However, exotic fermion mass operators using these bilinears must include the SM Higgs field as well as an exotic Higgs, and are thus non-renormalisable. An alternative approach is to add fewer exotic Higgses, such that some of the exotic fermions do not have renormalisable mass terms, but higher dimension operators respecting the gauge symmetries can give masses after VEV insertions.

When the exotics acquire mass through $U(1)'$ -breaking VEVs at the scale $\sim v'$, we expect that the masses of the gauge boson ($m_{Z'} \sim gv'$) and the exotics ($M \sim y'v'$) should be comparable: $m_{Z'} \sim M$. Any hierarchical splitting of $m_{Z'}$ or M from v' arises primarily

Bilinear	#1	#2	#3	#4
SM $\overline{\text{LH}}\text{-RH}$ bilinears (e.g. $z[\bar{Q}_L u_R]$)	-2	-2	-2	-2
$z[\bar{\chi}_L \chi_R]$	-	- 18	-18	9/2
$z[\bar{Q}'_L Q'_R]$	2	-2	-1	-
$z[\bar{u}'_L u'_R]$	7	5	1	9/2
$z[\bar{d}'_L d'_R]$	1	11	13	-9/2
$z[\bar{L}'_L L'_R]$	6	18	12	3
$z[\bar{e}'_L e'_R]$	-3	-9	-6	-3/2
$z[\bar{Q}'_L u'_R]$	3	2	-2	-
$z[\bar{Q}'_L d'_R]$	3	4	10	-
$z[\bar{Q}'_R u'_L]$	-6	-1	2	-
$z[\bar{Q}'_R d'_L]$	0	-5	-2	-
$z[\bar{L}'_L e'_R]$	-7	-15	61/4	-85/48
$z[\bar{L}'_R e'_L]$	-10	-24	37/4	-157/48
No. scalars for Yukawa terms	5	5	4	3
Min. number of scalars	2	3	2	2

TABLE 4.1: Charges of fermion bilinears for Models #1-#4. Also shown is the number of exotic scalars needed to give vector-like masses to all exotics after VEV insertions (not including SM Higgs), and to give masses to all exotics via a combination of renormalisable and non-renormalisable operators with mass dimension six or less. These models need multiple scalars to give all fermions masses.

due to couplings. Moreover, perturbativity of y' implies

$$M \lesssim v' \simeq \frac{m_{Z'}}{g'(m_{Z'})}. \quad (4.2)$$

Thus separating the Z' from the exotics requires a tuning of the Yukawa couplings such that $g' \ll y'$. In addition, the exotic fermions can not be made significantly heavier than v' .

4.1.3 The Scalar Sector of Model #1

Let us consider a specific example. Below, we outline a scalar sector for Model #1 which can give masses to all of the SM fermions and chiral exotics. To understand the charges required for exotic Higgses we should look at the net charge of the bilinear operators involving chiral exotic pairs. We give these for Models #1-#4 in Table 4.1. In Model #1, observe that most of these bilinears have different net charge, and thus five different scalars (with $|z| = 1, 2, 3, 6, 7$) are required for these states to acquire vector-like mass terms via renormalisable Yukawa terms with VEV insertions. We denote by S_q an exotic Higgs with $z[S_q] = q$.

Note that one could replace terms involving S_{-6} with non-renormalisable terms involving S_{-2} and S_{-3} . For example, instead of $S_{-6} \bar{L}'_L L'_R$ mass terms can also arise from

$$\left[\frac{c_1}{\Lambda_*} \langle S_{-3} \rangle^2 + \frac{c_2}{\Lambda_*^2} \langle S_{-2} \rangle^3 \right] \bar{L}'_L L'_R, \quad (4.3)$$

where Λ_* is the cutoff of the EFT. The operator involving S_{-3}^2 is dimension five, while the others are dimension six. However, if its coefficient is small, $c_1 \ll c_2$, or if $\langle S_{-3} \rangle \ll \langle S_{-2} \rangle$, this operator will not necessarily dominate. Thus the number of exotic Higgses required can be reduced (cf. Table 4.1), but at the expense of UV completeness.

Now let us consider an example Lagrangian for the scalar sector of Model #1. Suppose the SM Higgs H has charge $z[H] = -2$ and introduce two SM singlet scalars S_1 and S_4 with $U(1)'$ charges $z[S_1] = 1$ and $z[S_4] = 4$. With these states the SM Yukawa couplings can be constructed with a renormalisable interaction for the up-like quarks (useful for obtaining the large top Yukawa) and dimension five operators responsible for the down and lepton

Yukawas

$$\mathcal{L}_{\text{SM}} \supset y_u^i H^\dagger \bar{Q}_L u_R + \frac{y_d^i}{\Lambda_*} S_4 H \bar{Q}_L d_R + \frac{y_l^i}{\Lambda_*} S_4 H \bar{L}_L e_R + \text{h.c.} \quad (4.4)$$

The scale suppression of the higher dimension operators can help realise the fermion hierarchy, as in the Froggatt-Nielsen mechanism [97]. For the exotic fermions one can obtain vector-like masses via gauge invariant Yukawa terms involving the SM singlet scalars,

$$\mathcal{L}_{\text{Ex}} \supset \frac{y_{Q'}}{\Lambda_*} S_1^{\dagger 2} \bar{Q}'_L Q'_R + \frac{y_{u'}}{\Lambda_*^2} S_4^{\dagger 2} S_1 \bar{u}'_L u'_R + y_{d'} S_1^\dagger \bar{d}'_L d'_R + \frac{y_{L'}}{\Lambda_*^2} S_4^\dagger S_1^{\dagger 2} \bar{L}'_L L'_R + \frac{y_{e'}}{\Lambda_*} S_4 S_1^\dagger \bar{e}'_L e'_R + \dots \quad (4.5)$$

None of the leading SM mass terms involve S_1 , and in contradistinction all of the exotic fermion mass terms involve S_1 . Thus the magnitude of the $\langle S_1 \rangle$ is not restricted by the requirement that one reproduces the SM fermion masses and a large S_1 VEV can be used to decouple the exotic fermions. This results in a hierarchy between the exotic fermions, but we will not discuss this here. Moreover, a large $\langle S_1 \rangle$ breaks $U(1)'$ at a high scale, allowing for a Z' which is much heavier than the weak scale. This avoids electroweak precision constraints from tree-level Z - Z' mixing [16, 20, 49, 123], which for $m_{Z'} \gg m_Z$ require $m_{Z'} \gtrsim g'(14 \text{ TeV})$.

There are also mass terms from chiral bilinears, such as $\bar{Q}'_L u'_R$, which must be paired with a Higgs H field for $SU(2)$ invariance and a combination of S_1 and S_4 fields to conserve $U(1)'$ charge. As discussed above, mass operators containing these bilinears, e.g. $S_4^\dagger S_1 H^\dagger \bar{Q}'_L u'_R$, are non-renormalisable, but can affect the mass splittings between exotic fermions.

Giving mass to certain fields via higher dimension operators implies that the EFT should break down around Λ_* , and one might ask what manner of physics can give rise to such operators. As an example, consider the dimension five operator $S_4 H \bar{L}_L e_R$ in Eq. (4.4) which is responsible for the electron mass. This operator can arise from a vector-like pair of fermions ψ_L, ψ_R in the representation $(1, 1)_{-2,3}$ entering in the Lagrangian of the UV theory

$$L_{\text{UV}} \supset y_\psi H \bar{L}_L \psi_L + y'_\psi S_4 \bar{\psi}_L e_R + m_\psi \bar{\psi}_L \psi_R + \text{h.c.} \quad (4.6)$$

After integrating out ψ , one recovers the contact operator which gives mass to the electrons and the EFT cutoff can be identified as $\Lambda_* = \frac{m_\psi}{y_\psi y'_\psi}$. While the introduction of high dimension operators necessitates new physics (for instance new fermions) in the UV theory, these states could be significantly above the weak scale.

4.1.4 Mass Generation for Exotic Mirror Fermions

In anomaly free models arising from mirror constructions, such as Models #5 & #6, the situation is somewhat different. Since the exotic fermions are not introduced in pairs that are vector-like under the SM, but rather as copies of SM generations, one requires a new scalar which is a doublet under $SU(2)_L$ to construct renormalisable Yukawa terms. Since the VEV of such a scalar breaks electroweak symmetry, it is constrained by electroweak precision and Higgs measurements. Moreover, in this case the exotics can not be much above the weak scale. Viable exotics require Yukawas near the perturbative limit, which implies new physics at the TeV scale, and thus such scenarios will be generically constrained by collider searches.

Alternatively, we may introduce further exotic fermions which do not disrupt the anomaly cancellation, and then give masses to the exotics in the same fashion as in Section 4.1.2. This can be achieved if one supplements the mirror constructions, such as Models #5 & #6, with a full set of states with identical SM representations, zero $U(1)'$ charge, and opposite chirality to the existing exotic fermions. For example, for Model #5 one would add Q'_L , u'_R , d'_R , L'_L , e'_R with $z[Q'_L] = z[u'_R] = z[d'_R] = z[L'_L] = z[e'_R] = 0$. Since they are uncharged under $U(1)'$, they obviously do not contribute to any anomalies involving $U(1)'$. Furthermore, since these states mimic an entire generation of SM fermions, and the anomalies in the SM cancel generation by generation, it follows that this spectrum is anomaly free.

The benefit of doubling the number of exotics is that now one can form Yukawa terms for the anomaly cancelling exotics which give vector-like masses after VEV insertions, similar to Section 4.1.2. For a given anomaly cancelling RH exotic X_R one can form a LH-RH bilinear which has net charge $z[\bar{X}_L X_R] = z[X_R]$ (similarly for LH anomaly cancelling exotics). For Models #5 & #6, supplemented by a generation with opposite chirality and zero $U(1)'$ charge, all of the exotic $\bar{L}H$ -RH bilinears have net charge 1. Thus one can give mass to all of the exotic fermions through a single new SM singlet scalar field S with $z[S] = -1$

$$\mathcal{L}_{\text{Mir}} \supset S \bar{Q}'_L Q'_R + S \bar{u}'_L u'_R + S \bar{d}'_L d'_R + S \bar{L}'_L L'_R + S \bar{e}'_L e'_R . \quad (4.7)$$

This model has a minimal scalar sector, and is UV complete, at the price of doubling the fermion content of the theory.

4.2 Breakdown of Low Energy Theories

In this section we examine at what scale new physics is needed to mitigate a breakdown in the low energy theory, either due to a loss of renormalisability from uncanceled anomalies or, after introducing new fermions for anomaly cancellation, due to a loss of perturbativity of the $U(1)'$ gauge coupling g' .

4.2.1 The Non-Perturbative Limit

In the SM the hypercharges of fields are all $\mathcal{O}(1)$ and as a result the gauge coupling remains perturbative well beyond the Planck scale. However, as can be seen from Table 3.2, the exotics required for anomaly cancellation in axial vector extensions of the SM often carry large $U(1)'$ charges. As a result the $U(1)'$ gauge coupling g' may quickly run non-perturbative. Indeed, shortly after the coupling nears the non-perturbative limit one must reach a $U(1)'$ Landau pole. Near the scale at which the $U(1)'$ becomes non-perturbative either the theory enters a strong coupling regime or new physical states appear which maintain the theory in a weakly coupled completion.¹ In principle such new physics could be observable at collider experiments if it occurs near the TeV scale.

The running of g' is only initiated above the Z' mass, thus $g'(m_Z) = g'(m_{Z'})$. At energies $Q < m_{Z'}$ running is inhibited by the Z' mass, much as the Fermi constant G_F does not run. Above $m_{Z'}$ the $U(1)'$ coupling strength $\alpha' \equiv g'^2/4\pi$ runs with the energy scale Q ,

$$\frac{d\alpha'^{-1}}{d \ln Q} = -\frac{b}{2\pi} \quad \text{with} \quad b = \sum_f \frac{2}{3} z_f^2 + \sum_s \frac{1}{3} z_s^2, \quad (4.8)$$

where the sum runs over all $U(1)'$ charged Weyl fermions f and complex scalars s with charge z_i that are accessible at the scale Q and includes color and representation factors.

The scale at which g' becomes non-perturbative depends not only on the field content and charge assignments, but also the masses of any new fields. Below the TeV scale, we assume that only the SM fields, and DM states χ_L and χ_R (except for Model #1), are present. If the new fermions enter at the scale M , the running of g' to some UV scale Λ

¹New physics which enters at the Landau pole does not necessarily need to take part in anomaly cancellation. The low energy theory could transition to a different weakly coupled theory which remains anomalous, and now anomaly cancellation must take place in the new theory.

is described by

$$\alpha'^{-1}(\Lambda) = \alpha'^{-1}(m_{Z'}) - \int_{m_{Z'}}^M \frac{b_{m_Z}}{2\pi} d \ln Q - \int_M^\Lambda \frac{b_{m_Z} + b_M}{2\pi} d \ln Q, \quad (4.9)$$

where b_{m_Z} and b_M are defined as in Eq. (4.8), but now for b_{m_Z} the sum is over the SM states and DM, and for b_M we sum over only the new fermions required by anomaly cancellation. Specifically, the $U(1)'$ coupling runs non-perturbative ($\alpha'(\Lambda_P) \sim 1$) at the scale $Q = \Lambda_P$

$$\Lambda_P = M \exp \left[\frac{1}{b_M + b_{m_Z}} \left(b_{m_Z} \log \left[\frac{m_{Z'}}{M} \right] + \frac{2\pi}{\alpha'(m_Z)} - \frac{2\pi}{\alpha'(\Lambda_P)} \right) \right]. \quad (4.10)$$

There could be additional vector-like pairs of fermions, or new scalars, charged under $U(1)'$ which will increase running without altering the anomaly cancellation requirements. Indeed, one typically introduces scalars charged under $U(1)'$ to give masses to the exotics through a Higgs mechanism, as discussed in Section 4.1. Furthermore, certain states charged under $U(1)$ might be integrated out at some scale Λ_* leading to higher dimension operators in the low energy theory (as may be useful to give mass to some SM fermions or exotics, cf. eq. 4.6). If $\Lambda_* < \Lambda_P$, however, then these states must also in principle be included in the running of the $U(1)'$ gauge coupling above Λ_* . Here for simplicity we include only the new fermions required by anomaly cancellation in the $U(1)'$ gauge coupling running. Thus, our constraints may be weaker than in a complete model, but qualitatively they usually will not change. Note that for the spectra we consider, the pole for $U(1)_Y$ always lies above Λ_P .

Figure 4.1 shows the RG evolution of the $U(1)'$ coupling g' in Models #1-#6 with the assumption that $m_{Z'} \sim \text{TeV}$. The PURPLE contours indicate the scale Λ_P at which g' becomes non-perturbative for a given $g'(m_Z)$ and M . If g' starts out sufficiently small at the electroweak scale and the new fields are heavy, the Landau pole is reached only at very high scales. But observe that for weak scale couplings $g'(m_Z) \sim 0.1 - 1$ Landau poles can be a concern for all models we consider. At the threshold of strong coupling Λ_P one expects new physics with observable consequences. In particular, TeV scale non-perturbativity is evident in Models #1-4 with weak scale exotics, as indicated by the lightest contours in Figure 4.1. On the other hand, for sufficiently small $g'(m_Z)$ the $U(1)'$

coupling may not run to strong coupling until above 10^{18} GeV (which coincides with the Planck scale), as indicated by the darkest contour.

In the GREY region, $\Lambda_P < M$ and the running due to the low energy content alone will cause g' to reach its pole before the anomaly cancelling fermions enter, so that new physics is expected at this scale regardless of anomaly cancellation considerations. The boundary of this region saturates this bound, thus $M = \Lambda_P$ and $g'(M) = \sqrt{4\pi}$, and the scale at which g' runs non-perturbative can be read from the LH axis. The coupling at the weak scale is determined by the RG evolution, according to Eq. (4.10), from the UV scale $M = \Lambda_P$

$$\alpha'(m_Z) = \left(\frac{1}{\alpha'(\Lambda_P)} - \frac{b_{m_Z}}{2\pi} \log \left[\frac{m_Z}{\Lambda_P} \right] \right)^{-1}. \quad (4.11)$$

In other words, the trajectory of the boundary curve enveloping the grey region relates the scale M and $g'(m_Z)$ by the RG evolution backward from $g'(M) = \sqrt{4\pi}$ with only SM particle content plus the added DM (if present).

4.2.2 The Non-Renormalisable Limit

If a set of fermions is anomalous at a given energy scale, it should be anticipated that this is an EFT and at some higher scale M additional fermions (or another mechanism) enters to cancel the anomalies. Below the scale M the heavy chiral fermions which are integrated out generate Wess-Zumino terms which cancel the apparent anomalies in low energy theory [124–126]. However, the cutoff of the EFT in which the anomaly cancelling fermions are integrated out can not be made arbitrarily high without losing calculability. If a gauge anomaly remains uncanceled it eventually results in a loss of renormalisability. For an EFT with gauge anomalies there is a fundamental cutoff Λ_R at which renormalisability is lost, and for an anomalous U(1) gauge theory this is given by [126]

$$M \lesssim m_{Z'} \left(\frac{64\pi^3}{|g_R'^3 \mathcal{A}_{Z'Z'Z'}|} \right) \equiv \Lambda_R, \quad (4.12)$$

where $g_R' \equiv g'(\Lambda_R)$ and $\mathcal{A}_{Z'Z'Z'} = \text{Tr}[z^3]$ is the U(1)³ anomaly coefficient in the EFT below the scale of the exotics M . Therefore, the requirement that the gauge theory remains renormalisable places an upper limit on the scale of the anomaly cancelling exotics M .

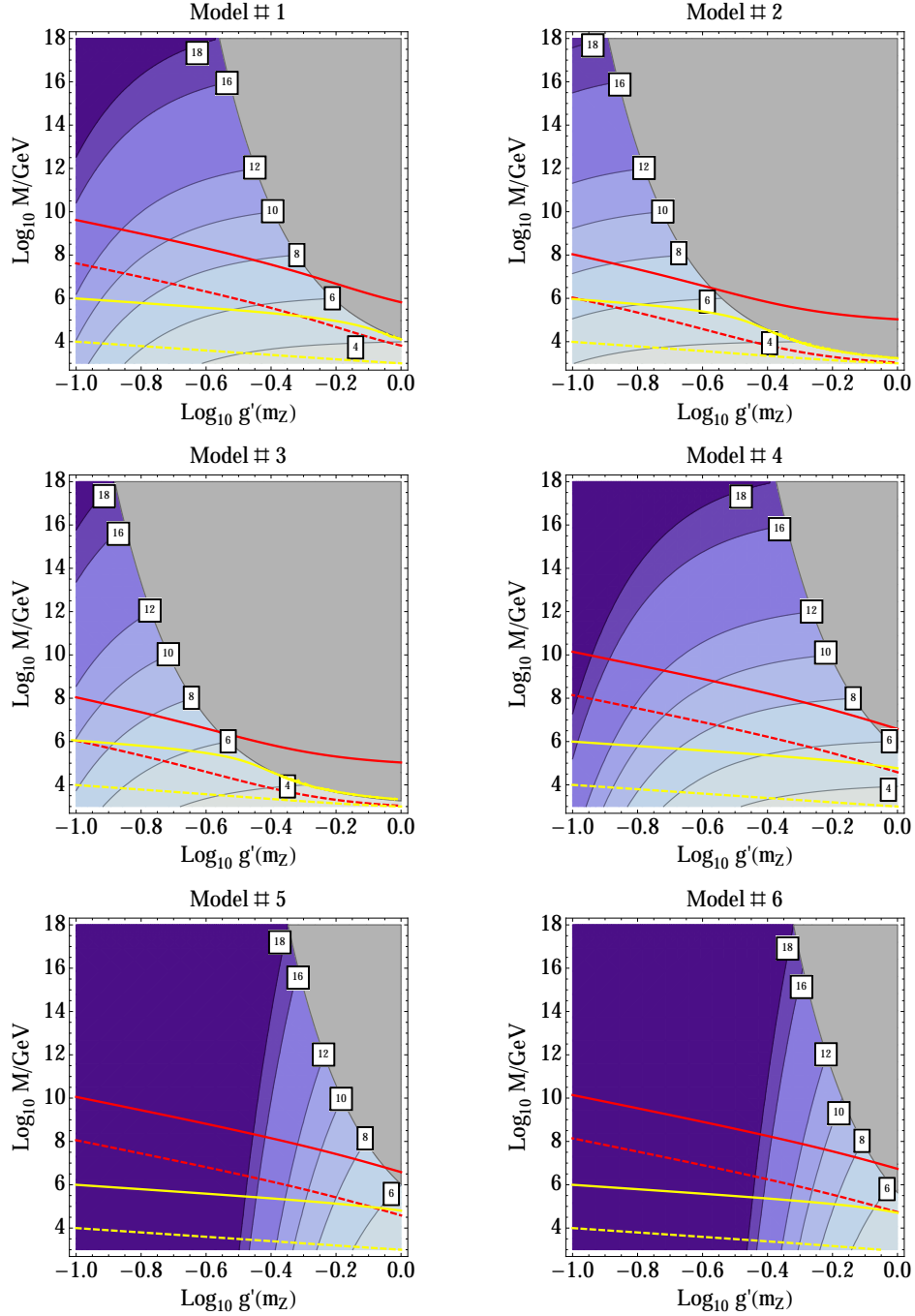


FIGURE 4.1: Assuming $m_{Z'} \simeq 1$ TeV and $m_{\text{DM}} \sim m_Z$ the PURPLE CONTOURS show the scale Λ_P at which the $U(1)'$ coupling g' runs non-perturbative in Models #1-#6. The boxes show values of $\text{Log}_{10}[\Lambda_P/\text{GeV}]$. The scale Λ_P depends on $g'(m_Z)$, and M , the scale of the anomaly cancelling fermions. Only the contributions from the SM fermions, DM, and anomaly cancelling fermions are used in the RG evolution. The GREY region indicates that $\Lambda_P < M$, and new physics enters at Λ_P regardless of M . The RED CURVES show the maximum scale at which exotics must enter to prevent the loss of renormalisability Λ_R for $m_{Z'} \sim 1$ TeV (DASHED), and 100 TeV (SOLID). For exotics which acquire mass through v' , the VEV that breaks $U(1)'$, M and m_Z are related. We show the restriction $M \lesssim v' \simeq m_{Z'}/g'$, as YELLOW CURVES for $m_{Z'} \sim 1$ TeV (DASHED), and 100 TeV (SOLID).

The anomaly cancelling exotics must enter at, or prior to, the scale Λ_R , as determined by Eq. (4.12). Moreover, if we suppose that the exotics enter at the highest possible scale, $M = \Lambda_R$, then Eq. (4.12) implies the following model independent upper bound on the coupling for a given set of charges

$$\frac{|g'_R|^3 \mathcal{A}_{Z'Z'Z'}}{64\pi^3} \lesssim \frac{m_{Z'}}{M} \lesssim 1, \quad (4.13)$$

since a reliable EFT must satisfy $m_{Z'} \lesssim \Lambda_R$. For $m_{Z'} \sim M$ this requirement does not significantly constrain the parameter space, but stronger bounds are obtained for specific values of $m_{Z'}$. To derive a useful constraint we take a range of values for M and find the coupling g_R which saturates the inequality Eq. (4.13) for $m'_Z = 1$ TeV and 100 TeV. Running g'_R from M to the scale $m_{Z'}$ (via Eq. (4.9)), gives a bound on the low energy coupling $g'(m_Z)$.

For $m_{Z'} \ll M$ the exotics must enter to prevent the loss of renormalisability prior to the scale at which one anticipates a Landau pole, i.e. $\Lambda_R \ll \Lambda_P$. Furthermore, the mass scale of the exotics is characteristically set by the $U(1)'$ breaking scale v' , i.e. $M \lesssim v' \simeq \frac{m_{Z'}}{g'(m_{Z'})}$ (cf. Eq. (4.2)). In this case the exotics must typically enter earlier than dictated by perturbativity or renormalisability considerations. The scale of EFT breakdown Λ_R and the requirement that $M \lesssim v'$ are both shown in Figure 4.1 for $m_{Z'} = 1$ TeV, and 100 TeV.

4.3 Dark Matter Freeze-out via an Axial Vector

One of the leading motivations for considering a new abelian gauge boson with only axial vector couplings to the SM fermions is the prospect of providing a potential mediator between DM and SM fermion interaction. As such it is of interest to consider the possibility of successful thermal freeze-out of the DM, with the relic density of DM determined by annihilation to SM states mediated by the axial vector. Here we will restrict ourselves to the scenario in which the charges of the DM χ and SM fermions f are fixed to be Model #2 of Table 3.2. Further, we assume that the Higgs is not charged under $U(1)'$, and only consider $\bar{\chi}\chi \rightarrow \bar{f}f$ annihilation. A similar analysis could be carried out for alternative models.

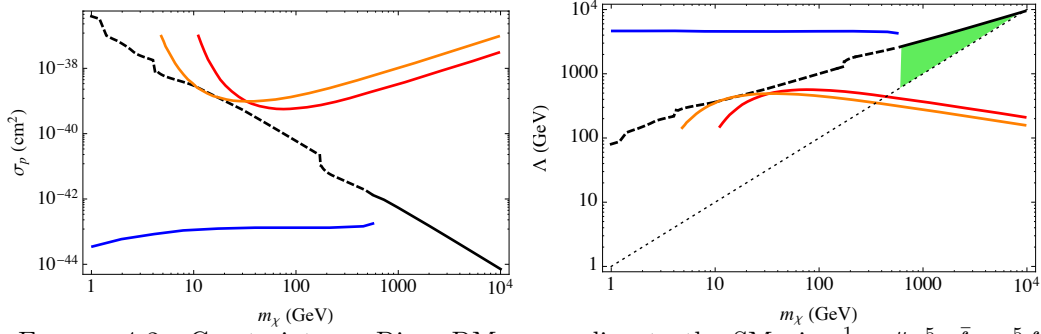


FIGURE 4.2: Constraints on Dirac DM χ coupling to the SM via $\frac{1}{\Lambda^2} \bar{\chi} \gamma^\mu \gamma^5 \chi \bar{f} \gamma_\mu \gamma^5 f$ coming from PICO60 (RED) [130], PICO2L (ORANGE) [131], and CMS monojet searches (BLUE) [132]. The LH panel shows the $\sigma_{\text{SD}}-m_\chi$ plane. The RH plot gives the same information in the $\Lambda-m_\chi$ plane. The BLACK curve shows the Λ such that DM freeze-out reproduces the correct relic density, the curve is dashed where such couplings are in tension with direct searches. For DM with mass $600 \text{ GeV} \lesssim m_\chi \lesssim 10 \text{ TeV}$ the correct relic density can be reproduced without conflicting with direct constraints. The GREEN SHADED region indicates parameter regions where the DM density set by freeze-out is below the observed relic density. The thin DOTTED LINE on RH plot indicates the regime $m_\chi \gtrsim \Lambda$ where the EFT is not reliable.

If the Z' is heavy relative to the DM and SM states, the mediator can be integrated out yielding a dimension six operator $\frac{1}{\Lambda^2} \bar{\chi} \gamma^\mu \gamma^5 \chi \bar{f} \gamma_\mu \gamma^5 f$ connecting DM with SM fermions, with $\Lambda \equiv m_{Z'}/g' \sqrt{(2z_q)(2z_{\text{DM}})}$. For Model #2 we have $\sqrt{4z_q z_{\text{DM}}} = 6$. The cross section for Dirac DM annihilating to SM quarks via this operator is [63]

$$\sigma_{\text{ann}} v = \frac{3m_\chi^2}{2\pi\Lambda^4} \sum_q \left(1 - \frac{m_q^2}{m_\chi^2}\right)^{1/2} \left[\frac{m_q^2}{m_\chi^2} + v^2 \left(\frac{8m_\chi^4 - 22m_q^2 m_\chi^2 + 17m_q^4}{24m_\chi^2(m_\chi^2 - m_q^2)} \right) \right] + \mathcal{O}(v^4). \quad (4.14)$$

where v is the DM relative velocity. Thus the requirement that the annihilation cross section is appropriate to give the observed DM relic density constrains the magnitude of Λ for a given DM mass m_χ . Following [127–129], in Figure 4.2 we show the value of Λ required to obtain the observed relic density as m_χ varies. Note that the EFT is no longer reliable if the DM mass exceeds the cutoff, so we require $m_{\text{DM}} \lesssim \Lambda$, as indicated by the dashed line in the RH panel of Figure 4.2. This EFT requirement can be re-expressed as a constraint on the Z' mass and coupling g' , as in Eq. (4.1).

The operator induces spin-dependent DM-nucleon scattering and thus can be searched for via direct detection experiments. For Dirac fermion DM scattering with quarks, mediated via a heavy axial vector the spin-dependent scattering cross section with protons is [127–129]

$$\sigma_p \approx \frac{4}{\pi\Lambda^4} \mu_p^2 \left(\sum_{q=u,d,s} \Delta_q^p \right)^2, \quad (4.15)$$

where $\mu_p \equiv \frac{m_\chi m_p}{m_\chi + m_p}$ is the reduced mass, and Δ_q^p is the spin content of the nucleon [133]; we use $\sum_q \Delta_q^p \approx 0.37$. A smaller Λ , from larger couplings or equivalently lighter mediators, corresponds to a higher scattering rate. Given the scattering cross section σ_p we can apply the current direct detection limits to the EFT, and derive a lower bound on Λ . We use the limit from the PICO experiment [130, 131] to put a constraint on Λ , see Figure 4.2. We have not included RG running, see e.g. [42], but this is expected to have only a mild effect in this case.

Additionally, indirect detection signals due to DM annihilation producing photons and neutrinos are searched for by Fermi [29], IceCube [134] and Super-Kamiokande [135]; these can provide complementary constraints. A full analysis is beyond the scope of this work, however see e.g. [105, 128] for further discussion.

The axial vector can also mediate DM production through collisions of SM states, and thus searches at colliders for events with missing energy constrain the production cross section. Figure 4.2 displays limits from CMS searches with $\sqrt{s} = 13$ TeV and 12.9 fb^{-1} [132]. The CMS analysis shown assumes a simplified model with $z_q g' = z_\chi g' = 0.05$. In this limit the mediator is heavy enough that it is not kinematically accessible, and we cutoff the limit before on-shell effects affect the line shape; small variations in the couplings can be absorbed into $m_{Z'}$ with little impact. An EFT should give a similar limit, and in the RH plot we refashion the CMS limit in terms of an EFT by identifying $\Lambda \equiv m_{Z'}/g' \sqrt{(2z_q)(2z_{\text{DM}})}$; this is strictly only reliable for $\sqrt{s} < m_{Z'}$. If the axial vector mass is comparable to LHC energies ($m_{Z'} \lesssim \sqrt{s} = 13$ TeV) the EFT may break down and this requires a UV completion, examples of which we have outlined above. For discussions of on-shell mediator effects see e.g. [20, 63, 66, 69, 108–110].

For $600 \text{ GeV} \lesssim m_\chi \lesssim 10 \text{ TeV}$ the DM relic density can be reproduced without conflict with constraints. This viable parameter space corresponds to $1 \text{ TeV} \lesssim \Lambda \lesssim 10 \text{ TeV}$, thus for moderate couplings (say $0.01 \lesssim g' \lesssim 1$) the axial vector is of order $60 \text{ GeV} \lesssim m_{Z'} \lesssim 60 \text{ TeV}$. However, LHC constraints typically require $m_{Z'} \gtrsim 1 \text{ TeV}$ for couplings $g' \sim \mathcal{O}(0.1)$ [136].

The above discussion assumes the DM relic abundance is set by freeze-out, in alternative scenarios these requirements will vary. For instance, in Asymmetric Dark Matter [137] one desires that the density of DM-antiDM pairs is reduced below the observed relic density, such that a DM-antiDM asymmetry can be responsible for the late time abundance. Thus

this scenario requires even more efficient annihilation, which shrinks the viable parameter space; see [63, 138] for studies of DM annihilation via $\bar{\chi}\gamma^\mu\gamma^5\chi\bar{f}\gamma_\mu\gamma^5f$ in Asymmetric Dark Matter. Furthermore, in parameter regions in which the DM density is not reduced below the observed relic density, the correct abundance might still be obtained via other mechanisms, e.g. entropy injection (e.g. [139]), DM freeze-in (e.g. [140–142]), or thermal inflation (e.g. [143, 144]).

4.4 Discussion

Axial vectors have been motivated in a number of different contexts. For instance, they appear commonly as mediators for DM interactions with SM states. While many studies consider scenarios with axial vector gauge bosons, they often neglect to confront the challenges of anomaly cancellation. Ensuring that a model is anomaly free is crucial for the gauge theory to be consistent, and successful anomaly cancellation typically requires new states which are charged under the SM gauge group. Moreover, as we have argued here, these new fermions can not be arbitrarily separated in mass from the axial vector.

Thus it is important to consider UV completions as these new exotics required for anomaly cancellation are potentially observable at colliders. In particular, unless $U(1)'$ charges differ in each SM generation, an axial vector which couples to quarks requires new colored fermions for anomaly cancellation. In the case of a universal axial vector with couplings to DM that thermally produce the observed relic density, the new colored fermions should be at the 1-10 TeV scale, and can be probed in the future.

Additionally, when the Z' is accessible at colliders, limits arise from resonance searches. Current LHC limits from dijet (dilepton) searches for axial vectors with $g' \sim 0.1$ typically require $m_{Z'} \gtrsim 1$ TeV ($m_{Z'} \gtrsim 3$ TeV) [66, 105, 136, 145], which would weaken somewhat if the Z' has a large branching fraction to DM, or not be applicable if the Z' is leptophilic (leptophobic). Both of these scenarios occur in the models we have discussed. In the case of Z - Z' mixing, there are also limits from electroweak precision constraints [16, 49, 123]. Moreover, if there are exotic Higgs states to give mass to the new fermions, this can lead to other bounds such as variations in Higgs couplings to SM states, see e.g. [146], or contributions to the invisible Higgs width [147, 148]. Furthermore, after $U(1)'$ breaking states with the same SM quantum numbers will generically mix (and beforehand if the

states have identical charges) this f - f' mixing is constrained by electroweak precision and flavour observables. However, these constraints are typically model dependent, see e.g. [149]. A full analysis of the constraints, and model dependence, of each of the scenario considered here is beyond the scope of this work.

In conclusion the purpose of *Chapter 3* and *4* has been two-fold: Firstly we have provided anomaly free, UV complete reference models for axial vector gauge bosons coupling to SM fermions. In the course of deriving the anomaly-free sets of fermions we have explored a number of general methods for constructing such models. Secondly, we wished to highlight that in neglecting the additional states required for anomaly cancellation, one omits a number of potentially important constraints, such as collider searches for anomaly cancelling exotics, the need for new scalars to give mass to exotics, the possibility of low $U(1)'$ Landau poles, and potentially the loss of renormalisability, all which should be taken into consideration in any full model.

Chapter 5

CONCLUSION

This thesis has explored SM and BSM phenomenology in the case of $U(1)'$ extension of the SM and the application to DM physics including the direct, in-direct detection of DM, and collider search at LHC. A comprehensive study of top-philic vector portal DM simplified models and anomaly cancellation for axial-vector DM mediators have been presented.

In the top-philic model study, the parameter space of DM and Z' masses are presented in order to reproduce the current relic density $\Omega_{\text{DM}} h^2 \approx 0.12$. We find that direct detection searches and EWPT of Z - Z' mixing provides the sharpest limits compared to in-direct and collider searches in the case that the DM and top couplings are fixed from the relic density. We further developed the first phenomenology method for addressing the ambiguity arising from the chirality of top by considering the ratio of cross sections in the mono-jet and mono-photon searches of DM at LHC.

Anomaly cancellation for $U(1)'$ extension of SM has been extensively studied in this thesis especially for the case that the Z' is a pure axial-vector. We have developed anomaly-free spectra and UV complete models for different motivated purposes. The theoretical and phenomenological limits coming from the anomaly cancelling exotics have been considered and these determine the parameter space for the future search of axial-vector Z' and the exotics. Moreover, we provide further constraints for the parameter space in the case that DM relic density is set by the freeze-out mechanism via the axial-vector Z' portal. Following our work, there has been further exploration of anomaly free models [150, 151] which build upon our results.

Searching for DM driven from the theory and phenomenology of BSM is an ongoing journey and we rely on the forthcoming experimental results to guide today's and the next generation physicists. This thesis provides a new insight for BSM in a minimal extension of SM scenario and has a potential to be tested in the near future.

Appendix A

AXIAL VECTOR VERSUS VECTOR IN SM AND BSM

A.1 Axial-Vector Verse Vector in $gg \rightarrow Z(or Z') + j$

In this appendix, we investigate the difference between the axial vector and vector contribution in loop-induced process, $gg \rightarrow Z(or Z') + j$, which strongly related to our DM mono-jet study for top-philic model. The production cross section of $gg \rightarrow Z(or Z') + j$ is determined generically by four parameters:

- the momentum of the jet p_t
- the loop fermion mass m_f
- the gauge coupling
- the mass of vector boson M_Z or $M_{Z'}$

When a vector boson couples to SM fermion contents with both axial and vector couplings, we find the axial vector contribution has the larger branch ratio for the cross section due to the loop structure in Figure A.1. The states of the jet: the jet from axial vector coupling is mainly a *initial state radiation (ISR)* and the vector coupling channel only has *final state radiation (FSR)* because of Furry theorem. We show the cross section difference in Figure A.2 and it shows the cross section for axial vector is about $\mathcal{O}(1)$ larger than the

vector for a given jet p_t . Then we further study the mass of loop fermion effect in the following subsections.

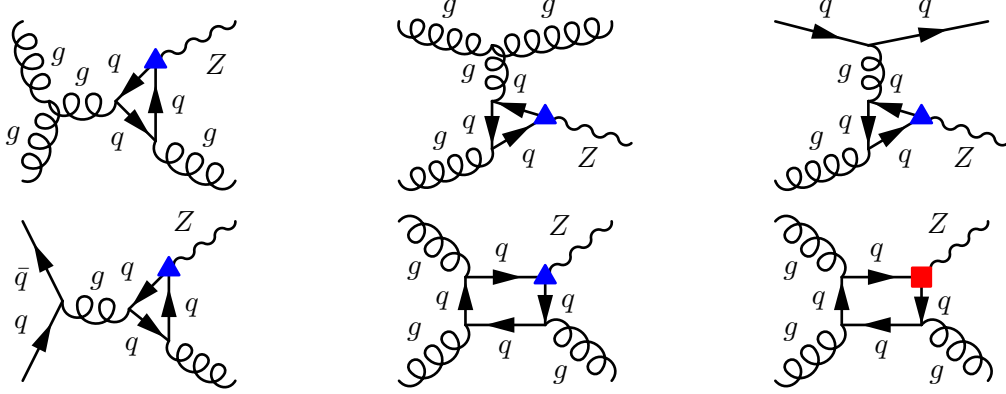


FIGURE A.1: The Feynman diagrams for $gg \rightarrow Z(\text{or } Z') + j$. The RED BOX vertex is the vector coupling of Z and the BLUE TRIANGULAR vertex is the axial vector coupling of Z . The jet from the axial vector coupling channel mainly is a initial state jet. On the other hand, the vector coupling diagram only has the final state jet.

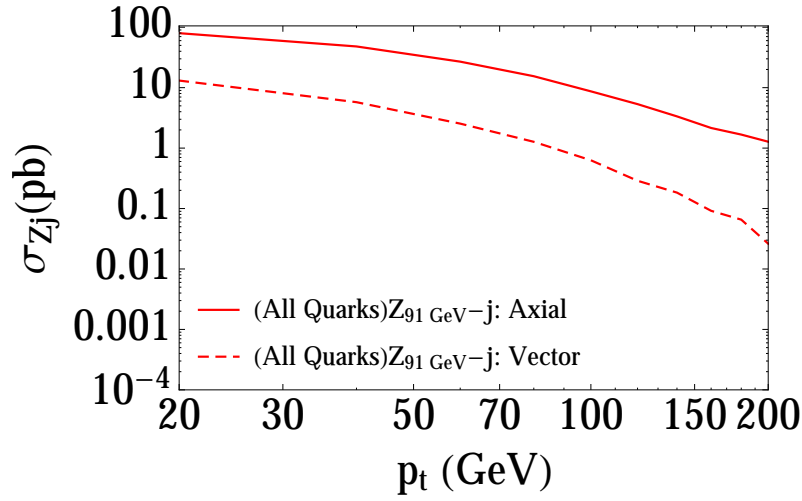


FIGURE A.2: $g g \rightarrow Z + j$ with all flavor quarks in the fermion loop.

A.1.1 In Standard Model $M_Z = 91$ GeV

In Figure A.2, we consider all flavor of quarks in the loop and we will study the effect from SM quark mass hierarchy, i.e. $m_t \gg m_q$ where q are other light flavor quarks, which leads to the the result that mass influences the production cross section which indeed is controlled by mass of top quark[152].

We assume the light flavor quarks are massless and massive top in the loop process of $gg \rightarrow Z + j$, i.e. $m_u = m_d = m_c = m_s = m_b = 0$ and $m_t = 172$ GeV and the axial-vector and vector couplings of Z are in the convention (for simplification purpose, $g_Z \equiv 1$):

$$g_{Vu} = g_z \times \left(\frac{1}{4} - \frac{2}{3}\sin^2\theta_w\right) \approx 0.096; \quad g_{Au} = g_z \times \left(\frac{1}{4}\right) = 0.25; \quad (\text{A.1})$$

$$g_{Vd} = g_z \times \left(-\frac{1}{4} + \frac{1}{3}\sin^2\theta_w\right) \approx -0.17; \quad g_{Ad} = g_z \times \left(-\frac{1}{4}\right) = -0.25; \quad (\text{A.2})$$

Then we scan the individual quark contribution for the axial vector Z production cross section at jet $p_t = 20$ GeV ($g_{Au} = -g_{Ad}$ and $g_Z = 1$) and the cross section is indeed determined by mass of top in Eq. (A.5):

$$\begin{aligned} \sigma_{up,A} &= 155.1 \text{ pb} ; \\ \sigma_{down,A} &= 155.8 \text{ pb} \\ &\approx \sigma_{up,A}; \\ \sigma_{charm,A} &= 157.6 \text{ pb} \\ &\approx \sigma_{up,A}; \\ \sigma_{uc,A} &= 623.2 \text{ pb} \\ &\approx (2 \times g_{Au})^2 \times \frac{\sigma_{up,A}}{g_{Au}^2} \\ &= 4 \times \sigma_{up,A}; \\ \sigma_{udc,A} &= 157.6 \text{ pb} \\ &\approx (2 \times g_{Au} + 1 \times g_{Ad})^2 \times \frac{\sigma_{up,A}}{g_{Au}^2} \\ &= (2 \times g_{Au} - 1 \times g_{Au})^2 \times \frac{\sigma_{up,A}}{g_{Au}^2} \\ &= \sigma_{up,A}; \end{aligned} \quad (\text{A.3})$$

$$\begin{aligned} \sigma_{udcsb,A} &= 155 \text{ pb} \\ &\approx (2 \times g_{Au} + 3 \times g_{Ad})^2 \times \frac{\sigma_{up,A}}{g_{Au}^2} \\ &= (2 \times g_{Au} - 3 \times g_{Au})^2 \times \frac{\sigma_{up,A}}{g_{Au}^2} \\ &= \sigma_{up,A}; \end{aligned} \quad (\text{A.4})$$

$$\sigma_{top,A} = 79.87 \text{ pb}$$

$$\begin{aligned}
\sigma_{udcsb+ \text{ massless top},A} &= 0 \text{ pb} \\
&\approx (3 \times g_{Au} + 3 \times g_{Ad})^2 \times \frac{\sigma_{up,A}}{g_{Au}^2} \\
&= (3 \times g_{Au} - 3 \times g_{Au})^2 \times \frac{\sigma_{up,A}}{g_{Au}^2} \\
&= 0 \times \sigma_{up,A}; \\
\sigma_{udcsb+ 172 \text{ GeV top},A} &= 79.71 \text{ pb} \\
&\approx (2 \times g_{Au} + 3 \times g_{Ad})^2 \times \frac{\sigma_{up,A}}{g_{Au}^2} - \sigma_{top,A} \\
&= \sigma_{udcsb,A} - \sigma_{top,A}
\end{aligned} \tag{A.5}$$

While the vector Z production cross section at the same jet $p_t = 20 \text{ GeV}$ ($g_{Vu} = 0.096$, $g_{Vd} = -0.17$ and $g_Z = 1$):

$$\begin{aligned}
\sigma_{up,V} &= 1.198 \text{ pb}; \\
\sigma_{down,V} &= 3.721 \text{ pb}; \\
\sigma_{charm,V} &= 1.188 \text{ pb} \\
&\approx \sigma_{up,V}; \\
\sigma_{uc,V} &= 4.788 \text{ pb} \\
&\approx (2 \times g_{Vu})^2 \times \frac{\sigma_{up,V}}{g_{Vu}^2} \\
&= 4 \times \sigma_{up,V}; \\
\sigma_{udc,V} &= 0.06274 \text{ pb} \\
&\approx (2 \times g_{Vu} + 1 \times g_{Vd})^2 \times \frac{\sigma_{up,V}}{g_{Vu}^2};
\end{aligned} \tag{A.6}$$

$$\begin{aligned}
\sigma_{udcsb,V} &= 13.14 \text{ pb} \\
&\approx (2 \times g_{Vu} + 3 \times g_{Vd})^2 \times \frac{\sigma_{up,V}}{g_{Vu}^2};
\end{aligned} \tag{A.7}$$

$$\begin{aligned}
\sigma_{top,V} &= 0.004511 \text{ pb} \\
\sigma_{udcsb+ \text{ massless Top},V} &= 6.4 \text{ pb} \\
&\approx (3 \times g_{Vu} + 3 \times g_{Vd})^2 \times \frac{\sigma_{up,V}}{g_{Vu}^2}; \\
\sigma_{udcsb+ 172 \text{ GeV Top},V} &= 13.1 \text{ pb} \\
&\approx (2 \times g_{Vu} + 3 \times g_{Vd})^2 \times \frac{\sigma_{up,V}}{g_{Vu}^2} - \sigma_{top,V} \\
&= \sigma_{udcsb,V} - \sigma_{top,V} \\
&\approx \sigma_{udcsb,V};
\end{aligned} \tag{A.8}$$

We show the $\sigma - p_t$ as in Figure A.2 for axial vector and vector for the above individual channels:

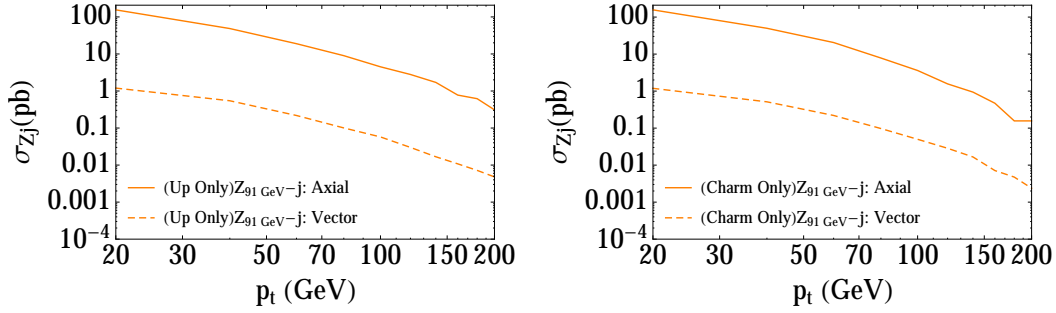


FIGURE A.3: LEFT: $g g \rightarrow Z + j$ with only up quark. RIGHT: $g g \rightarrow Z + j$ with only charm quark

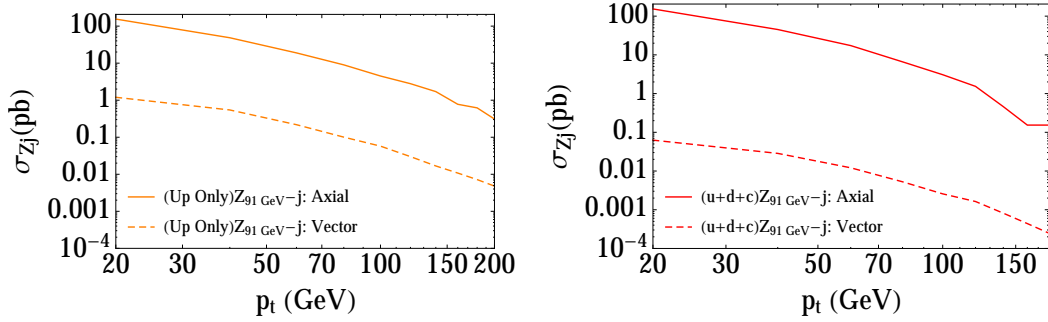


FIGURE A.4: LEFT: $g g \rightarrow Z + j$ with up and charm. RIGHT: $g g \rightarrow Z + j$ with up, down and charm. These two plots show the cross section combination from Eq. (A.3) and Eq. (A.6).

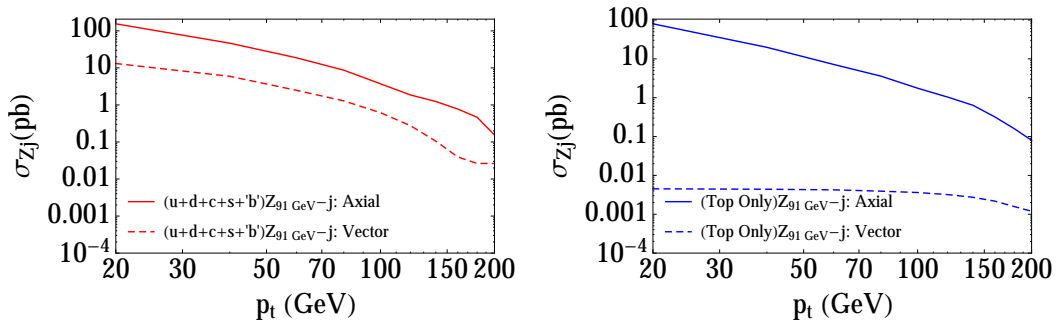


FIGURE A.5: LEFT: $g g \rightarrow Z + j$ with $u+d+c+s+b'$. RIGHT: $g g \rightarrow Z + j$ with top only. The combination of these two plots will lead to Figure A.2 and cancellation effect from Eq. (A.5) only happens for axial vector coupling since the vector contribution from Eq. (A.8) is negligible.

The contribution from massive top to the cross section for vectorial Z is relatively smaller than light quarks. It can be understood by considering the threshold of the center mass energy \sqrt{s} to produce massive top in the loop plus a loop-induced radiative jet (FSR) which is harder than the axial vector case which has a ISR jet. We demonstrate the histogram plot for the threshold energy differences in Figure A.6 and A.7 (jet $p_t = 20$ GeV and total number of events = 1,000):

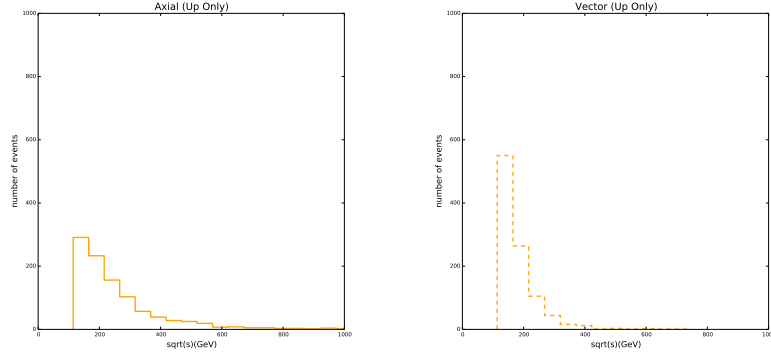


FIGURE A.6: The histogram plot of \sqrt{s} to produce $Z(91 \text{ GeV}) + j(20 \text{ GeV})$ with only massless up quark in the loop. LEFT: $g g \rightarrow Z_{91 \text{ GeV}} \text{ (Axial)} + j$ with up only. RIGHT: $g g \rightarrow Z_{91 \text{ GeV}} \text{ (Vector)} + j$ with up only. Both plots show the threshold of \sqrt{s} are about the same for axial vector and vector coupling for ISR or FSR since the loop fermion is massless.

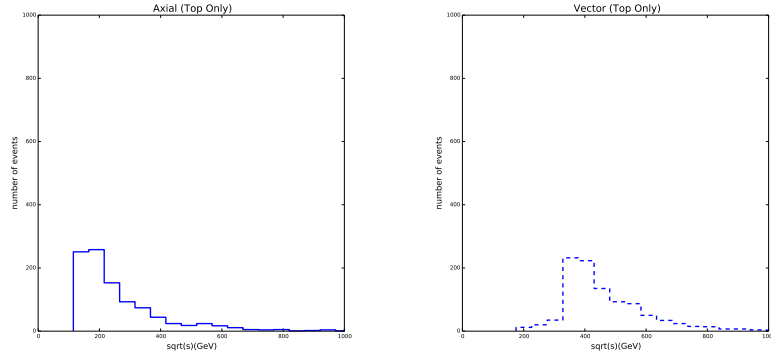


FIGURE A.7: The histogram plot of \sqrt{s} to produce $Z(91 \text{ GeV}) + j(20 \text{ GeV})$ with only massive top in the loop. LEFT: $g g \rightarrow Z_{91 \text{ GeV}} \text{ (Axial)} + j$ with top only. RIGHT: $g g \rightarrow Z_{91 \text{ GeV}} \text{ (Vector)} + j$ with top only. The production of a FSR from vector coupling Z needs more \sqrt{s} due to the massive top in the loop.

A.1.2 Heavy Z' with fixed couplings $g_A=g_V=0.1$

We rescale the coupling $g_A=g_V=0.1$ for simplification purpose and discuss the case of heavy vector boson Z' production. We follow the same procedure as the discussion in SM. In Figure A.8, we show the axial vector and vector production difference of Z in the cases of light loop fermion and massive top quark with our couplings simplification which is consistent with our previous results. The vector coupling contribution is suppressed by the FSR when massive top is in the loop.

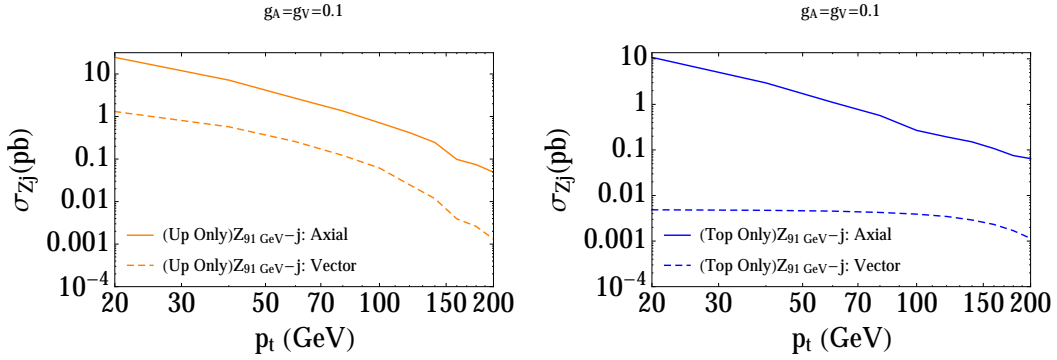


FIGURE A.8: LEFT: $g g \rightarrow Z + j$ with up only when $g_A=g_V=0.1$. $M_Z = 91$ GeV. RIGHT: $g g \rightarrow Z + j$ with top only when $g_A=g_V=0.1$. $M_Z = 91$ GeV

Then we increase the vector boson mass to 1 TeV:

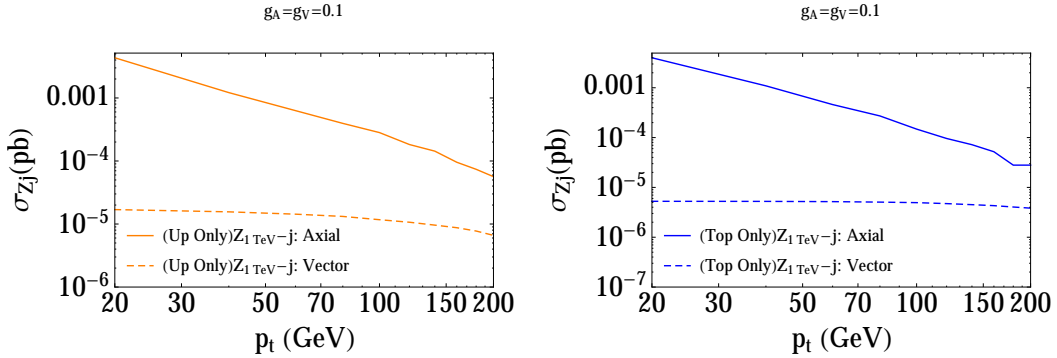


FIGURE A.9: LEFT: $g g \rightarrow Z' + j$ with up only when $g_A=g_V=0.1$. $M_{Z'} = 1$ TeV. RIGHT: $g g \rightarrow Z + j$ with top only when $g_A=g_V=0.1$. $M_{Z'} = 1$ TeV

When Z' mass becomes heavier than the top mass, the cross section differences become the same for both light quark and top. The center mass energy threshold histograms have shown the minimal $\sqrt{s} \gtrsim 1$ TeV in Figure A.10 and A.10.

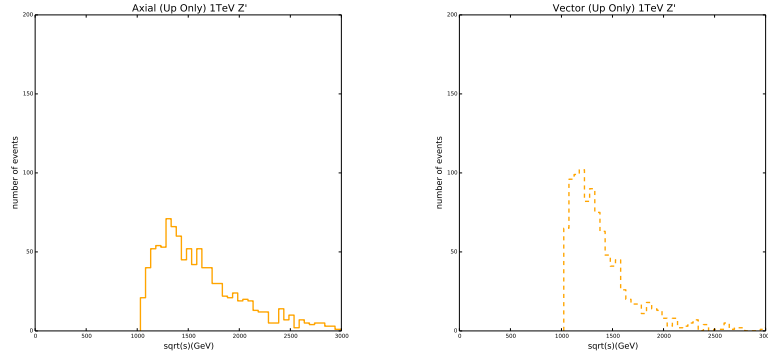


FIGURE A.10: LEFT: $g g \rightarrow Z_{1TeV}$ (Axial) + j with up quark only. RIGHT: $g g \rightarrow Z_{91GeV}$ (Vector) + j with up quark only

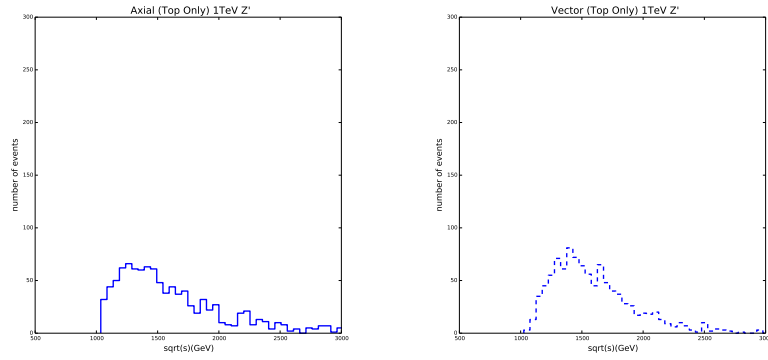


FIGURE A.11: LEFT: $g g \rightarrow Z_{1TeV}$ (Axial) + j with top quark only. RIGHT: $g g \rightarrow Z_{91GeV}$ (Vector) + j with top quark only

The summary of this appendix is the axial vector coupling of a vector boson Z (or Z') dominating contribution to the $gg \rightarrow Z$ (or Z') + j production cross section. We investigate the loop structure and show the center mass energy threshold difference due to the state of the jet along with Z (or Z') which supports our top-philic Z' and axial vector studies where we mainly focus on the axial vector coupling of Z' .

Appendix B

Copyright Permissions

4/25/2017

Creative Commons — Attribution 4.0 International — CC BY 4.0



[Creative Commons](#)

Creative Commons License Deed

Attribution 4.0 International (CC BY 4.0)

This is a human-readable summary of (and not a substitute for) the [license](#).
[Disclaimer](#)

You are free to:



Share — copy and redistribute the material in any medium or format



Adapt — remix, transform, and build upon the material
for any purpose, even commercially.

The licensor cannot revoke these freedoms as long as you follow the license terms.



Under the following terms:



Attribution — You must give [appropriate credit](#), provide a link to the license, and [indicate if changes were made](#). You may do so in any reasonable manner, but not in any way that suggests the licensor endorses you or your use.

No additional restrictions — You may not apply legal terms or [technological measures](#) that legally restrict others from doing anything the license permits.

Notices:

You do not have to comply with the license for elements of the material in the public domain or where your use is permitted by an applicable [exception or limitation](#).

No warranties are given. The license may not give you all of the permissions necessary for your intended use. For example, other rights such as [publicity, privacy, or moral rights](#) may limit how you use the material.

ELSEVIER

Q

SEARCH

CART

≡

MENU

Personal use

Authors can use their articles, in full or in part, for a wide range of scholarly, non-commercial purposes as outlined below:

- Use by an author in the author’s classroom teaching (including distribution of copies, paper or electronic)
- Distribution of copies (including through e-mail) to known research colleagues for their personal use (but not for Commercial Use)
- Inclusion in a thesis or dissertation (provided that this is not to be published commercially)
- Use in a subsequent compilation of the author’s works
- Extending the Article to book-length form
- Preparation of other derivative works (but not for Commercial Use)
- Otherwise using or re-using portions or excerpts in other works

ELSEVIER

Q

SEARCH

CART

≡

MENU

These rights apply for all Elsevier authors who publish their article as either a subscription article or an open access article. In all cases we require that all Elsevier authors always include a full acknowledgement and, if appropriate, a link to the final published version hosted on Science Direct.

CITED LITERATURE

- [1] F. Englert and R. Brout. Broken symmetry and the mass of gauge vector mesons. *Phys. Rev. Lett.*, 13:321–323, Aug 1964. doi: 10.1103/PhysRevLett.13.321.
- [2] Georges Aad et al. Combined search for the Standard Model Higgs boson using up to 4.9 fb^{-1} of pp collision data at $\sqrt{s} = 7 \text{ TeV}$ with the ATLAS detector at the LHC. *Phys. Lett.*, B710:49–66, 2012. doi: 10.1016/j.physletb.2012.02.044.
- [3] Serguei Chatrchyan et al. Combined results of searches for the standard model Higgs boson in pp collisions at $\sqrt{s} = 7 \text{ TeV}$. *Phys. Lett.*, B710:26–48, 2012. doi: 10.1016/j.physletb.2012.02.064.
- [4] F. Zwicky. Die Rotverschiebung von extragalaktischen Nebeln. *Helvetica Physica Acta*, 6:110–127, 1933.
- [5] Maxim Markevitch, A. H. Gonzalez, D. Clowe, A. Vikhlinin, L. David, W. Forman, C. Jones, S. Murray, and W. Tucker. Direct constraints on the dark matter self-interaction cross-section from the merging galaxy cluster 1E0657-56. *Astrophys. J.*, 606:819–824, 2004. doi: 10.1086/383178.
- [6] K. G. Begeman, A. H. Broeils, and R. H. Sanders. Extended rotation curves of spiral galaxies: Dark haloes and modified dynamics. *Mon. Not. Roy. Astron. Soc.*, 249:523, 1991.
- [7] Vernon D. Barger and R. J. N. Phillips. Collider physics: 1993. In *7th Summer School Jorge Andre Swieca: Particles and Fields Sao Paulo, Brazil, January 10-23, 1993*, pages 0064–168, 1993.
- [8] Paul Langacker. The Physics of Heavy Z' Gauge Bosons. *Rev. Mod. Phys.*, 81: 1199–1228, 2009. doi: 10.1103/RevModPhys.81.1199.

- [9] B. Pontecorvo. Inverse beta processes and nonconservation of lepton charge. *Sov. Phys. JETP*, 7:172–173, 1958. [Zh. Eksp. Teor. Fiz.34,247(1957)].
- [10] Ziro Maki, Masami Nakagawa, and Shoichi Sakata. Remarks on the unified model of elementary particles. *Prog. Theor. Phys.*, 28:870–880, 1962. doi: 10.1143/PTP.28.870.
- [11] Nicola Cabibbo. Unitary Symmetry and Leptonic Decays. *Phys. Rev. Lett.*, 10: 531–533, 1963. doi: 10.1103/PhysRevLett.10.531. [,648(1963)].
- [12] Makoto Kobayashi and Toshihide Maskawa. CP Violation in the Renormalizable Theory of Weak Interaction. *Prog. Theor. Phys.*, 49:652–657, 1973. doi: 10.1143/PTP.49.652.
- [13] Ling-Lie Chau and Wai-Yee Keung. Comments on the Parametrization of the Kobayashi-Maskawa Matrix. *Phys. Rev. Lett.*, 53:1802, 1984. doi: 10.1103/PhysRevLett.53.1802.
- [14] C. Patrignani et al. Review of Particle Physics. *Chin. Phys.*, C40(10):100001, 2016. doi: 10.1088/1674-1137/40/10/100001.
- [15] Bob Holdom. Two U(1)’s and Epsilon Charge Shifts. *Phys. Lett.*, B166:196–198, 1986. doi: 10.1016/0370-2693(86)91377-8.
- [16] K. S. Babu, Christopher F. Kolda, and John March-Russell. Implications of generalized Z - Z-prime mixing. *Phys. Rev.*, D57:6788–6792, 1998. doi: 10.1103/PhysRevD.57.6788.
- [17] Daniel Feldman, Zuowei Liu, and Pran Nath. The Stueckelberg Z-prime Extension with Kinetic Mixing and Milli-Charged Dark Matter From the Hidden Sector. *Phys. Rev.*, D75:115001, 2007. doi: 10.1103/PhysRevD.75.115001.
- [18] Michael E. Peskin and Tatsu Takeuchi. Estimation of oblique electroweak corrections. *Phys. Rev.*, D46:381–409, 1992. doi: 10.1103/PhysRevD.46.381.
- [19] Anson Hook, Eder Izaguirre, and Jay G. Wacker. Model Independent Bounds on Kinetic Mixing. *Adv. High Energy Phys.*, 2011:859762, 2011. doi: 10.1155/2011/859762.

- [20] Felix Kahlhoefer, Kai Schmidt-Hoberg, Thomas Schwetz, and Stefan Vogl. Implications of unitarity and gauge invariance for simplified dark matter models. *JHEP*, 02:016, 2016. doi: 10.1007/JHEP02(2016)016.
- [21] Mads T. Frandsen, Felix Kahlhoefer, Subir Sarkar, and Kai Schmidt-Hoberg. Direct detection of dark matter in models with a light Z' . *JHEP*, 09:128, 2011. doi: 10.1007/JHEP09(2011)128.
- [22] S. D. Drell and Tung-Mow Yan. Massive Lepton Pair Production in Hadron-Hadron Collisions at High-Energies. *Phys. Rev. Lett.*, 25:316–320, 1970. doi: 10.1103/PhysRevLett.25.316. [Erratum: *Phys. Rev. Lett.*25,902(1970)].
- [23] Puneet Batra, Bogdan A. Dobrescu, and David Spivak. Anomaly-free sets of fermions. *J. Math. Phys.*, 47:082301, 2006. doi: 10.1063/1.2222081.
- [24] JoAnne L. Hewett and Thomas G. Rizzo. Low-Energy Phenomenology of Superstring Inspired $E(6)$ Models. *Phys. Rept.*, 183:193, 1989. doi: 10.1016/0370-1573(89)90071-9.
- [25] Paul Langacker and Jing Wang. $U(1)$ -prime symmetry breaking in supersymmetric $E(6)$ models. *Phys. Rev.*, D58:115010, 1998. doi: 10.1103/PhysRevD.58.115010.
- [26] D. S. Akerib et al. Results on the Spin-Dependent Scattering of Weakly Interacting Massive Particles on Nucleons from the Run 3 Data of the LUX Experiment. *Phys. Rev. Lett.*, 116(16):161302, 2016. doi: 10.1103/PhysRevLett.116.161302.
- [27] D. S. Akerib et al. Results from a search for dark matter in the complete LUX exposure. *Phys. Rev. Lett.*, 118(2):021303, 2017. doi: 10.1103/PhysRevLett.118.021303.
- [28] Andi Tan et al. Dark Matter Results from First 98.7 Days of Data from the PandaX-II Experiment. *Phys. Rev. Lett.*, 117(12):121303, 2016. doi: 10.1103/PhysRevLett.117.121303.
- [29] M. Ackermann et al. Searching for Dark Matter Annihilation from Milky Way Dwarf Spheroidal Galaxies with Six Years of Fermi Large Area Telescope Data. *Phys. Rev. Lett.*, 115(23):231301, 2015. doi: 10.1103/PhysRevLett.115.231301.

- [30] M. Incaglion behalf of the AMS02 Collaboration. AMS02 results after 4 years of data taking on the International Space Station. *Nuovo Cim.*, C39(4):313, 2017. doi: 10.1393/ncc/i2016-16313-y.
- [31] O. Adriani et al. Time Dependence of the Electron and Positron Components of the Cosmic Radiation Measured by the PAMELA Experiment between July 2006 and December 2015. *Phys. Rev. Lett.*, 116(24):241105, 2016. doi: 10.1103/PhysRevLett.116.241105.
- [32] Morad Aaboud et al. Search for dark matter at $\sqrt{s} = 13$ TeV in final states containing an energetic photon and large missing transverse momentum with the ATLAS detector. 2017.
- [33] Morad Aaboud et al. Search for new phenomena in final states with an energetic jet and large missing transverse momentum in pp collisions at $\sqrt{s} = 13$ TeV using the ATLAS detector. *Phys. Rev.*, D94(3):032005, 2016. doi: 10.1103/PhysRevD.94.032005.
- [34] CMS Collaboration. Search for dark matter in association with a top quark pair at $\sqrt{s}=13$ TeV. 2016.
- [35] P. A. R. Ade et al. Planck 2015 results. XIII. Cosmological parameters. *Astron. Astrophys.*, 594:A13, 2016. doi: 10.1051/0004-6361/201525830.
- [36] Miguel Escudero, Asher Berlin, Dan Hooper, and Meng-Xiang Lin. Toward (Finally!) Ruling Out Z and Higgs Mediated Dark Matter Models. *JCAP*, 1612:029, 2016. doi: 10.1088/1475-7516/2016/12/029.
- [37] Jalal Abdallah et al. Simplified Models for Dark Matter and Missing Energy Searches at the LHC. 2014.
- [38] Felix Kahlhoefer. Review of LHC Dark Matter Searches. *Int. J. Mod. Phys.*, A32:1730006, 2017. doi: 10.1142/S0217751X1730006X.
- [39] L. D. Landau. On the angular momentum of a system of two photons. *Dokl. Akad. Nauk Ser. Fiz.*, 60(2):207–209, 1948. doi: 10.1016/B978-0-08-010586-4.50070-5.
- [40] Chen-Ning Yang. Selection Rules for the Dematerialization of a Particle Into Two Photons. *Phys. Rev.*, 77:242–245, 1950. doi: 10.1103/PhysRev.77.242.

- [41] A. Liam Fitzpatrick, Wick Haxton, Emanuel Katz, Nicholas Lubbers, and Yiming Xu. The Effective Field Theory of Dark Matter Direct Detection. *JCAP*, 1302:004, 2013. doi: 10.1088/1475-7516/2013/02/004.
- [42] Francesco D’Eramo, Bradley J. Kavanagh, and Paolo Panci. You can hide but you have to run: direct detection with vector mediators. *JHEP*, 08:111, 2016. doi: 10.1007/JHEP08(2016)111.
- [43] Gregory D. Martinez. A robust determination of Milky Way satellite properties using hierarchical mass modelling. *Mon. Not. Roy. Astron. Soc.*, 451(3):2524–2535, 2015. doi: 10.1093/mnras/stv942.
- [44] Alex Geringer-Sameth, Savvas M. Koushiappas, and Matthew Walker. Dwarf galaxy annihilation and decay emission profiles for dark matter experiments. *Astrophys. J.*, 801(2):74, 2015. doi: 10.1088/0004-637X/801/2/74.
- [45] Brian Patt and Frank Wilczek. Higgs-field portal into hidden sectors. 2006.
- [46] John March-Russell, Stephen M. West, Daniel Cumberbatch, and Dan Hooper. Heavy Dark Matter Through the Higgs Portal. *JHEP*, 07:058, 2008. doi: 10.1088/1126-6708/2008/07/058.
- [47] G. D’Ambrosio, G. F. Giudice, G. Isidori, and A. Strumia. Minimal flavor violation: An Effective field theory approach. *Nucl. Phys.*, B645:155–187, 2002. doi: 10.1016/S0550-3213(02)00836-2.
- [48] Ulrich Haisch, Felix Kahlhoefer, and James Unwin. The impact of heavy-quark loops on LHC dark matter searches. *JHEP*, 07:125, 2013. doi: 10.1007/JHEP07(2013)125.
- [49] K. A. Olive et al. Review of Particle Physics. *Chin. Phys.*, C38:090001, 2014. doi: 10.1088/1674-1137/38/9/090001.
- [50] Kingman Cheung, Kentarou Mawatari, Eibun Senaha, Po-Yan Tseng, and Tzu-Chiang Yuan. The Top Window for dark matter. *JHEP*, 10:081, 2010. doi: 10.1007/JHEP10(2010)081.
- [51] Nicolas Greiner, Kyoungchul Kong, Jong-Chul Park, Seong Chan Park, and Jan-Christopher Winter. Model-Independent Production of a Top-Philic Resonance at the LHC. *JHEP*, 04:029, 2015. doi: 10.1007/JHEP04(2015)029.

- [52] Biplob Bhattacharjee, Debajyoti Choudhury, Keisuke Harigaya, Shigeki Matsumoto, and Mihoko M. Nojiri. Model Independent Analysis of Interactions between Dark Matter and Various Quarks. *JHEP*, 04:031, 2013. doi: 10.1007/JHEP04(2013)031.
- [53] C. B. Jackson, Geraldine Servant, Gabe Shaughnessy, Tim M. P. Tait, and Marco Taoso. Higgs in Space! *JCAP*, 1004:004, 2010. doi: 10.1088/1475-7516/2010/04/004.
- [54] C. B. Jackson, Géraldine Servant, Gabe Shaughnessy, Tim M. P. Tait, and Marco Taoso. Gamma Rays from Top-Mediated Dark Matter Annihilations. *JCAP*, 1307:006, 2013. doi: 10.1088/1475-7516/2013/07/006.
- [55] Yue Zhang. Top Quark Mediated Dark Matter. *Phys. Lett.*, B720:137–141, 2013. doi: 10.1016/j.physletb.2013.01.063.
- [56] Peter Cox, Anibal D. Medina, Tirtha Sankar Ray, and Andrew Spray. Novel collider and dark matter phenomenology of a top-philic $Z^?$. *JHEP*, 06:110, 2016. doi: 10.1007/JHEP06(2016)110.
- [57] Vardan Khachatryan et al. Search for dark matter, extra dimensions, and unparticles in monojet events in proton-proton collisions at $\sqrt{s} = 8$ TeV. *Eur. Phys. J.*, C75(5):235, 2015. doi: 10.1140/epjc/s10052-015-3451-4.
- [58] Georges Aad et al. Search for new phenomena in final states with an energetic jet and large missing transverse momentum in pp collisions at $\sqrt{s} = 8$ TeV with the ATLAS detector. *Eur. Phys. J.*, C75(7):299, 2015. doi: 10.1140/epjc/s10052-015-3517-3, 10.1140/epjc/s10052-015-3639-7. [Erratum: *Eur. Phys. J.* C75,no.9,408(2015)].
- [59] Patrick J. Fox, Roni Harnik, Joachim Kopp, and Yuhsin Tsai. Missing Energy Signatures of Dark Matter at the LHC. *Phys. Rev.*, D85:056011, 2012. doi: 10.1103/PhysRevD.85.056011.
- [60] Jessica Goodman, Masahiro Ibe, Arvind Rajaraman, William Shepherd, Tim M. P. Tait, and Hai-Bo Yu. Constraints on Light Majorana dark Matter from Colliders. *Phys. Lett.*, B695:185–188, 2011. doi: 10.1016/j.physletb.2010.11.009.
- [61] Arvind Rajaraman, William Shepherd, Tim M. P. Tait, and Alexander M. Wijangco. LHC Bounds on Interactions of Dark Matter. *Phys. Rev.*, D84:095013, 2011. doi: 10.1103/PhysRevD.84.095013.

-
- [62] Jessica Goodman, Masahiro Ibe, Arvind Rajaraman, William Shepherd, Tim M. P. Tait, and Hai-Bo Yu. Constraints on Dark Matter from Colliders. *Phys. Rev.*, D82: 116010, 2010. doi: 10.1103/PhysRevD.82.116010.
- [63] John March-Russell, James Unwin, and Stephen M. West. Closing in on Asymmetric Dark Matter I: Model independent limits for interactions with quarks. *JHEP*, 08: 029, 2012. doi: 10.1007/JHEP08(2012)029.
- [64] Ulrich Haisch, Felix Kahlhoefer, and Emanuele Re. QCD effects in mono-jet searches for dark matter. *JHEP*, 12:007, 2013. doi: 10.1007/JHEP12(2013)007.
- [65] Ulrich Haisch and Emanuele Re. Simplified dark matter top-quark interactions at the LHC. *JHEP*, 06:078, 2015. doi: 10.1007/JHEP06(2015)078.
- [66] Mikael Chala, Felix Kahlhoefer, Matthew McCullough, Germano Nardini, and Kai Schmidt-Hoberg. Constraining Dark Sectors with Monojets and Dijets. *JHEP*, 07: 089, 2015. doi: 10.1007/JHEP07(2015)089.
- [67] Patrick J. Fox and Ciaran Williams. Next-to-Leading Order Predictions for Dark Matter Production at Hadron Colliders. *Phys. Rev.*, D87(5):054030, 2013. doi: 10.1103/PhysRevD.87.054030.
- [68] Linda M. Carpenter, Andrew Nelson, Chase Shimmin, Tim M. P. Tait, and Daniel Whiteson. Collider searches for dark matter in events with a Z boson and missing energy. *Phys. Rev.*, D87(7):074005, 2013. doi: 10.1103/PhysRevD.87.074005.
- [69] Andrea De Simone, Gian Francesco Giudice, and Alessandro Strumia. Benchmarks for Dark Matter Searches at the LHC. *JHEP*, 06:081, 2014. doi: 10.1007/JHEP06(2014)081.
- [70] Philip Harris, Valentin V. Khoze, Michael Spannowsky, and Ciaran Williams. Closing up on Dark Sectors at Colliders: from 14 to 100 TeV. *Phys. Rev.*, D93(5): 054030, 2016. doi: 10.1103/PhysRevD.93.054030.
- [71] Stephen L. Adler and William A. Bardeen. Absence of higher order corrections in the anomalous axial vector divergence equation. *Phys. Rev.*, 182:1517–1536, 1969. doi: 10.1103/PhysRev.182.1517.

- [72] Adam Alloul, Neil D. Christensen, Céline Degrande, Claude Duhr, and Benjamin Fuks. FeynRules 2.0 - A complete toolbox for tree-level phenomenology. *Comput. Phys. Commun.*, 185:2250–2300, 2014. doi: 10.1016/j.cpc.2014.04.012.
- [73] Thomas Hahn. Generating Feynman diagrams and amplitudes with FeynArts 3. *Comput. Phys. Commun.*, 140:418–431, 2001. doi: 10.1016/S0010-4655(01)00290-9.
- [74] J. Alwall, R. Frederix, S. Frixione, V. Hirschi, F. Maltoni, O. Mattelaer, H. S. Shao, T. Stelzer, P. Torrielli, and M. Zaro. The automated computation of tree-level and next-to-leading order differential cross sections, and their matching to parton shower simulations. *JHEP*, 07:079, 2014. doi: 10.1007/JHEP07(2014)079.
- [75] Torbjorn Sjostrand, Stephen Mrenna, and Peter Z. Skands. PYTHIA 6.4 Physics and Manual. *JHEP*, 05:026, 2006. doi: 10.1088/1126-6708/2006/05/026.
- [76] J. de Favereau, C. Delaere, P. Demin, A. Giammanco, V. Lemaître, A. Mertens, and M. Selvaggi. DELPHES 3, A modular framework for fast simulation of a generic collider experiment. *JHEP*, 02:057, 2014. doi: 10.1007/JHEP02(2014)057.
- [77] Yang Bai, Hsin-Chia Cheng, Jason Gallicchio, and Jiayin Gu. Stop the Top Background of the Stop Search. *JHEP*, 07:110, 2012. doi: 10.1007/JHEP07(2012)110.
- [78] Ahmed Ismail, Wai-Yee Keung, Kuo-Hsing Tsao, and James Unwin. Axial Vector Z' and Anomaly Cancellation. 2016.
- [79] Daniel Abercrombie et al. Dark Matter Benchmark Models for Early LHC Run-2 Searches: Report of the ATLAS/CMS Dark Matter Forum. 2015.
- [80] R. Adam et al. Planck 2015 results. I. Overview of products and scientific results. *Astron. Astrophys.*, 594:A1, 2016. doi: 10.1051/0004-6361/201527101.
- [81] Joseph Bramante and James Unwin. Superheavy Thermal Dark Matter and Primordial Asymmetries. *JHEP*, 02:119, 2017. doi: 10.1007/JHEP02(2017)119.
- [82] Asher Berlin, Dan Hooper, and Gordan Krnjaic. Thermal Dark Matter From A Highly Decoupled Sector. *Phys. Rev.*, D94(9):095019, 2016. doi: 10.1103/PhysRevD.94.095019.
- [83] Michael S. Turner and Frank Wilczek. Positron Line Radiation from Halo WIMP Annihilations as a Dark Matter Signature. *Phys. Rev.*, D42:1001–1007, 1990. doi: 10.1103/PhysRevD.42.1001.

-
- [84] Joseph Silk and Mark Srednicki. Cosmic Ray anti-Protons as a Probe of a Photino Dominated Universe. *Phys. Rev. Lett.*, 53:624, 1984. doi: 10.1103/PhysRevLett.53.624.
- [85] John R. Ellis, R. A. Flores, K. Freese, S. Ritz, D. Seckel, and Joseph Silk. Cosmic Ray Constraints on the Annihilations of Relic Particles in the Galactic Halo. *Phys. Lett.*, B214:403–412, 1988. doi: 10.1016/0370-2693(88)91385-8.
- [86] Edward A. Baltz and L. Wai. Diffuse inverse Compton and synchrotron emission from dark matter annihilations in galactic satellites. *Phys. Rev.*, D70:023512, 2004. doi: 10.1103/PhysRevD.70.023512.
- [87] Ilias Cholis, Gregory Dobler, Douglas P. Finkbeiner, Lisa Goodenough, and Neal Weiner. The Case for a 700+ GeV WIMP: Cosmic Ray Spectra from ATIC and PAMELA. *Phys. Rev.*, D80:123518, 2009. doi: 10.1103/PhysRevD.80.123518.
- [88] Juan Zhang, Xiao-Jun Bi, Jia Liu, Si-Ming Liu, Peng-Fei Yin, Qiang Yuan, and Shou-Hua Zhu. Discriminating different scenarios to account for the cosmic $e^+/-$ excess by synchrotron and inverse Compton radiation. *Phys. Rev.*, D80:023007, 2009. doi: 10.1103/PhysRevD.80.023007.
- [89] Adam Martin, Jessie Shelton, and James Unwin. Fitting the Galactic Center Gamma-Ray Excess with Cascade Annihilations. *Phys. Rev.*, D90(10):103513, 2014. doi: 10.1103/PhysRevD.90.103513.
- [90] Jeremy Mardon, Yasunori Nomura, Daniel Stolarski, and Jesse Thaler. Dark Matter Signals from Cascade Annihilations. *JCAP*, 0905:016, 2009. doi: 10.1088/1475-7516/2009/05/016.
- [91] Marco Cirelli, Eugenio Del Nobile, and Paolo Panci. Tools for model-independent bounds in direct dark matter searches. *JCAP*, 1310:019, 2013. doi: 10.1088/1475-7516/2013/10/019.
- [92] D. S. Akerib et al. LUX-ZEPLIN (LZ) Conceptual Design Report. 2015.
- [93] CMS Collaboration. Search for dark matter and graviton produced in association with a photon in pp collisions at $\sqrt{s} = 13$ TeV. 2016.
- [94] Rafael A. Porto and A. Zee. The Private Higgs. *Phys. Lett.*, B666:491–495, 2008. doi: 10.1016/j.physletb.2008.08.001.

- [95] Nima Arkani-Hamed, Andrew G. Cohen, and Howard Georgi. Electroweak symmetry breaking from dimensional deconstruction. *Phys. Lett.*, B513:232–240, 2001. doi: 10.1016/S0370-2693(01)00741-9.
- [96] Hsin-Chia Cheng and Ian Low. Little hierarchy, little Higgses, and a little symmetry. *JHEP*, 08:061, 2004. doi: 10.1088/1126-6708/2004/08/061.
- [97] C. D. Froggatt and Holger Bech Nielsen. Hierarchy of Quark Masses, Cabibbo Angles and CP Violation. *Nucl. Phys.*, B147:277–298, 1979. doi: 10.1016/0550-3213(79)90316-X.
- [98] S. Dawson and E. Furlan. A Higgs Conundrum with Vector Fermions. *Phys. Rev.*, D86:015021, 2012. doi: 10.1103/PhysRevD.86.015021.
- [99] Hong-Jian He, Christopher T. Hill, and Timothy M. P. Tait. Top quark seesaw, vacuum structure and electroweak precision constraints. *Phys. Rev.*, D65:055006, 2002. doi: 10.1103/PhysRevD.65.055006.
- [100] The ATLAS collaboration. Search for pair production of vector-like top quarks in events with one lepton and an invisibly decaying Z boson in $\sqrt{s} = 13$ TeV pp collisions at the ATLAS detector. 2017.
- [101] The ATLAS collaboration. Search for new phenomena in the dilepton final state using proton-proton collisions at $\sqrt{s} = 13$ TeV with the ATLAS detector. 2015.
- [102] Georges Aad et al. Search for high-mass dilepton resonances in pp collisions at $\sqrt{s} = 8$ TeV with the ATLAS detector. *Phys. Rev.*, D90(5):052005, 2014. doi: 10.1103/PhysRevD.90.052005.
- [103] Maria Beltran, Dan Hooper, Edward W. Kolb, Zosia A. C. Krusberg, and Tim M. P. Tait. Maverick dark matter at colliders. *JHEP*, 09:037, 2010. doi: 10.1007/JHEP09(2010)037.
- [104] Shigeki Matsumoto, Satyanarayan Mukhopadhyay, and Yue-Lin Sming Tsai. Singlet Majorana fermion dark matter: a comprehensive analysis in effective field theory. *JHEP*, 10:155, 2014. doi: 10.1007/JHEP10(2014)155.
- [105] Thomas Jacques, Andrey Katz, Enrico Morgante, Davide Racco, Mohamed Rameez, and Antonio Riotto. Complementarity of DM searches in a consistent simplified model: the case of Z' . *JHEP*, 10:071, 2016. doi: 10.1007/JHEP10(2016)071.

- [106] Mihailo Backovic, Alberto Mariotti, and Diego Redigolo. Di-photon excess illuminates Dark Matter. *JHEP*, 03:157, 2016. doi: 10.1007/JHEP03(2016)157.
- [107] Dan Hooper. Z' mediated dark matter models for the Galactic Center gamma-ray excess. *Phys. Rev.*, D91:035025, 2015. doi: 10.1103/PhysRevD.91.035025.
- [108] Oleg Lebedev and Yann Mambrini. Axial dark matter: The case for an invisible Z' . *Phys. Lett.*, B734:350–353, 2014. doi: 10.1016/j.physletb.2014.05.025.
- [109] Oliver Buchmueller, Matthew J. Dolan, Sarah A. Malik, and Christopher McCabe. Characterising dark matter searches at colliders and direct detection experiments: Vector mediators. *JHEP*, 01:037, 2015. doi: 10.1007/JHEP01(2015)037.
- [110] Giorgio Arcadi, Yann Mambrini, and Francois Richard. Z-portal dark matter. *JCAP*, 1503:018, 2015. doi: 10.1088/1475-7516/2015/03/018.
- [111] David E. Morrissey and James D. Wells. The Tension between gauge coupling unification, the Higgs boson mass, and a gauge-breaking origin of the supersymmetric mu-term. *Phys. Rev.*, D74:015008, 2006. doi: 10.1103/PhysRevD.74.015008.
- [112] Michael B. Green and John H. Schwarz. Anomaly Cancellation in Supersymmetric D=10 Gauge Theory and Superstring Theory. *Phys. Lett.*, B149:117–122, 1984. doi: 10.1016/0370-2693(84)91565-X.
- [113] Curtis G. Callan, Jr. and Jeffrey A. Harvey. Anomalies and Fermion Zero Modes on Strings and Domain Walls. *Nucl. Phys.*, B250:427–436, 1985. doi: 10.1016/0550-3213(85)90489-4.
- [114] Jeffrey A. Harvey. TASI 2003 lectures on anomalies. 2005.
- [115] Claudio A. Scrucca and Marco Serone. Anomalies in field theories with extra dimensions. *Int. J. Mod. Phys.*, A19:2579–2642, 2004. doi: 10.1142/S0217751X04018518.
- [116] Edward Witten. An $SU(2)$ Anomaly. *Phys. Lett.*, B117:324–328, 1982. doi: 10.1016/0370-2693(82)90728-6.
- [117] L. F. Li and Frank Wilczek. Price of Fractionally Charged Particles in a Unified Model. *Phys. Lett.*, B107:64–68, 1981. doi: 10.1016/0370-2693(81)91148-5.
- [118] Tom Banks and Nathan Seiberg. Symmetries and Strings in Field Theory and Gravity. *Phys. Rev.*, D83:084019, 2011. doi: 10.1103/PhysRevD.83.084019.

- [119] Stephen M. Barr, B. Bednarz, and C. Benesh. Anomaly Constraints and New U(1) Gauge Bosons. *Phys. Rev.*, D34:235, 1986. doi: 10.1103/PhysRevD.34.235.
- [120] Paul Langacker and Michael Plumacher. Flavor changing effects in theories with a heavy Z' boson with family nonuniversal couplings. *Phys. Rev.*, D62:013006, 2000. doi: 10.1103/PhysRevD.62.013006.
- [121] Wolfram Research Inc. Mathematica, Version 9.0.
- [122] G. C. Branco, P. M. Ferreira, L. Lavoura, M. N. Rebelo, Marc Sher, and Joao P. Silva. Theory and phenomenology of two-Higgs-doublet models. *Phys. Rept.*, 516: 1–102, 2012. doi: 10.1016/j.physrep.2012.02.002.
- [123] Jens Erler, Paul Langacker, Shoaib Munir, and Eduardo Rojas. Improved Constraints on Z-prime Bosons from Electroweak Precision Data. *JHEP*, 08:017, 2009. doi: 10.1088/1126-6708/2009/08/017.
- [124] T. Sterling and M. J. G. Veltman. Decoupling in Theories With Anomalies. *Nucl. Phys.*, B189:557–574, 1981. doi: 10.1016/0550-3213(81)90581-2.
- [125] Eric D’Hoker and Edward Farhi. Decoupling a Fermion Whose Mass Is Generated by a Yukawa Coupling: The General Case. *Nucl. Phys.*, B248:59–76, 1984. doi: 10.1016/0550-3213(84)90586-8.
- [126] John Preskill. Gauge anomalies in an effective field theory. *Annals Phys.*, 210: 323–379, 1991. doi: 10.1016/0003-4916(91)90046-B.
- [127] Andriy Kurylov and Marc Kamionkowski. Generalized analysis of weakly interacting massive particle searches. *Phys. Rev.*, D69:063503, 2004. doi: 10.1103/PhysRevD.69.063503.
- [128] Maria Beltran, Dan Hooper, Edward W. Kolb, and Zosia C. Krusberg. Deducing the nature of dark matter from direct and indirect detection experiments in the absence of collider signatures of new physics. *Phys. Rev.*, D80:043509, 2009. doi: 10.1103/PhysRevD.80.043509.
- [129] A. Liam Fitzpatrick, Dan Hooper, and Kathryn M. Zurek. Implications of CoGeNT and DAMA for Light WIMP Dark Matter. *Phys. Rev.*, D81:115005, 2010. doi: 10.1103/PhysRevD.81.115005.

- [130] C. Amole et al. Dark matter search results from the PICO-60 CF₃I bubble chamber. *Phys. Rev.*, D93(5):052014, 2016. doi: 10.1103/PhysRevD.93.052014.
- [131] C. Amole et al. Dark Matter Search Results from the PICO-2L C₃F₈ Bubble Chamber. *Phys. Rev. Lett.*, 114(23):231302, 2015. doi: 10.1103/PhysRevLett.114.231302.
- [132] CMS Collaboration. Search for dark matter in final states with an energetic jet, or a hadronically decaying W or Z boson using 12.9 fb⁻¹ of data at $\sqrt{s} = 13$ TeV. 2016.
- [133] Hai-Yang Cheng and Cheng-Wei Chiang. Revisiting Scalar and Pseudoscalar Couplings with Nucleons. *JHEP*, 07:009, 2012. doi: 10.1007/JHEP07(2012)009.
- [134] M. G. Aartsen et al. Improved limits on dark matter annihilation in the Sun with the 79-string IceCube detector and implications for supersymmetry. *JCAP*, 1604(04):022, 2016. doi: 10.1088/1475-7516/2016/04/022.
- [135] K. Choi et al. Search for neutrinos from annihilation of captured low-mass dark matter particles in the Sun by Super-Kamiokande. *Phys. Rev. Lett.*, 114(14):141301, 2015. doi: 10.1103/PhysRevLett.114.141301.
- [136] The ATLAS collaboration. Search for New Phenomena in Dijet Events with the ATLAS Detector at $\sqrt{s}=13$ TeV with 2015 and 2016 data. 2016.
- [137] Kathryn M. Zurek. Asymmetric Dark Matter: Theories, Signatures, and Constraints. *Phys. Rept.*, 537:91–121, 2014. doi: 10.1016/j.physrep.2013.12.001.
- [138] Matthew R. Buckley. Asymmetric Dark Matter and Effective Operators. *Phys. Rev.*, D84:043510, 2011. doi: 10.1103/PhysRevD.84.043510.
- [139] Graciela B. Gelmini and Paolo Gondolo. Neutralino with the right cold dark matter abundance in (almost) any supersymmetric model. *Phys. Rev.*, D74:023510, 2006. doi: 10.1103/PhysRevD.74.023510.
- [140] Lawrence J. Hall, Karsten Jedamzik, John March-Russell, and Stephen M. West. Freeze-In Production of FIMP Dark Matter. *JHEP*, 03:080, 2010. doi: 10.1007/JHEP03(2010)080.
- [141] Xiaoyong Chu, Thomas Hambye, and Michel H. G. Tytgat. The Four Basic Ways of Creating Dark Matter Through a Portal. *JCAP*, 1205:034, 2012. doi: 10.1088/1475-7516/2012/05/034.

- [142] Fatemeh Elahi, Christopher Kolda, and James Unwin. UltraViolet Freeze-in. *JHEP*, 03:048, 2015. doi: 10.1007/JHEP03(2015)048.
- [143] Lam Hui and Ewan D. Stewart. Superheavy dark matter from thermal inflation. *Phys. Rev.*, D60:023518, 1999. doi: 10.1103/PhysRevD.60.023518.
- [144] David H. Lyth and Ewan D. Stewart. Thermal inflation and the moduli problem. *Phys. Rev.*, D53:1784–1798, 1996. doi: 10.1103/PhysRevD.53.1784.
- [145] Vardan Khachatryan et al. Search for physics beyond the standard model in dilepton mass spectra in proton-proton collisions at $\sqrt{s} = 8$ TeV. *JHEP*, 04:025, 2015. doi: 10.1007/JHEP04(2015)025.
- [146] David Curtin et al. Exotic decays of the 125 GeV Higgs boson. *Phys. Rev.*, D90(7): 075004, 2014. doi: 10.1103/PhysRevD.90.075004.
- [147] Robert E. Shrock and Mahiko Suzuki. Invisible Decays of Higgs Bosons. *Phys. Lett.*, B110:250, 1982. doi: 10.1016/0370-2693(82)91247-3.
- [148] CMS Collaboration. Searches for invisible Higgs boson decays with the CMS detector. 2016.
- [149] Anupama Atre, Georges Azuelos, Marcela Carena, Tao Han, Erkan Ozcan, Jose Santiago, and Gokhan Unel. Model-Independent Searches for New Quarks at the LHC. *JHEP*, 08:080, 2011. doi: 10.1007/JHEP08(2011)080.
- [150] Yonatan Kahn, Gordan Krnjaic, Siddharth Mishra-Sharma, and Tim M. P. Tait. Light Weakly Coupled Axial Forces: Models, Constraints, and Projections. 2016.
- [151] John Ellis, Malcolm Fairbairn, and Patrick Tunney. Anomaly-Free Dark Matter Models are not so Simple. 2017.
- [152] J. J. van der Bij and E. W. Nigel Glover. Z Boson Production and Decay via Gluons. *Nucl. Phys.*, B313:237–257, 1989. doi: 10.1016/0550-3213(89)90317-9.

Vita

Kuo-Hsing Tsao

Education:

- Ph.D. Physics, University of Illinois at Chicago, expected May 2017.
Thesis: *Theory and Phenomenology Beyond the Standard Model and Dark Matter Physics*
Advisor: Wai-Yee Keung
- M.S. Physics, National Taiwan Normal University, Taipei, Taiwan, 2009.
Thesis: *Supersymmetry Breaking by Metastable Vacua*
Advisor: Chia-Hung Chang
- B.S. Physics, National Chung Cheng University, Chiayi, Taiwan, 2007.

Publications:

1. Ahmed Ismail, Wai-Yee Keung, Kuo-Hsing Tsao and James Unwin. *Nuclear Physics B* (dx.doi.org/10.1016/j.nuclphysb.2017.03.001).

Research Presentations:

1. Seminar Talk: “Top-philic Z' at the LHC & Axial Vector Z' and Anomaly Cancellation”, National Taiwan Normal University, Taipei, Taiwan, 2017.
2. Talk: “The 4th International Workshop on Dark Matter, Dark Energy and Matter-antimatter Asymmetry”, National Center for Theoretical Sciences, Hsinchu, Taiwan, 2016.
3. Talk: “The 2011 Phenomenology Symposium”, Madison, USA, 2011.

Schools Attended:

1. The 7th Joint Fermilab-CERN Hadron Collider Summer School, Batavia, Illinois, USA, August 6-17, 2012.

Teaching Experience:

Lab Assistant	Electricity and Magnetism
Lab Assistant	Introductory Mechanics
Lab Assistant	Astrophysics
Lab Assistant	Modern Physics
Grading Assistant	Quantum Mechanics
Grading Assistant	Classical Mechanics
Grading Assistant	Statistical Mechanics
Grading Assistant	Electricity and Magnetism
Grading Assistant	Particle Physics